1999

Control of a high-frequency rectifier

Linda J. Murdoch
University of Wollongong

CONTROL OF A

HIGH-FREQUENCY RECTIFIER

A thesis submitted in fulfilment of the requirements

for the award of the degree

MASTER OF ENGINEERING (Honours)

from

UNIVERSITY OF WOLLONGONG

by

LINDA J. MURDOCH, B.E.

School of Electrical, Computer and
Telecommunications Engineering
1999

ABSTRACT

The quality of the electricity supply can be affected by the operation of power conversion equipment such as ac/dc rectifiers and ac/dc/ac converters. Power conversion equipment such as this is widely used in industrial, commercial and domestic applications and the number of applications that use power conversion equipment is rapidly increasing.

The conventional power conversion systems that are implemented have been developed to supply the required waveform to the load without regard for the effect that this has on the supply. The operation of these systems can produce a large number of harmonics on the supply, which reduces the quality of the supply and causes problems such as an increase in losses and inefficient operation.

Developments in power conversion equipment have included the introduction of conversion equipment which is capable of operating at high switching frequencies. This type of system can be operated in such a way as to produce minimal supply distortion.

This thesis considers one such system and focuses on the control of the high-frequency rectifier for which a number of control strategies are presented. Rather than controlling the rectifier based on a cycle-by-cycle assessment of the system, these strategies consider the capability of the system based on the overall form of the system trajectories. An understanding of these trajectories has allowed the development of control strategies with a high speed of response.

ACKNOWLEDGMENTS

For their guidance and support I would like to thank my supervisors Dr Don Platt and Associate Professor Vic Gosbell.

For financial assistance I would like to thank the Energy Research and Development Corporation and the Energy Efficient Research Centre.

For their support, understanding and patience I thank my family and friends.

TABLE OF CONTENTS

LIST OF FIGURES

LIST OF TABLES

LIST OF SYMBOLS

C	DC bus capacitor
$\underline{e}$	Supply voltage vector
$\underline{E}$	Supply voltage vector (assumed constant)
e_a, e_b, e_c	Three phase supply voltages
e_{par}	Component of supply voltage vector parallel to switching vector
e_{perp}	Component of supply voltage vector perpendicular to switching vector
E_S	Supply voltage (DC source circuit)
f	Natural frequency of oscillation
$\underline{i}$	Supply current vector
i_a, i_b, i_c	Three phase supply currents
i_d	Component of supply current vector parallel to supply voltage vector
i_q	Component of supply current vector perpendicular to supply voltage vector
i_{par}	Component of supply current vector parallel to switching vector
i_{perp}	Component of supply current vector perpendicular to switching vector
i_L	Inductor current
i_{L0}	Initial inductor current

i_{out}	Rectifier output current
I_{out}	Rectifier output current (assumed constant)
i_{inv}	Current to inverter (rectifier output current)
$\underline{i}_{LL}$	Converter load current vector
i_{la}, i_{lb}, i_{lc}	Three phase converter load currents
L	Supply side inductance
L_L	Load inductance
R_L	Load resistance
S	Switching mode (1, -1 or 0)
$\underline{S}$	Switching vector
S_a, S_b, S_c	Three phase switching mode
S_d	Component of switching vector parallel to supply voltage vector
S_q	Component of switching vector perpendicular to supply voltage vector
S_{dR}	Weighted combination of S_d for adjacent modes
S_{qR}	Weighted combination of S_q for adjacent modes
v_{cap}	DC bus capacitor voltage
v_{cap0}	Initial dc bus capacitor voltage
w_1, w_2	Weighting factors for adjacent modes
ω	Natural frequency
Z	Characteristic impedance

Z_0	Current scaling factor
θ	Angle between supply voltage vector and the closest switching vector

CHAPTER 1
INTRODUCTION

The three phase ac to ac converter is a circuit commonly used in applications such as three phase induction machine control to allow variable speed operation. The converter is used to control the flow of power from the supply to the load and also to control the waveshape at the output. The use of a controllable rectifier on the supply side allows bidirectional operation and allows control of the supply currents as well. The aim of this report is to provide an understanding of the rectifier system trajectories and to introduce rectifier control strategies based on these trajectories.

This chapter provides the background to the work, an overview of the circuit considered, the aims of the control strategy and an overview of rectifier control strategies published by other researchers.

1.1 Background

The type of circuit under consideration in this report is the voltage source converter; that is an ac/dc/ac converter where the dc link represents a voltage source to the output stage. The rectifier is the focus of this report and developments in the hardware and control of the rectifier are considered in this chapter. The first voltage source converter to be considered is that with an uncontrolled or phase controlled rectifier as the input stage. Circuit developments that are also considered here are the hard-switched and soft-switched converters.

1.1.1 Uncontrolled and Phase Controlled Rectifier

In the past, diode rectifiers were commonly used for three phase ac to dc conversion. The conversion was uncontrolled. Power flows in one direction only, that is from the ac side to the dc side of the bridge. The disadvantages of using this type of circuit are that the dc bus voltage is uncontrolled, the ac supply currents are not sinusoidal and have a large harmonic content and the power factor is poor.

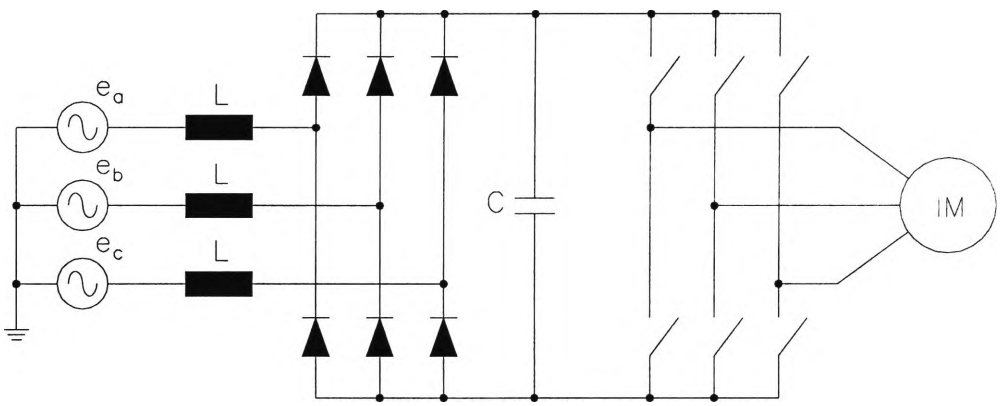

Figure 1 Three phase converter with diode rectifier

The use of line frequency phase-controlled (thyristor) rectifiers was also common as it allowed the dc bus voltage to be controlled. In this type of circuit the thyristors can be turned on by the application of a control signal but they can only be turned off by the power circuit; that is when the current through the device goes negative. The problems with this type of circuit are similar; the ac supply currents are not sinusoidal and have large harmonic content, and the power factor decreases as the thyristor firing angle increases.

The types of problems caused by high levels of harmonics in the supply current include:

- an increase in losses and therefore heating of equipment;
- errors in metering;
- malfunction of equipment.

There is an increasing demand for variable speed drives so, as the use of these types of circuits increases, the level of harmonic distortion of the supply would tend to increase also. With increasingly severe standards controlling supply harmonics injection, more sophisticated rectifier systems have been developed.

1.1.2 Hard Switched Converter

Since the introduction of controllable switches, ac/dc/ac converters have frequently made use of these devices which include insulated gate bipolar transistors (IGBTs), gate turn off thyristors (GTOs), bipolar junction transistors (BJTs) and metal oxide semiconductor field effect transistors (MOSFETs). The turn on and turn off of these devices is controlled and they are capable of switching at frequencies much greater than the supply frequency, allowing high-frequency operation.

The converter circuit is shown below with IGBT switching devices with anti-parallel diodes. The circuit is referred to as hard-switched because when the switches operate they are required to switch the line currents with the full dc bus voltage across them.

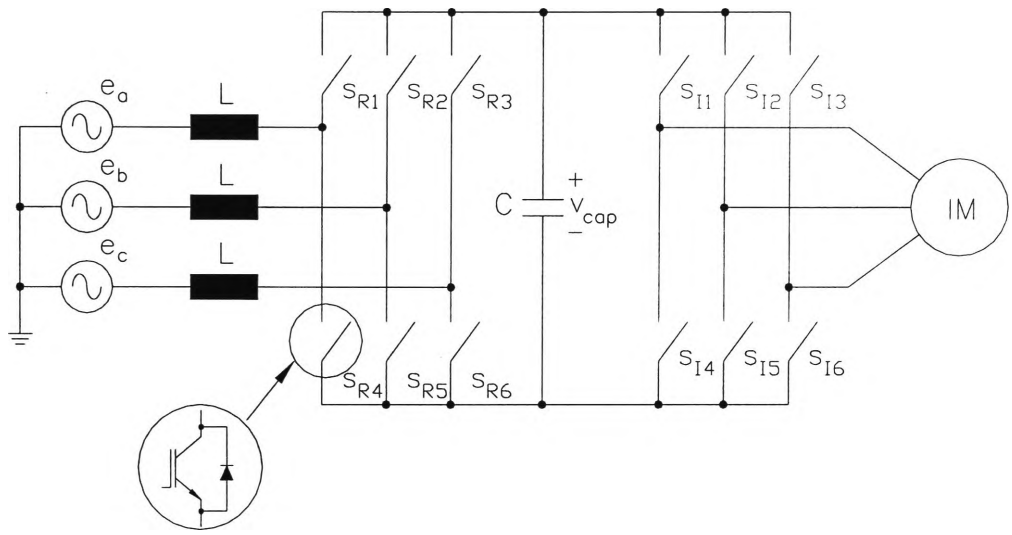

Figure 2 Three phase converter with controllable hard-switched rectifier

The introduction of controllable switches has allowed the use of pulse-width modulation (PWM) rectifier control techniques with the following typical control aims:

- Sinusoidal supply currents (reduced harmonics);
- Unity power factor on the supply side;
- Bidirectional capability.

Another consideration in the control of the rectifier is the competitive need to reduce the size of the dc bus capacitor, which can lead to a reduction in cost as well as a reduction in volume.

Thus the control of the rectifier involves operating the switching devices in the rectifier bridge in order to control the supply currents and dc bus voltage. The devices may be switched at a fixed or variable frequency. Various control strategies are reported in the literature which attempt to meet these aims. Some of the most common strategies are discussed below.

The focus of this discussion is on the control of the rectifier, and there are two important aspects which are discussed separately:

- Choice of target;
- Control of switches to achieve target.

1.1.2.1 Choice of Target

In order to meet the desired control aims the variables to be controlled are the dc bus voltage and the supply currents. The rectifier control strategies derive target values for the variables in a number of different ways.

The control schemes typically aim to maintain a constant dc bus voltage in an attempt to match the power from the supply with the power drawn by the load.

Ooi et al [1]-[4] discuss a limit that restricts the choice of capacitor voltage target, which is referred to as the "current waveform distortion limit". Briefly, the current waveform distortion limit specifies a minimum limit on the capacitor voltage which must be exceeded to "ensure that there is sufficient voltage to force the supply currents through the inductances to track the desired template waveforms". This limit is discussed in Chapter 4.4.4.

For the supply current reference, the supply voltage waveforms are often used as templates for the supply currents in order to achieve unity power factor. This also allows phase shifting if a different power factor (leading or lagging) is required. The derivation of the supply current reference involves the calculation of the required magnitude for the reference waveform.

In the control strategy presented by Ooi et al [1]-[4], the supply current reference

magnitude is based on proportional feedback of the dc bus voltage error. The problems with proportional feedback include the steady-state error in the dc bus voltage that results.

Phase shifting is included in the derivation of the current reference for the predictive current controller with fixed switching frequency (PCFF) [5],[6],[7]. The operation of this control strategy is discussed in Chapter 1.1.2.2. Phase shift compensation is introduced into the reference waveform to account for the phase shift introduced by the control strategy. The supply voltage is used as a template with phase shift applied.

The current reference is more often based on a combination of feedback of the dc bus voltage error (proportional or PI regulated) as well as load feedforward. This improves the response of the dc bus voltage to changes in the load. Load feedforward has been implemented in a PCFF control system by Chen and Blaabjerg [7] where the load feedforward is the rectifier output current (that is, the current drawn from the dc bus by the inverter bridge and load), which is then added to the PI dc bus voltage feedback term. More typically the load feedforward is based on an output power estimate. The output power estimation utilised by Habetler [8] is based on the power delivered to the motor load from the inverter, which is calculated from an estimation of the electrical torque of the motor and the stator frequency.

Early control techniques were based on references for per-phase currents. The supply currents can also be represented as a vector and the control is then based on a current reference vector. The supply voltage is also represented by a vector and

these vectors are transformed to a rotating (dq) reference frame which is aligned with the supply voltage vector. Since unity power factor is required the component of the supply current vector reference in quadrature with the supply voltage vector is set to zero. The reference supply current then specifies the magnitude of the vector. This type of control is termed space vector control as presented by Habetler [8].

Habetler [8] derives the current reference magnitude from a combination of a dc bus voltage feedback term and an output power estimation. A parameter which determines the weighting of these two components is used to tradeoff the control performance under steady state and transient conditions. If greater weighting is applied to the dc bus voltage feedback term then the steady state performance is improved. On the other hand, greater weighting applied to the output power estimation term will improve the transient performance.

Recent research has considered quasi-direct converters, which are ac/dc/ac converters with minimum dc bus capacitor size, as reported by Kim and Sul [9] and also by Malesani et al [10]. Typically electrolytic capacitors have been used as the dc bus capacitor. Electrolytic capacitors are relatively large and heavy. Thus the motivation behind reducing the size of the capacitor is to replace the electrolytic capacitor with ceramic capacitors. In order to reduce the size of the capacitor it is necessary to achieve a very tight power balance.

The load feedforward presented by Malesani et al [10] low pass filters the rectifier output current to get the average rectifier output current. The current reference magnitude is calculated by multiplying this current by a constant which takes into

account the efficiency of the rectifier and the supply and dc link voltages. DC bus voltage feedback is used as well as the output power estimation to account for any errors in the power estimation, as may be caused by changing load characteristics for example.

Kim and Sul [9] take advantage of the computational power of modern DSPs for real time power estimation. Their estimate of output power includes the machine losses (copper loss in the stator and rotor of the machine, iron losses plus the mechanical output power) as well as the switching and conduction losses of the semiconductor devices. These last losses are difficult to estimate and so the estimation has thus been based on the line currents. This output power estimation is combined with proportional dc bus voltage feedback and the control also incorporates a PI regulator with low gains and limited range to account for any errors in the power estimation.

1.1.2.2 Control of Switches

Once the current reference has been calculated the switching of the controllable bridge must be controlled in order to force the currents to follow the reference.

A common method of rectifier control is hysteresis current control (HCC). This type of control has been implemented by Ooi et al [1]-[4]. HCC involves switching the devices in the rectifier bridge so that the currents remain within a small tolerance of the reference value; that is, switching occurs when the current error exceeds the upper and lower hysteresis bands which are either side of the reference. A problem with HCC is that the switching frequency, and therefore switching losses, can be high if the size of the hysteresis band is small. The

switching frequency varies with changes in rectifier output current so the switching stresses are difficult to predict.

Phase and amplitude control (PAC), or indirect current control, has evolved from HCC. This technique is based on sinusoidal PWM. Instead of deriving the magnitude of the current reference from the dc bus voltage error, the proportional error is used to derive the amplitude of the PWM modulating voltage waveform. The phase of this waveform is controlled to give adjustable power factor. This method has been considered by Dixon and Ooi [11], Wernekinck et al [12] and Wu et al [13]. The derivation of the modulating voltage waveform equates to determining the required rectifier voltage (voltage at the rectifier input terminals), and the supply currents are thus controlled indirectly by changing the phase and amplitude of this voltage. Sinusoidal PWM is used to determine the switching instants from the intersection of the modulating sinusoidal waveform with a triangular carrier. A problem with PAC is that it produces a dc offset on the supply currents.

Predictive current control with fixed switching frequency (PCFF) is a control technique presented by Wu et al [5],[6] which does not produce the dc offset of the PAC strategy. A current reference is calculated based on dc bus voltage feedback and load feedforward. Given the current reference, the required change in current for each phase is determined. PCFF is used to calculate the required rectifier voltages for achieving the desired change in current. From this a switching pattern is constructed for each phase by comparing the voltage to a triangular carrier and the intersections give the switching instants for each leg of the rectifier bridge. As implied by the name of the strategy, the switching

frequency is constant and therefore the switching stresses are predictable. There is a delay of one switching period for the supply currents to follow the reference so the derivation of the current reference generally includes phase compensation as discussed in Chapter 1.1.2.1.

Another predictive control strategy has been presented by Habetler [8]. This space vector control strategy controls the supply current vector in the rotating dq reference frame. The available rectifier switching modes are represented as vectors and this strategy involves calculating the duty cycle for each switching mode which will give the required change in the supply current vector in a single cycle. Every half cycle the required rectifier voltage vector is determined and this differs from the PCFF strategy which calculates the required rectifier voltage only once per cycle. The first stage of the space vector control is to select the switching modes to be applied. They will be those with vectors adjacent to the required rectifier voltage vector. The next step is to determine the duration for which each of these two modes should be applied, or the duty cycle. The switching period is constant and the zero mode is applied over the remainder of the period. The zero mode application is equally distributed at either end of the half-switching cycle. If under transient conditions it is not possible to achieve the reference in a single cycle then in this case the zero mode is not applied. The modes that are applied are those that drive the current towards the reference.

Chen and Blaabjerg [7] also use a predictive space vector based control strategy.

Other approaches to the control of the rectifier include sliding mode, neural networks and fuzzy logic. There are also many different combinations for the two

aspects of the control; that is the coupling of the target selection with the control strategy for switching operation.

As mentioned previously, hard-switching involves switching the line currents with the full dc bus voltage across the switching devices. This results in switching stresses and switching power losses that increase linearly with the switching frequency. The switching frequency (and therefore performance) of the system is limited due to the switching losses and switching stresses which cause:

- production of heat;
- reduced system efficiency;
- component degradation;
- possible component failure.

The switching operation also causes electromagnetic interference (EMI) due to the rapid changes in voltage and current. Higher switching frequency is possible if the switching losses can be decreased. This is achieved using soft-switching.

1.1.3 Soft-Switched Converter

Soft-switched converters switch the semiconductor devices when the voltage across them or the current through them is equal to zero. Therefore the switching losses will be minimal. A brief overview of the zero voltage switching resonant circuit is provided below.

The resonant dc link (RDCL) converter was proposed by Divan [14]. Soft-switching is possible because of the resonant action of the bus voltage which is due to the addition of parallel LC components to the dc bus. The circuit for the

resonant dc link converter is similar to that of a hard-switched converter with the addition of the resonant components as shown below.

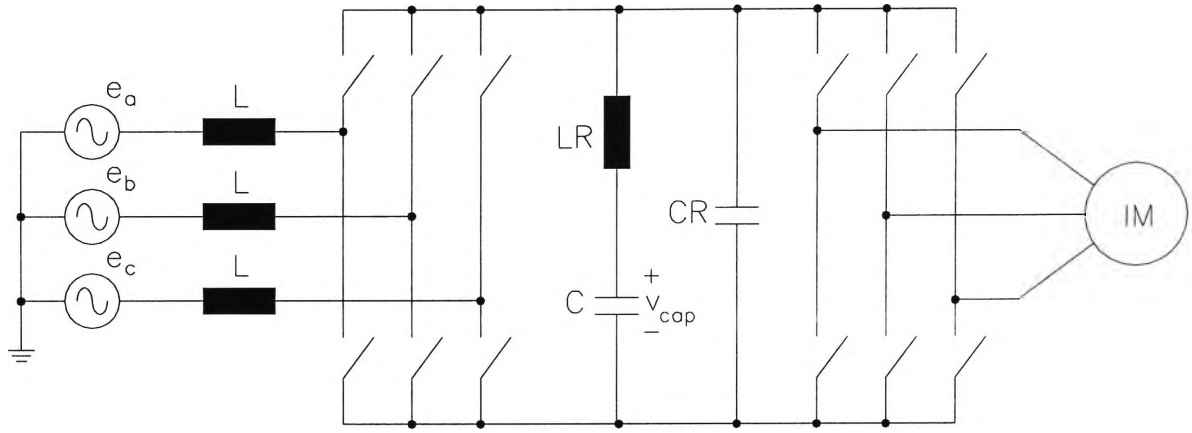

Figure 3 Three phase resonant dc link converter

Since the switching devices operate with zero voltage across them, reduced switching stresses and power losses occur which allows:

- the elimination of snubbers, resulting in less circuit hardware
- improved circuit reliability
- reduced EMI
- less heat produced
  - improved efficiency
  - reduced equipment size
- higher frequency operation
  - better control of current waveforms
  - less acoustic noise

While detail of the operation of the resonant dc link converter is not provided here, a brief overview of some rectifier control aspects are considered.

The aims of the control of the rectifier in the resonant dc link converter are the same as those presented for the hard-switched converter. That is:

- Sinusoidal supply currents (reduced harmonics);
- Unity power factor on the supply side;
- Bidirectional capability;
- Reduced size of the dc bus capacitor.

For a soft-switched converter the switching instants are constrained to the part of the switching period when the voltage is zero. The types of strategies generally used are referred to as discrete pulse modulation (DPM) strategies.

Control strategies for the RDCL rectifier include space vector control which is similar in manner to that presented for the hard-switched rectifier. An example is presented by Habetler and Divan [15]. The current vector reference is again derived from load feedforward in the form of output power estimation. The control considers the rotating (dq) frame of reference and the selection of switching mode to apply at a particular switching instant involves a number of steps. The modes which would drive the supply current vector towards the supply voltage vector (to give unity power factor) are determined. Of these, the modes are selected that will drive the current towards the required current magnitude according to a sliding mode equation. This equation includes a parameter to weight the dc bus voltage and supply current magnitude control components. The value given to this parameter will influence the relative steady state and transient performance. If more than one mode satisfies these selection aspects then the mode that gives the minimum dc bus voltage ripple is selected.

Research has also considered the application of PWM to the soft-switched converter as DPM strategies can result in significant harmonic components at frequencies below the switching or resonant frequency. These developments consider the synchronisation of the switching instants with a PWM type control strategy.

One characteristic of the operation of the RDCL converter is the high peak voltages imposed on the switching devices during the switching period due to the resonant operation. Methods of reducing the peak voltage include active clamping, which involves additional hardware and more complex control.

1.2 Thesis Aims

The circuit considered in this report is the hard-switched three phase ac/dc/ac rectifier which would typically form the input stage to a high-frequency converter as shown in Figure 4. This is the circuit that was discussed in Chapter 1.1.2. The converter is shown connected to the supply and an induction motor load below.

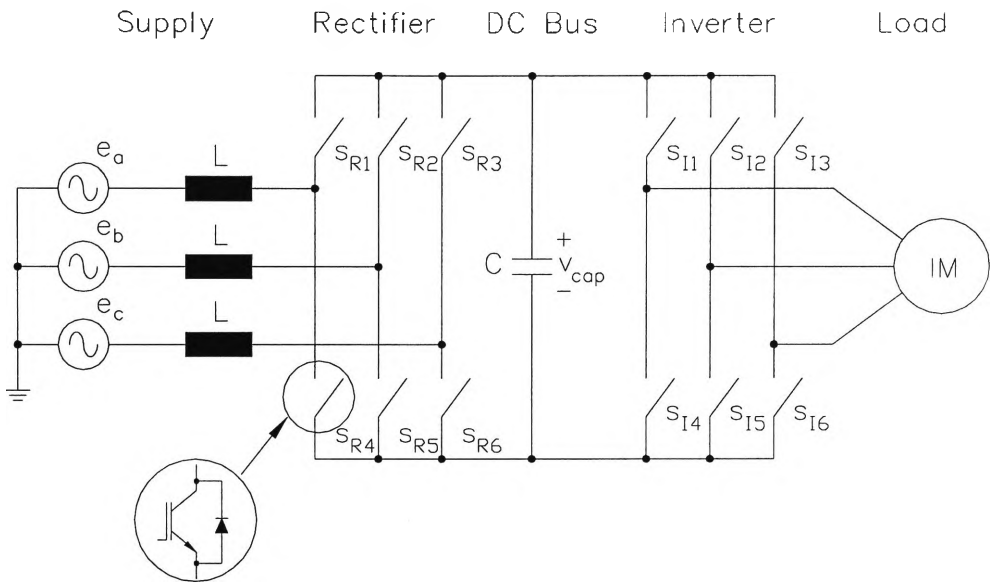

Figure 4 Three phase converter hardware

The three phase ac supply, and associated line inductance L, is connected to the rectifier bridge. The rectifier consists of six bi-directional switches, typically made up of insulated gate bipolar transistors (IGBT) with antiparallel diodes. The rectifier is connected to a capacitor which forms the dc bus. The inverter bridge, which is identical in construction to the rectifier, is connected between the dc bus and the load.

During forward operation, the switches in the rectifier bridge allow the supply to be connected to the dc bus in order to charge the dc bus capacitor. At the same time the switches in the inverter bridge allow the dc bus voltage to be connected to the load in order to drive the load currents. During reverse (regenerative) operation, the switches allow power to flow in the reverse direction.

The rectifier is operated such that each of the three phases of the supply and load are connected to either the positive or negative side of the dc bus capacitor. For example, if switch S_{R1} is closed then S_{R4} will be open and supply phase-a will be

connected to the positive side of the dc bus capacitor. Alternatively, if switch S_{R1} is open then S_{R4} is closed and supply phase-a will be connected to the negative side of the dc bus capacitor. The configuration of the switches at each switching instant is selected in order to push currents and voltage towards target values to meet the required control aims.

1.2.1 Control Aims

The aim of this report is the analysis of the rectifier trajectories and the development of methods of controlling the high-frequency rectifier based on this analysis. The following control considerations are applied:

- unity power factor on the supply side (supply currents in phase with supply voltages),
- minimise line current harmonics,
- reversible power flow,
- desired current to load,
- minimal capacitor voltage ripple so that the capacitor size can be minimised,
- fast response,

In order that the control strategies developed be applicable to the resonant dc link rectifier, where the switching instants will generally be set by the resonant operation, the control is based on a fixed switching frequency.

1.3 Outline of the Report

The report looks first at a simple single phase dc source circuit and analyses the

system equations and trajectories. This analysis provides an insight into the use of system trajectories for stable control of the state variables.

An analysis of the three phase high-frequency switched rectifier is presented in Chapter 3, on the basis of a simplified ac/dc/ac converter circuit. The results presented include the system equations and the trajectories for the rectifier state variables.

As discussed in Chapter 1.1.2, the control of the rectifier has two components. The first is the derivation of the references for the state variables. The second is the implementation of a control strategy which is used to select the switching mode to be applied at each switching instant. In Chapter 4 the first of these aspects is considered. Further analysis of the rectifier system trajectories is used as the basis of the selection of target values for the rectifier state variables. The control strategy implementation is considered in Chapter 5, where several techniques based on the system trajectories are presented. Simulation results for each are presented.

In order to show that the rectifier control strategies can be applied to the full ac/dc/ac converter system, in Chapter 6 one of the rectifier control schemes developed is coupled with an inverter control scheme to allow control of the high-frequency converter. Simulation results under both steady state and transient conditions are presented.

CHAPTER 2
DC SOURCE ANALYSIS

2.1 Introduction

In order to gain an insight into the use of system trajectories for the control of state space variables, a simple dc source circuit is considered. The dc source circuit is similar in representation to a single phase approximation of the three phase rectifier, with the ac supply replaced by a dc source. The dc source circuit that is considered has three possible switching configurations and the state space equations and trajectories for each are presented.

2.2 Circuit

The dc source circuit is shown in Figure 5. On the supply side the circuit consists of a dc source E_S connected to a supply inductance L. The supply is connected to the output stage via two switches and this connection can be made in one of three possible configurations by varying the positions of the switches. The output stage consists of a capacitor C and a constant output current I_{out}. This circuit is a form of step-up (boost) converter.

The position of the switches that connect the supply to the capacitor is represented by S where either:

- S=1 when the supply is connected across the capacitor as indicated : the

inductor L is connected to the positive side of the capacitor (positive active switching mode);

- S=-1 when the supply connections across the capacitor are reversed (negative active switching mode);
- S=0 when the supply is not connected to the capacitor (zero switching mode).

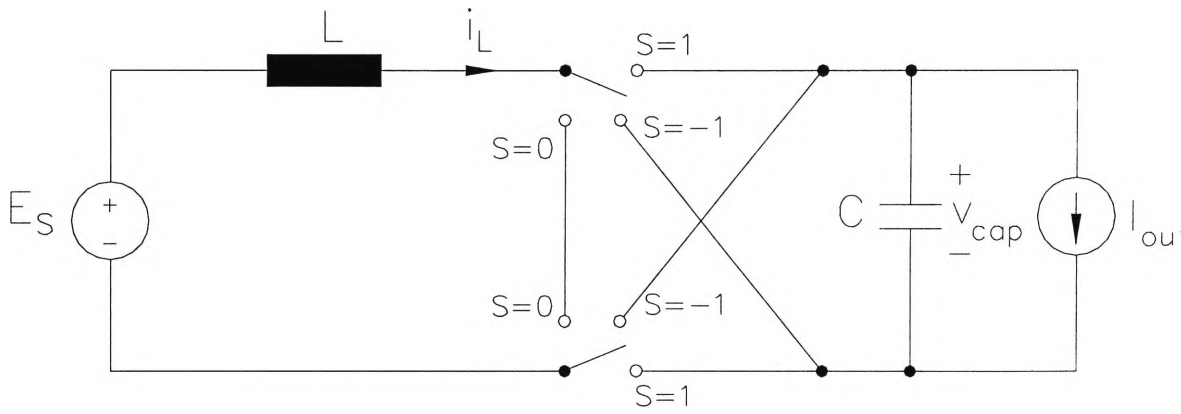

Figure 5 DC source circuit

The state variables in the dc source circuit are the inductor current i_L and the capacitor voltage v_{cap}.

During a zero switching mode the supply is disconnected from the output stage. There is a positive voltage (E_S) across the inductor and the inductor current increases. The capacitor voltage decreases as the output current flows.

During an active switching mode the supply is connected to the output stage in the forward or reverse direction. The change in inductor current depends on the difference between the supply voltage and the capacitor voltage and their relative signs. The change in capacitor voltage depends on the difference between the inductor current and output current and their relative signs.

The equations for the state variables are given below.

$$\frac{dv_{cap}}{dt} = \frac{1}{C}\left(Si_L - I_{out}\right) \tag{1}$$

$$\frac{di_L}{dt} = \frac{1}{L}\left(E_S - Sv_{cap}\right) \tag{2}$$

For the active switching modes, the equations for the state variables are given by:

$$v_{cap}(t) = SE_S + \left(v_{cap0} - SE_S\right)\cos\omega t + Z\left(Si_{L0} - I_{out}\right)\sin\omega t \tag{3}$$

$$i_L(t) = Si_{out} + \frac{\left(E_S - Sv_{cap0}\right)}{Z}\sin\omega t + \left(i_{L0} - SI_{out}\right)\cos\omega t \tag{4}$$

For the zero switching mode the equations for the state variables are given by:

$$v_{cap}(t) = v_{cap0} - \frac{I_{out}}{C}t \tag{5}$$

$$i_L(t) = i_{L0} + \frac{E_S}{L}t \tag{6}$$

where:

- v_{cap0} is the initial value of the capacitor voltage
- i_{L0} is the initial value of the inductor current
- $\omega = \sqrt{\frac{1}{LC}}$
- $Z = \sqrt{\frac{L}{C}}$

By graphing capacitor voltage versus inductor current the change in the state variables with time can be analysed. Examples of the trajectories for the three

switching modes are shown in Figure 6 for a positive output current and various initial conditions. The inductor current axis has been scaled by Z which results in circular trajectories for the active modes.

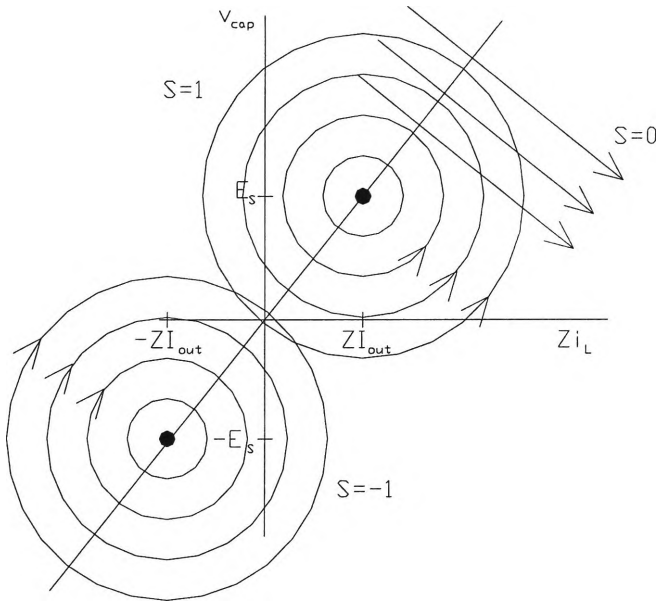

Figure 6 DC circuit trajectories

In the (v_{cap}, Zi_L) plane the active modes give circular trajectories, the radius of which depend on the initial conditions. The centre of the trajectories is given by:

$$\left(Zi_L, v_{cap}\right) = \left(SZI_{out}, SE_S\right) \tag{7}$$

The zero modes give straight line trajectories which are perpendicular to the line through the centre of the active mode trajectories (and the origin).

On the line through the centre of the active mode trajectories:

$$\frac{v_{cap}}{i_L} = \frac{E_S}{I_{out}} \tag{8}$$

Since the power out of the source is given by $E_S i_L$ and the power into the 'load' is given by $v_{cap} I_{out}$, Equation 8 gives the conditions for which a balance of power in

the circuit occurs. Therefore, if the operating point lies on the line through the centre of the active mode trajectories, then the power in the circuit is balanced.

Of the operating points for which the power in the system is balanced, special consideration must be given to points above the centre of the circular trajectories for the positive active switching mode. As shown below, at these points stable control of the state variables is possible due to the relative directions and shape of the trajectories. In the example presented in Figure 7, the circular active mode and straight line zero mode trajectories are used to oscillate about the point labelled 'T'.

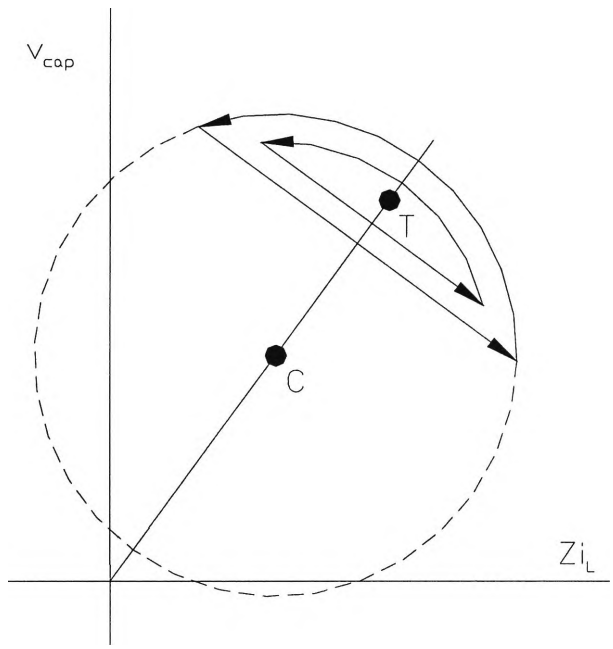

Figure 7 Trajectories for stable operation

It is also possible to utilise the circular and straight line trajectories to move between points on the line of power balance, or to move to the line from other points in the plane.

2.3 Summary

The dc source circuit considered has three possible switching modes. These have been referred to as positive and negative active switching modes and the zero switching mode. An analysis of the equations and trajectories for the state variables for each of these switching modes has been presented, where the state variables are the inductor current and capacitor voltage.

The trajectories for the active switching modes are shown to be circular (when the inductor current is appropriately scaled) and the radius of the trajectories depend on the initial conditions. The line through the centre of the active mode trajectories also passes through the origin and it has been shown that a balance of power in the circuit occurs when the operating point lies on this line (referred to here as the line of power balance). The trajectories for the zero switching mode are straight lines perpendicular to the line of power balance.

For operating points on the line of power balance and above the centre of the circular trajectories (for the positive active switching mode), it is possible to achieve stable control by taking advantage of the shape of the circular and straight line trajectories.

In the following chapter the equations and trajectories for the state variables for the three phase ac to dc rectifier are considered and related to those discussed above.

CHAPTER 3

ANALYSIS OF THE HIGH-FREQUENCY SWITCHED RECTIFIER

3.1 Introduction

The high-frequency switched rectifier to be considered forms the input stage of a three phase ac/dc/ac converter.

The aim is to analyse the rectifier in isolation and develop methods of rectifier control that utilise the shape of the system trajectories to meet several aims, mainly sinusoidal supply currents at unity power factor and constant capacitor voltage. The development of these control strategies is presented in three parts which are addressed in the following three chapters. The first is a detailed analysis of the shape and characteristics of the system trajectories. The next area considered is the choice of target operating point. The final aspect is the control rules implemented in an attempt to reach the target, which are based on the system trajectories.

In this chapter an analysis of the dynamic behaviour of the high-frequency switched rectifier is presented. The aim is to investigate in detail the shape and characteristics of the system trajectories.

The circuit considered in the analysis of the rectifier operation represents a simplified converter circuit, which allows results for the rectifier to be derived

which may be applied to the full converter system.

The rectifier considered has eight possible switching configurations and equations for the state variables for each configuration are derived. These equations apply irrespective of variation in the supply voltage or output current. A study of the equations for the state variables results in an understanding of the form of the system trajectories. A detailed analysis of the trajectories is presented for the system for which the response of the rectifier is fast compared to the supply frequency and the output current is assumed constant.

This chapter covers first the circuit considered for the rectifier analysis. The equations for the state variables and the system trajectories are then presented. The characteristics of these trajectories are discussed in some detail.

3.2 Rectifier Circuit

To analyse the operation of the high-frequency switched rectifier, the three phase ac/dc/ac converter system shown in Figure 4 can be approximated by that shown in Figure 8, where a current source represents the current drawn by the three phase inverter and inductive load.

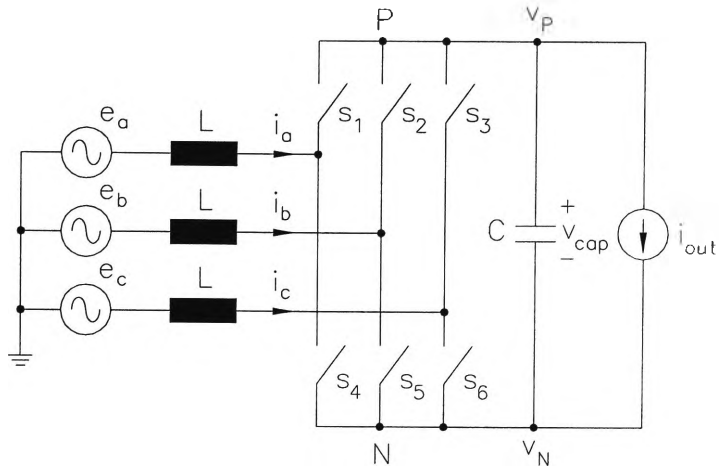

Figure 8 Simplified circuit for switched rectifier

The rectifier connects the three phase ac supply, and associated line inductance L, to the dc bus capacitor and current source.

3.3 Equations

A theoretical investigation of the system allows equations for the state variables for the switched rectifier to be derived. The state variables considered are the dc bus voltage (v_{cap}) and the supply current vector $\underline{i}$ where:

$$\underline{i} = i_a + i_b e^{j(2\pi/3)} + i_c e^{j(4\pi/3)} \tag{9}$$

The following vectors can also be defined:

$$\underline{e} = e_a + e_b e^{j(2\pi/3)} + e_c e^{j(4\pi/3)} \tag{10}$$

$$\underline{S} = S_a + S_b e^{j(2\pi/3)} + S_c e^{j(4\pi/3)} \tag{11}$$

where $\underline{e}$ is the supply voltage vector and $\underline{S}$ is the 'switching vector' which represents the distinct switching mode of the rectifier. The variables S_a, S_b and S_c from Equation 11 describe the switching configurations of the three phases of the

rectifier bridge. The a-phase will be connected to either P or N as illustrated in Figure 8, and this switching configuration is described by S_a where:

- $S_a = 1$ if the a-phase is connected to P
- $S_a = 0$ if the a-phase is connected to N.

Similarly S_b and S_c are defined for the b- and c-phases. Each of the eight possible switching modes (and switching vectors) is uniquely labelled using the three bits S_a, S_b and S_c. For example $\underline{S}_{110}$ identifies the switching vector that is applied when the a- and b-phases are connected to P and the c-phase is connected to N. A rectifier switching mode can be classified as:

- a zero switching mode if $\underline{S} = 0$
- an active switching mode otherwise.

As illustrated in Figure 9, for each of the six active switching modes there is a switching vector with unit magnitude and for the zero switching modes there are vectors with length equal to zero. The opposite switching vectors (for example $\underline{S}_{110}$ and $\underline{S}_{001}$) are referred to here as complementary.

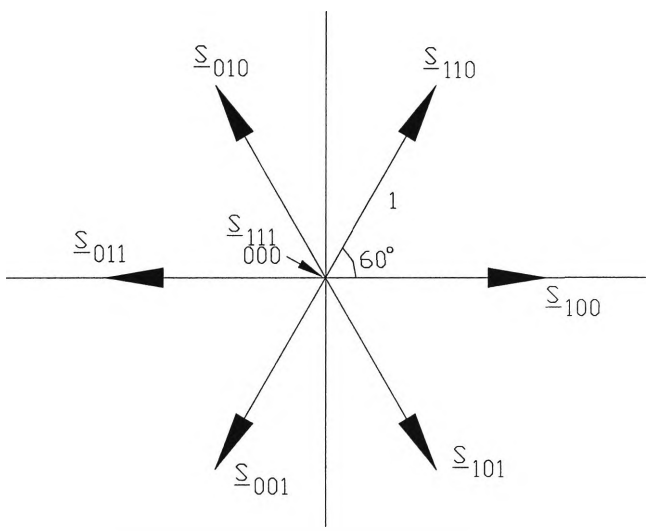

Figure 9 Rectifier switching vectors

It is shown in Appendix A, that the change in current and voltage are given by the system equations below:

$$\frac{d\underline{i}}{dt} = \frac{1}{L}\left(\underline{e} - \underline{S}v_{cap}\right) \tag{12}$$

$$\frac{dv_{cap}}{dt} = \frac{1}{C}\left(\frac{2}{3}\underline{S}\cdot\underline{i} - i_{out}\right) \tag{13}$$

where $\underline{S}\cdot\underline{i}$ is the dot product of the vectors $\underline{S}$ and $\underline{i}$.

Since an aim of the rectifier control system is to control the supply current vector to be in phase with the supply voltage vector, it is useful to consider:

- the component of the supply current vector in phase with the supply voltage vector (i_d)
- the component of the supply current vector out of phase with the supply voltage vector (i_q)

The corresponding equations for these variables are:

$$\frac{di_d}{dt} = \frac{1}{L}\left(|\underline{e}| - S_d v_{cap}\right) \tag{14}$$

$$\frac{di_q}{dt} = -\frac{S_q v_{cap}}{L} \tag{15}$$

where S_d and S_q are the components of $\underline{S}$ in phase and out of phase with $\underline{e}$ respectively.

For a particular active switching mode, the vectors $\underline{i}$ and $\underline{e}$ may be expressed in terms of components parallel and perpendicular to $\underline{S}$, which are denoted i_{par} and

i_{perp}, e_{par} and e_{perp} respectively. Different values of these parallel and perpendicular components exist for each active switching mode. The resultant decoupled equations for the active switching modes as derived in Appendix B are:

$$LC\frac{d^2 i_{par}}{dt^2} = C\frac{de_{par}}{dt} - \left(\frac{2}{3}i_{par} - i_{out}\right) \tag{16}$$

$$LC\frac{d^2 v_{cap}}{dt^2} = \frac{2}{3}\left(e_{par} - v_{cap}\right) - L\frac{di_{out}}{dt} \tag{17}$$

$$\frac{di_{perp}}{dt} = \frac{e_{perp}}{L} \tag{18}$$

These equations apply irrespective of variation in the supply voltage or the output current.

3.4 System Trajectories

The system equations allow the form of the state space trajectories to be determined. In order to gain an insight into the shape of the trajectories in a single control cycle, it is revealing to consider the form of these trajectories over a longer period. It is useful to assume that the supply voltage and output current are constant based on the fact that they will vary little over a single control period as described below:

- Since the period over which the control effort is applied is small compared to one supply cycle, it is reasonable to assume that the supply voltage is constant over the period. For example, the period of a 50Hz supply cycle is 20mS. At a control frequency of 10kHz the period of a control cycle is

0.1mS, and during this time the supply voltage would have changed little.

- Due to the inductive nature of the converter load, during a control period the change in converter load current (and therefore rectifier output current) is small. Therefore it is reasonable to assume that the output current is constant over this period. It is recognised that this assumption does not hold at the end of a control cycle, when the rectifier output current can undergo a step change as the inverter switching mode changes.

While these assumptions of constant supply voltage and output current do not hold with time, they are adopted with the aim of analysing the form of the trajectories in a single control cycle. An example of the state space trajectories that result from a variable supply are presented in Appendix D.

Based on these assumptions, the equations for the supply currents and capacitor voltage given a constant supply voltage ($\underline{E}$) and constant output current (I_{out}) are presented in Appendix C. An analysis of the state space trajectories provides an insight into how the state variables change from any point in the ($\underline{i}$, v_{cap}) space on application of each switching mode. This forms the basis of the selection of the switching mode at each control interval. For the remainder of this chapter, and for the discussion of control strategies in later chapters, it is assumed that the supply voltage and output current are constant. Variations in supply voltage and output current are taken into consideration when the control strategies are implemented in simulations in Chapter 5.

If the system trajectories are plotted in the three-dimensional ($\underline{i}$, v_{cap}) space, the trajectories for the zero modes are straight lines. The equations for the changes in $\underline{i}$ and v_{cap} that result are given below. These equations have been derived from

Equations 12 and 13.

$$\frac{d\underline{i}}{dt} = \frac{\underline{E}}{L} \tag{19}$$

$$\frac{dv_{cap}}{dt} = -\frac{I_{out}}{C} \tag{20}$$

The above equations show that $\underline{i}$ changes in the direction of the supply voltage vector and v_{cap} changes at a rate proportional to I_{out}.

For the active modes, the decoupled equations show that there is a LC oscillation involving i_{par} and v_{cap} (Equations 16 and 17), and i_{perp} changes at a constant rate (Equation 18). Therefore the trajectories for the active modes are helices with the (i_{par}, v_{cap}) plane being the plane of oscillation. The natural frequency of oscillation is given by:

$$f = \frac{1}{2\pi}\sqrt{\frac{2}{3LC}} \tag{21}$$

The helices progress in the i_{perp} direction at a rate proportional to E_{perp} as given by Equation 18. The direction of drift is at 90 degrees to the switching vector applied due to the circulating currents in the two supply phases connected together at the positive or negative dc bus.

Figure 10 shows an example of the trajectories that result if active modes 011 or 100 are applied for a given fixed supply voltage and output current.

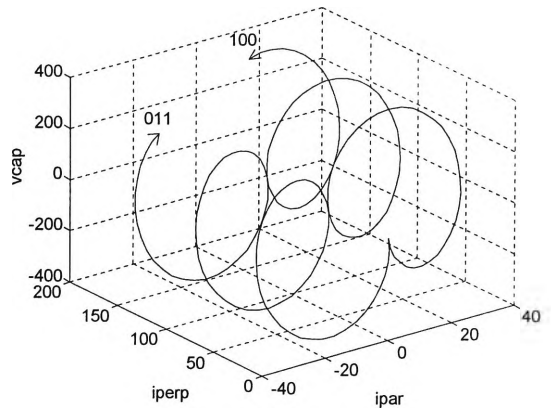

Figure 10 Trajectories for modes 011 and 100

3.4.1 Analysis of the Active Mode Trajectories

For each active mode the projection of the helical trajectory onto the ($Z_0 i_{par}$, v_{cap}) plane for that mode will give a circular trajectory, where Z_0 is a scaling factor given by:

$$Z_0 = \sqrt{\frac{2L}{3C}} \tag{22}$$

The centre of the circular trajectory is given by:

$$\left(Z_0 i_{par}, v_{cap}\right) = \left(\frac{3}{2} Z_0 I_{out}, e_{par}\right) \tag{23}$$

Examples of trajectories for a particular switching mode are shown below, where the radius of the circular trajectory depends on the initial conditions. The trajectory rotates anticlockwise when viewed as a projection in the S direction.

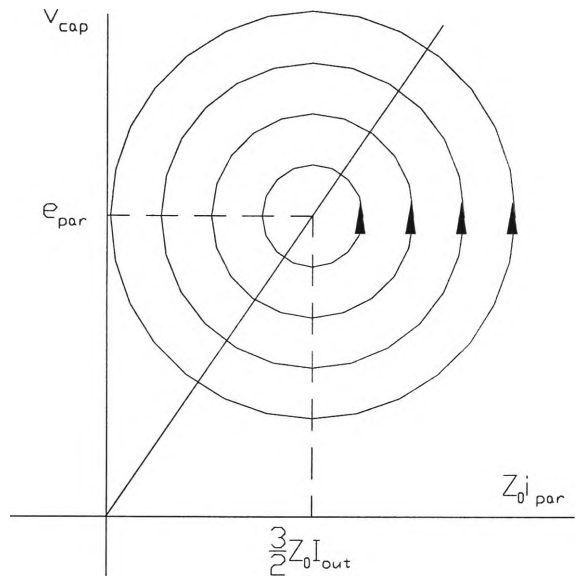

Figure 11 Active mode trajectories

Consider what the trajectories look like in terms of v_{cap} and i_d (the current in phase with the supply voltage vector $\underline{E}$). There are two cases to consider:

- $\underline{E}$ is aligned with a switching vector (that is $\underline{E}$ is at an angle of 0°, 60°, 120°, etc).
- $\underline{E}$ is not aligned with a switching vector.

If $\underline{E}$ is aligned with a particular switching vector, then i_d is equal to the current in phase with that switching vector (i_{par}). On application of the aligned switching mode, the trajectories in the ($Z_0 i_d$, v_{cap}) plane are the same as the circular trajectories presented in Figure 11. From Equations 13 and 14 the value of i_d and v_{cap} at the centre of the circles can be derived:

$$i_d = \frac{1}{S_d}\left(\frac{3}{2} I_{out} - S_q i_q\right) \tag{24}$$

$$v_{cap} = \frac{|\underline{E}|}{S_d} \tag{25}$$

Since $\underline{E}$ is aligned with the switching vector in this case, $S_d = 1$ and $S_q = 0$.

The centre of the circular trajectory when $\underline{E}$ is aligned with the switching vector can thus be simplified to:

$$\left(Z_0 i_d, v_{cap}\right) = \left(\frac{3}{2} Z_0 I_{out}, |\underline{E}|\right) \tag{26}$$

Since S_q is zero there is no change in i_q (from Equation 15) and the trajectory in three-dimensions is circular not helical.

If $\underline{E}$ is not aligned with a switching vector then a weighted combination of the two switching vectors adjacent to $\underline{E}$ will give a resultant trajectory that is very close to circular when projected on to the $(Z_0 i_d, v_{cap})$ plane. The weighting given to the adjacent switching modes is relative to the angle between each switching vector and the supply voltage vector. For example, if $\underline{E}$ is equidistant between adjacent modes then the modes would be weighted equally. Otherwise, the mode closest to $\underline{E}$ would be applied most often. Examples of the resultant trajectories are shown below.

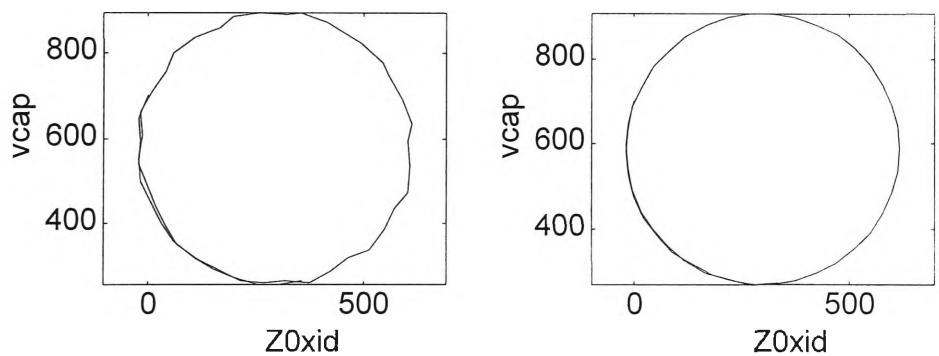

(a) Supply angle 20° (b) Supply angle 30°

Figure 12 Resultant trajectories

The 'centre' of the resultant trajectory is derived from Equations 24 and 25. In this case, S_d and S_q are replaced by S_{dR} and S_{qR} which are weighted combinations of S_d and S_q for each of the adjacent vectors. The value of i_d and v_{cap} at the centre of the trajectories is given by:

$$i_d = \frac{1}{S_{dR}}\left(\frac{3}{2}I_{out} - S_{qR}i_q\right) \tag{27}$$

$$v_{cap} = \frac{|\underline{E}|}{S_{dR}} \tag{28}$$

where

$$S_{dR} = \frac{(60-\theta)}{60}\cos\theta + \frac{\theta}{60}\cos(60-\theta) \tag{29}$$

$$S_{qR} = \frac{(60-\theta)}{60}\sin\theta + \frac{\theta}{60}\sin(60-\theta) \tag{30}$$

and

θ is the angle between $\underline{E}$ and the closest switching vector

An example of the parallel and perpendicular components of each of the switching vectors are shown graphically in Figure 13.

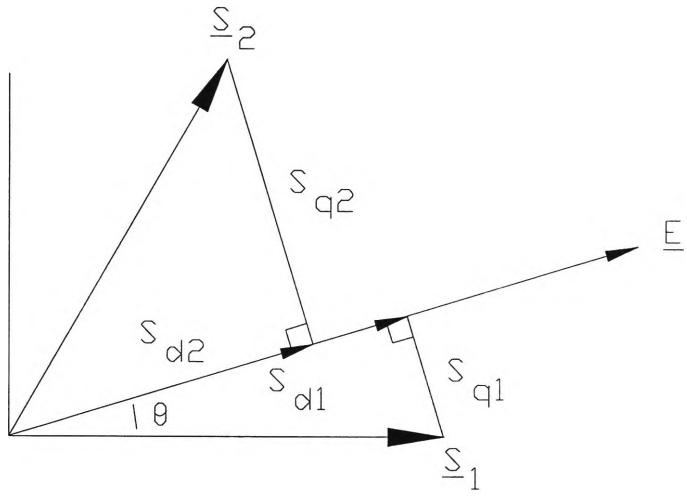

Figure 13 Components of S

Since S_q is of opposite sign for the two switching vectors adjacent to E, we find that one of the modes selected causes i_q to increase and the other causes i_q to decrease (refer to Equation 15). If the weighting with which the modes are selected is relative to the angles between them and the supply voltage vector, then the net drift of i_q can be controlled to average zero.

In summary, for any angle of the supply voltage it is appropriate to assume that it is possible to follow circular trajectories in the ($Z_0 i_d$, v_{cap}) plane with no net drift of i_q. Equation 31 below represents the centre of the circular trajectories.

$$\left(Z_0 i_d, v_{cap}\right) = \left(\frac{1}{S_{dR}} \left[\frac{3}{2} I_{out} - S_{qR} i_q \right], \frac{|\underline{E}|}{S_{dR}} \right) \tag{31}$$

This equation applies for all angles of the supply voltage. In the case where the supply voltage vector is aligned with a switching vector then $S_{dR}=1$ and $S_{qR}=0$. The equation then becomes that presented earlier (Equation 26).

3.4.2 Analysis of the Zero Mode Trajectories

In the ($Z_0 i_d$, v_{cap}) plane, the zero mode trajectories are straight lines perpendicular

to the line through the centre of the circular active mode trajectory. An example is shown below.

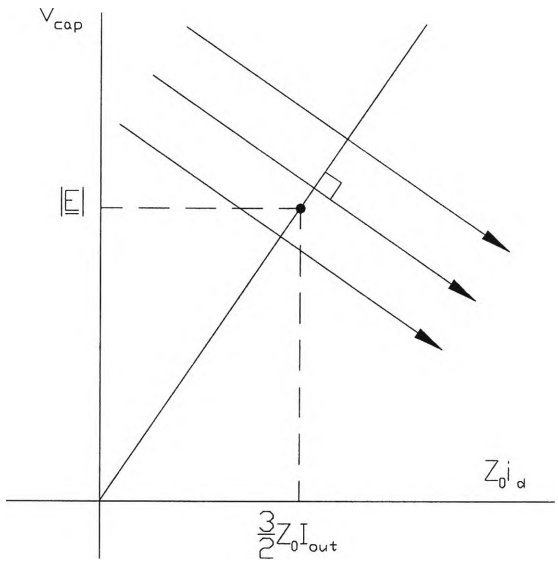

Figure 14 Zero mode trajectories

3.4.3 Characteristics of the Trajectories

Figure 15 shows an example of the trajectories for two complementary active switching modes and a zero switching mode. This figure is very similar to that presented for the dc source circuit in Figure 6. The variables v_C and i_C represent the capacitor voltage and in phase current respectively at the circle centre.

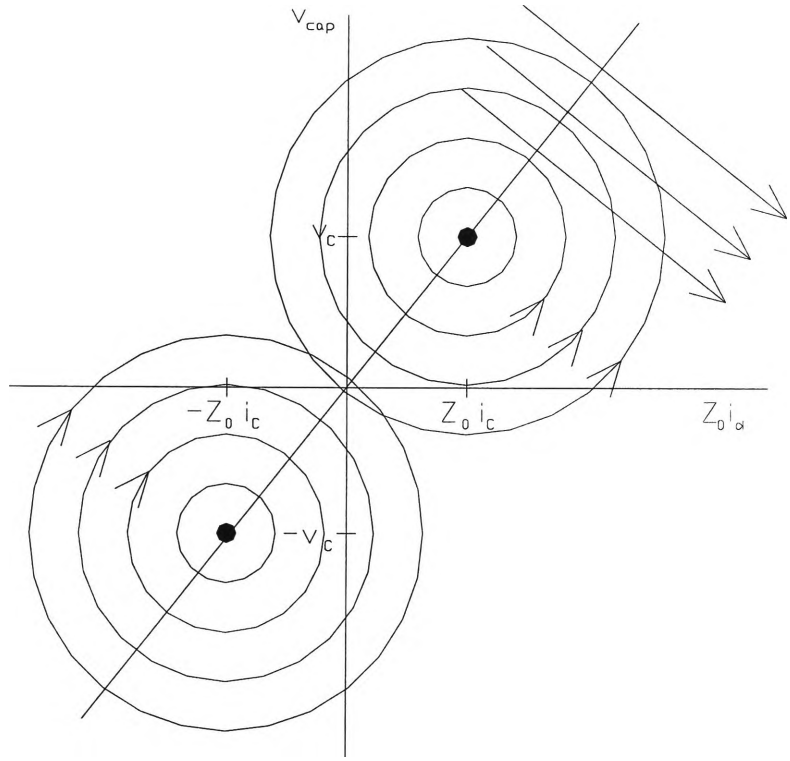

Figure 15 Example of active and zero mode trajectories

Some general observations can be made from a graphical analysis of the active mode trajectories. The direction of change of v_{cap} and i_d can be predicted by considering the position of the operating point in the ($Z_0 i_d$, v_{cap}) plane relative to the centre of the trajectory. For example, it can be seen from the two-dimensional projection in Figure 16 that the direction of the change in capacitor voltage is determined by the value of current relative to the current at the centre of the circular trajectory. For this example, if the value of $Z_0 i_d$ is to the left of the centre of the trajectory, then the capacitor voltage will decrease initially.

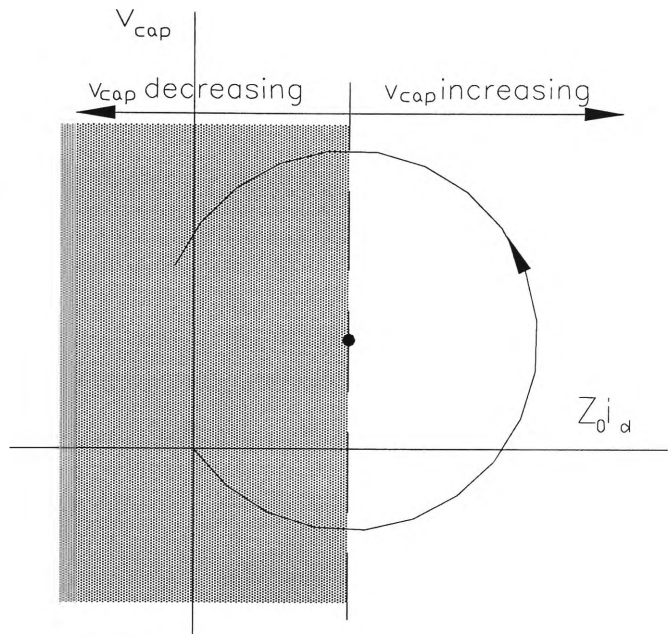

Figure 16 Effect of switching on capacitor voltage

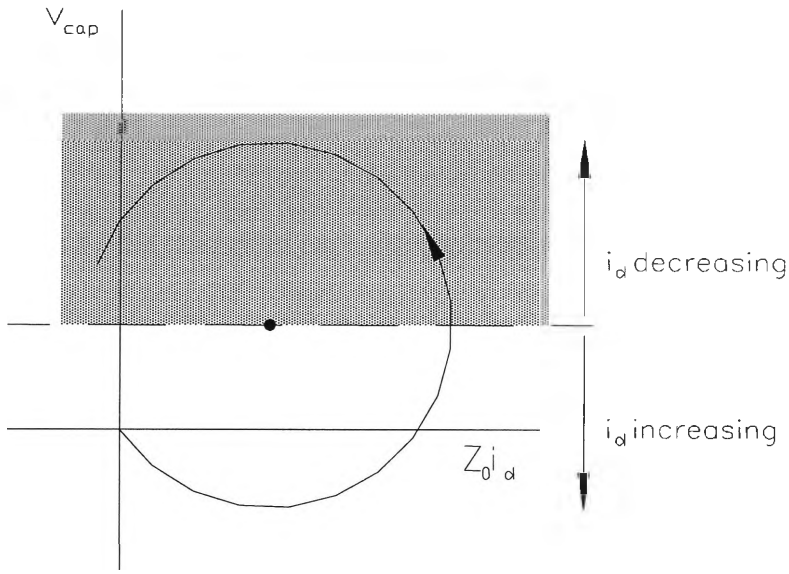

Figure 17 Effect of switching on supply current

In a similar manner, the change in the supply current is determined by the value of capacitor voltage relative to the voltage at the centre of the circular trajectory. For example, as shown in Figure 17, if v_{cap} is higher than the voltage at the centre of the trajectory then i_d will decrease initially.

At every point in the three-dimensional (i, v_{cap}) space, the effect of each switching

mode can be predicted by analysing the shape of the state space trajectories in this manner. For example, regions are formed in the current plane by plotting the longitudinal axes of the helical trajectories for the six active switching modes. These regions are shown in Figure 18.

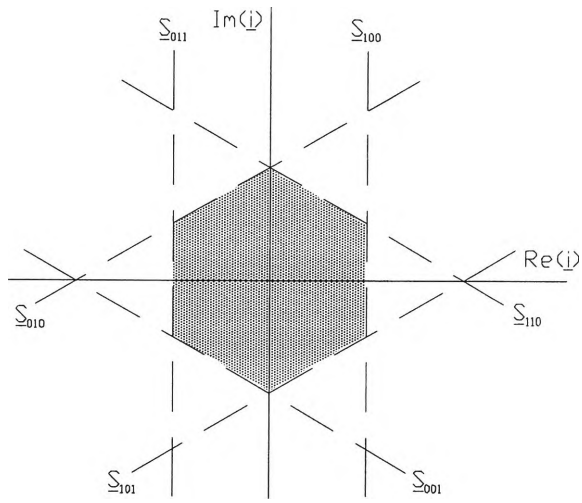

Figure 18 Regions in current plane defined by axes of helical trajectories

For every value of i the change in capacitor voltage due to the application of a switching mode is found by identifying the region that the vector lies in. When the supply current vector lies in the region that is shaded in Figure 18, the application of any switching mode will cause the capacitor voltage to decrease initially while the load current is positive.

3.5 Summary

The rectifier circuit considered is a simplified converter with a current source representing the current drawn from the dc bus by the inverter and three phase load. The state variables for the system are the supply currents (represented by the vector i) and the dc bus capacitor voltage.

There are eight possible rectifier switching modes, and equations for the state variables have been derived for these active and zero switching modes. These equations apply irrespective of variation in the supply voltage or the output current.

A study of the decoupled system equations has resulted in an understanding of the form of the system trajectories. When the response of the rectifier is fast compared to the supply frequency and the output current is assumed constant, the active mode trajectories are helical with the direction and rate of progression dependent on the position of the supply voltage vector. The zero mode trajectories are straight lines.

When the capacitor voltage and the component of the supply current in phase with the supply voltage are considered, it has been shown that it is possible to achieve circular trajectories. When the supply voltage is aligned with a switching vector, the circular trajectory results from the application of a single mode (that which is aligned). Otherwise a circular trajectory results from a weighted combination of adjacent modes.

In the following chapter the trajectories from a point are considered to develop simple rules for the choice of target values for the state variables.

CHAPTER 4
CHOICE OF RECTIFIER TARGET

4.1 Introduction

Control of the switched rectifier is based on an attempt to achieve the state variables at target values. The target values represent a target operating point in the ($\underline{i}$, v_{cap}) space.

This chapter considers the selection of the target operating point based on further analysis of the rectifier system trajectories. The aim is to select target operating points that allow stable control. A method of classification of operating points is introduced, which is referred to here as 'maintainability'. A study of the region defined by the trajectories from a point allows the maintainability to be investigated so that stable operating points in the ($\underline{i}$, v_{cap}) space can be identified.

An analysis of maintainability is also used to select the set of trajectories (and therefore switching modes) that can be used to reach the target point and to maintain that position.

This chapter first considers the rectifier control aims as they form the basis of the target point selection. The concept of maintainability is then described and general examples are presented. Maintainability as it applies to the rectifier is described and used to identify target operating points and rectifier switching modes to achieve stable control.

4.2 Control Aims

The choice of target values for the rectifier state variables must take into account the system requirements and also the aim of achieving unity power factor on the supply side. This forms the basis of the choice of target values for v_{cap}, i_d and i_q as described below.

- The target value of capacitor voltage is given by the system requirements. For example, the required dc bus voltage of the circuit might be specified as 700V.
- Since unity power factor is required, the target value of i_q is zero. This means that the supply voltage vector can be used as a template for the target supply current vector.

This chapter investigates the selection of target values for i_d which define the magnitude of the target supply current vector.

4.3 Definition of Maintainability

The operating points in state space can be described using a classification that is referred to here as 'maintainability'. Maintainability classifies operating points based on an analysis of the trajectories from each point, into two types:

- 'Maintainable' operating points;
- 'Unmaintainable' operating points.

Maintainable operating points are those for which it is possible to switch between the trajectories from the operating point in such a way that will allow the state

variables to return to their original values. An example in two-dimensions of the trajectories from a maintainable point is given in Figure 19.

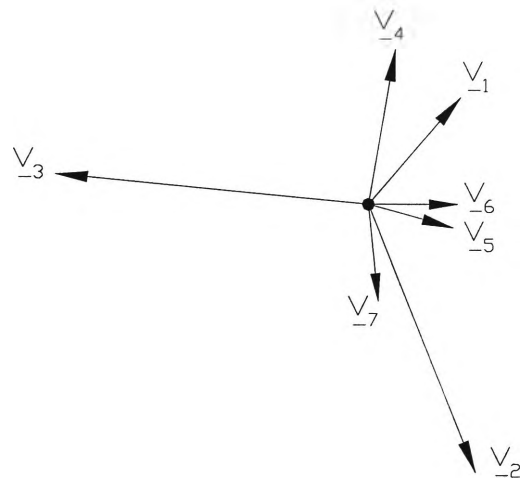

Figure 19 Trajectories from maintainable operating point

Vectors $\underline{V}_1$ to $\underline{V}_7$ represent the changes in the state variables that result on application of each of seven switching modes. It is possible to switch between these switching modes and return to the original operating point as shown in Figure 20(a).

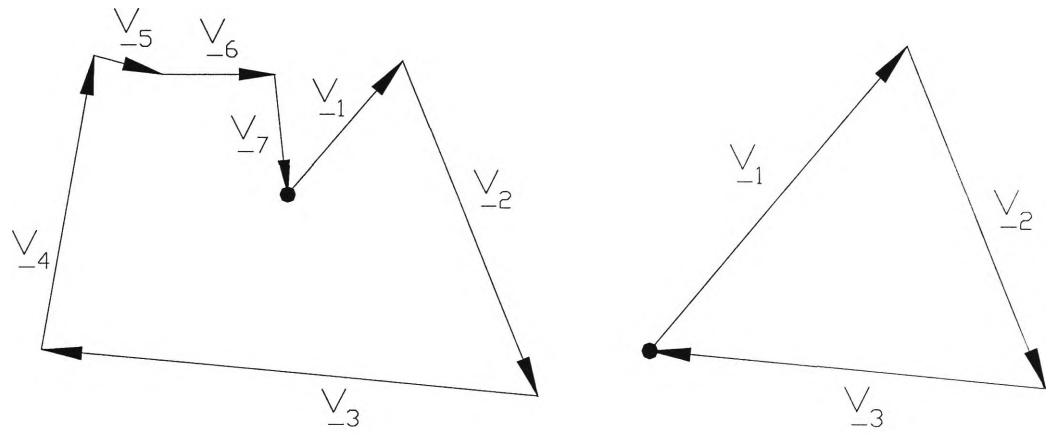

(a) (b)

Figure 20 Trajectories from maintainable operating point

It is possible for the state variables to return to their original values by applying a

subset of the available switching modes as illustrated in Figure 20(b). How closely the state variables remain to a maintainable operating point depends on the amount of time for which each switching mode is applied. This depends on the switching frequency and whether or not it is variable.

If an operating point is unmaintainable then it is not possible to switch between the trajectories from the point and have the state variables return to their original values. An example is shown in Figure 21.

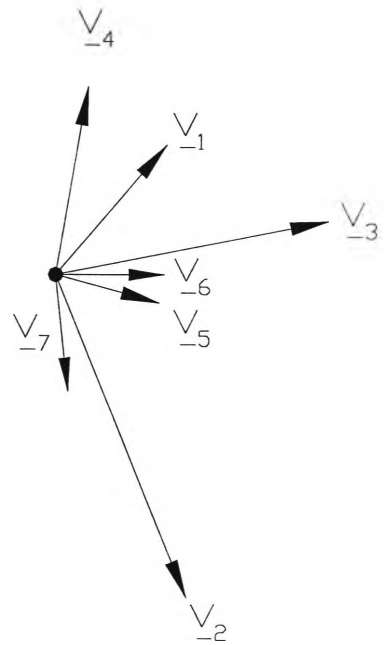

Figure 21 Trajectories from unmaintainable operating point

It is not possible to return to the original operating point by switching between the available switching modes for the example given in Figure 21.

Maintainability can be checked graphically. As shown in Figure 22, the trajectories from an operating point define a region. If this region encloses the operating point then it will be possible to move along the available trajectories in such a way that allows the state variables to return to their original values. The

original operating point is thus classified as maintainable. An example is presented in Figure 22(a). If the region defined by the trajectories from a point does not enclose the point then the operating point is classified as unmaintainable. An example is presented in Figure 22(b).

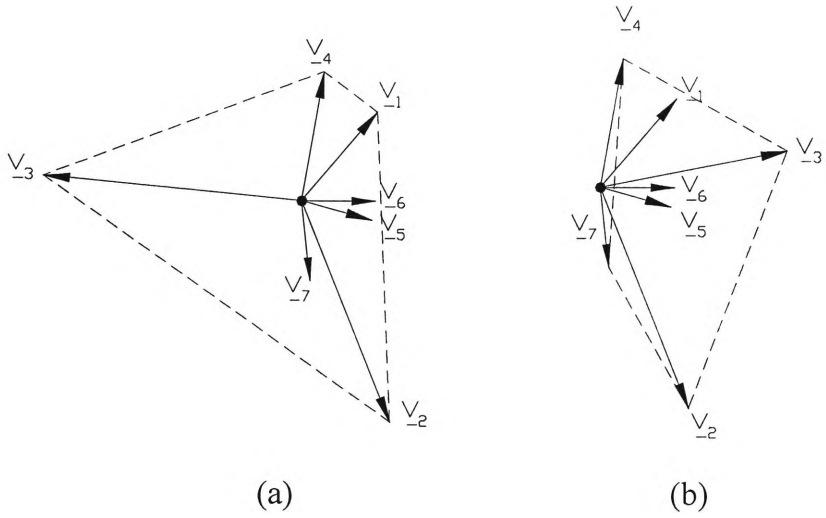

Figure 22 Region defined by trajectories (a) Maintainable (b) Unmaintainable

It should be noted that regions defined by subsets of the trajectories from the point also enclose a maintainable operating point. In Figure 22(a) for example, regions defined by trajectories $\underline{V}_1$, $\underline{V}_2$ and $\underline{V}_3$, or $\underline{V}_3$, $\underline{V}_6$ and $\underline{V}_7$, amongst others, enclose the operating point. Therefore for this two-dimensional example, a maintainable operating point can be maintained by applying the three switching modes for which the trajectories define a triangular region enclosing the operating point.

These ideas can also be extended to three-dimensions. In this case the switching mode trajectories from an operating point define a region in three-dimensional space, and the operating point is maintainable if the point is enclosed in that region. As an example, consider a case for which there are seven available switching modes. Checking for maintainability corresponds to solving Equation

32 and finding the coefficients λ_1 to λ_7 where $\lambda_i \geq 0$.

$$\lambda_1 \underline{V}_1 + \lambda_2 \underline{V}_2 + \lambda_3 \underline{V}_3 + \lambda_4 \underline{V}_4 + \lambda_5 \underline{V}_5 + \lambda_6 \underline{V}_6 + \lambda_7 \underline{V}_7 = 0 \tag{32}$$

If a solution exists for which at least two of the coefficients are non-zero then the operating point is maintainable, but there will be an infinite number of solutions. The results can be normalised by setting one of the coefficients to unity. For an operating point that is maintainable it is again possible to use a subset of the available trajectories to maintain the point. For this reason some of the coefficients in Equation 32 may be equal to zero.

These ideas can be applied to the rectifier system.

4.4 Application to Rectifier

The concept of maintainability is applicable to the control of the three phase rectifier because it shows that, for some (unmaintainable) operating points, it is not possible to achieve stable control. The aim then is to find target points that are maintainable. To determine which points are maintainable the rectifier trajectories need to be investigated further.

4.4.1 Rectifier Trajectories

At a given operating point in state space ($\underline{i}$, v_{cap}) there are seven possible trajectories corresponding to the available switching modes. The helical active mode trajectories can be approximated in a single control cycle by the straight line tangents at the operating point. The change in current and capacitor voltage for these tangents are defined by Equations 33 and 34.

$$\frac{dv_{cap}}{dt} = \frac{1}{C}\left(\frac{2}{3}\underline{S}\cdot\underline{i} - I_{out}\right) = \frac{1}{C}\left(\frac{2}{3}i_{par} - I_{out}\right) \tag{33}$$

$$\frac{d\underline{i}}{dt} = \frac{1}{L}\left(\underline{E} - \underline{S}v_{cap}\right) \tag{34}$$

For a single control period the region defined by the six tangents and the zero mode trajectory is a hexagon in the current plane as illustrated below. The operating point has been represented as the origin.

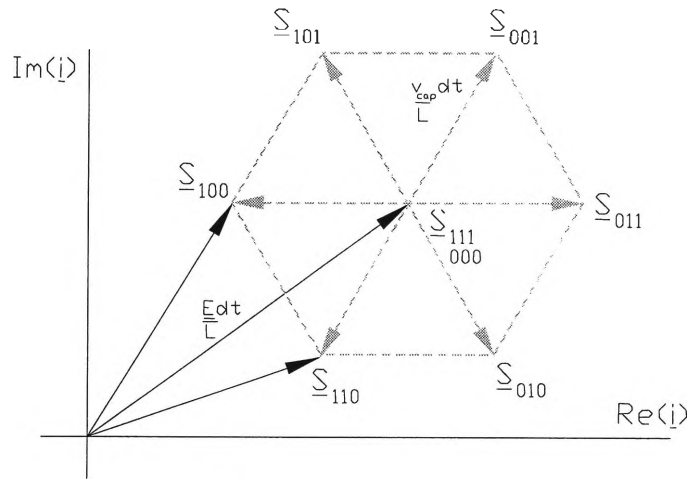

Figure 23 Possible di vectors

The centre of the hexagon is defined by the zero mode trajectory and it is offset from the operating point by:

$$\text{Centre Offset} = \underline{E}\frac{dt}{L} \tag{35}$$

The size of the hexagon is defined by the active mode trajectories and the distance from the centre of the hexagon to each vertex is given by:

$$\text{Size} = v_{cap}\frac{dt}{L} \tag{36}$$

The seven points that define the hexagon (and centre) all lie in a plane in the three-dimensional ($\underline{i}$, v_{cap}) space. An example in three-dimensions is presented in Figure 24.

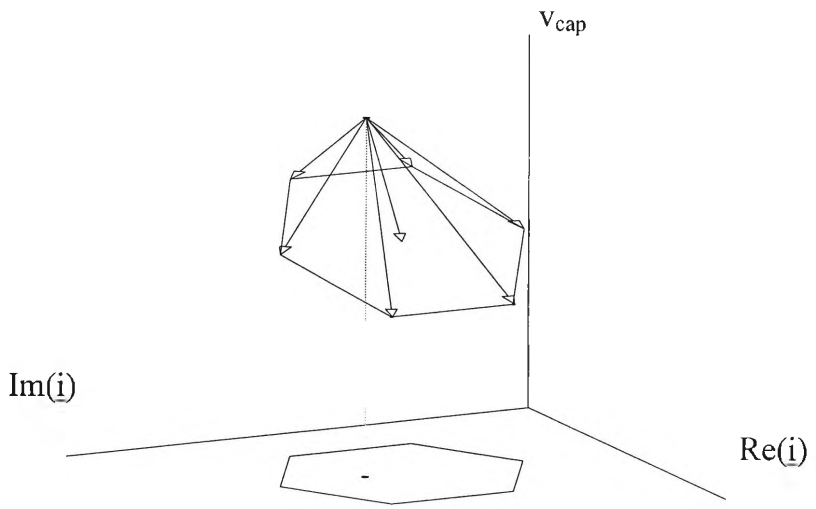

Figure 24 Hexagon defined by trajectories

Equation 33 defines the position of each of the seven points along the v_{cap} axis (relative to the operating point). For each switching mode this distance is proportional to i_{par}, which is the component of the current vector parallel to the switching vector. An example is given in Figure 25. The highest vertex of the hexagon will be that which represents the switching vector that is closest to $\underline{i}$. The orientation of the hexagon in three-dimensional space changes as the current vector moves.

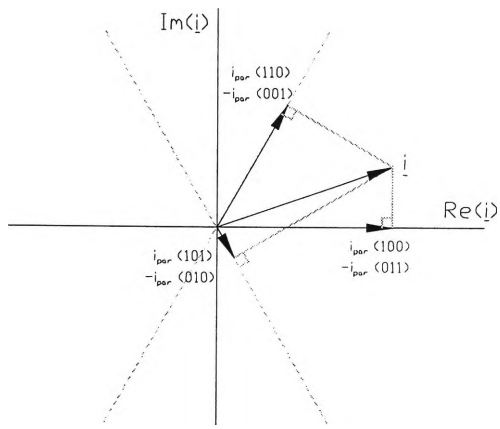

Figure 25 Component of current vector parallel to switching vectors

The plane defined by the trajectories is characterised by the following equation:

$$L\,\mathrm{Re}(\underline{i})\frac{d\,\mathrm{Re}(\underline{i})}{dt}+L\,\mathrm{Im}(\underline{i})\frac{d\,\mathrm{Im}(\underline{i})}{dt}+\frac{3}{2}Cv_{cap}\frac{dv_{cap}}{dt}-\underline{i}\cdot\underline{E}+\frac{3}{2}v_{cap}I_{out}=0 \qquad (37)$$

where

- Re(i) is the real component of the supply current vector
- Im(i) is the imaginary component of the supply current vector
- i·E is the dot product of the vectors i and E.

4.4.2 Rectifier Maintainability Criteria

As outlined above, the region defined by the seven trajectories from an operating point is a hexagon in a plane. A rectifier operating point is maintainable if the defined region encloses the point, which is the case if both of the following criteria are satisfied:

1. The point is on the plane;
2. The point is inside the hexagon as a projection on the current plane.

Figure 24 is an example of an operating point that meets the second of these criteria but not the first.

These criteria define limits on the state variables and these are discussed further below. The criteria are specified in terms of equations that apply to the state variables. The criteria are also related to operating points in the ($\underline{i}$, v_{cap}) space and described in terms of the state space trajectories in the two-dimensional ($Z_0 i_d$, v_{cap}) plane.

4.4.2.1 Criterion 1: Operating point on the plane

The first criterion is met when the perpendicular distance from the operating point to the plane is zero. The distance is given by the following equation:

$$\text{Distance from operating point to plane} = \left| \frac{2}{\sqrt{3}} \frac{\left(\underline{E} \cdot \underline{i} - \frac{3}{2} v_{cap} I_{out}\right)}{\sqrt{\frac{4}{3} L^2 \left(\text{Re}(\underline{i})^2 + \text{Im}(\underline{i})^2\right) + 3C^2 v_{cap}^2}} \right| \quad (38)$$

The distance from the operating point to the plane is zero when the numerator of Equation 38 is zero, that is when:

$$\left(\underline{E} \cdot \underline{i} - \frac{3}{2} v_{cap} I_{out}\right) = 0 \quad (39)$$

Therefore the criterion that the operating point be on the plane defined by the trajectories may be written in terms of the following equation for v_{cap}:

$$v_{cap} = \frac{2}{3} \frac{\underline{E} \cdot \underline{i}}{I_{out}} \quad (40)$$

As described in Chapter 4.2, in order to achieve unity power factor the target value

of i_q is zero. Therefore the plane in the ($\underline{i}$, v_{cap}) space that satisfies the first criterion can be reduced to a line. The equation of this line has been derived by rearranging Equation 40 and setting i_q equal to zero:

$$i_d = \frac{3}{2}\frac{v_{cap} I_{out}}{|\underline{E}|} \tag{41}$$

The same equation describes the line through the centre of the circular trajectories in the ($Z_0 i_d$, v_{cap}) plane as presented in Chapter 3.4.1. Therefore, the first maintainability criterion is satisfied by operating points on the line through the centre of the circular trajectories in the v_{cap} versus $Z_0 i_d$ plane.

4.4.2.2 Criterion 2: Operating point inside hexagon in current plane

The hexagon in the current plane is shown in Figure 23. The offset of the centre from the operating point is proportional to $\underline{E}$, and the size of the hexagon is proportional to v_{cap} (see Equations 35 and 36). Therefore, whether the operating point is enclosed in the hexagon depends on v_{cap} compared to $|\underline{E}|$.

The criterion that the operating point be inside the hexagon (as a projection on the current plane) may be written in terms of a limit on v_{cap} as given by Equation 42. In this equation θ is the angle between the supply voltage vector and the closest switching vector.

$$v_{cap} > \frac{2}{\sqrt{3}}|\underline{E}|\cos(30° - \theta) \tag{42}$$

Equation 42 imposes a minimum limit on v_{cap} and, in the ($Z_0 i_d$, v_{cap}) plane, this limit represents the capacitor voltage at the centre of the circular active mode

trajectories (or resultant trajectory when two adjacent modes are being implemented). For example, when $\underline{E}$ is aligned with a switching vector the criterion becomes:

$$v_{cap} > |\underline{E}| \tag{43}$$

This is the value of v_{cap} at the centre of the circular trajectory.

Therefore operating points for which v_{cap} exceeds the value at the centre of the circular trajectory satisfy the second maintainability criterion.

When using this limit in a practical control system it is useful to consider the limit on v_{cap} that will be met by maintainable operating points regardless of the position of $\underline{E}$. This is the limit defined graphically by an inscribed circle in the hexagon as illustrated in Figure 26.

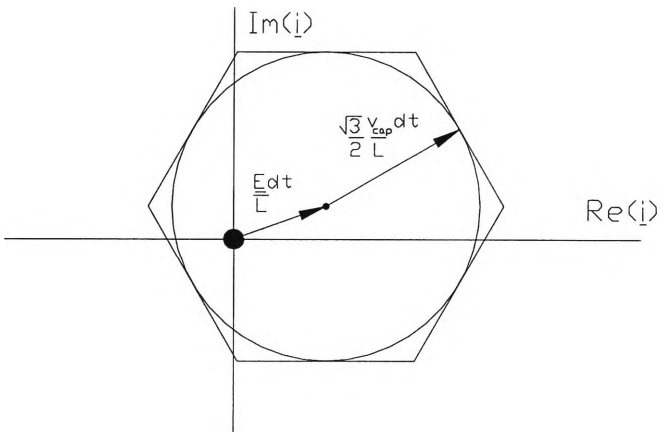

Figure 26 Maintainability criterion

This limit on v_{cap} is defined by the case whereby $\underline{E}$ is equidistant from adjacent switching vectors, as described by Equation 44. This shows that the capacitor voltage limit in this case is equal to the peak line-to-line supply voltage.

$$v_{cap} > \frac{2}{\sqrt{3}}|\underline{E}|$$
$$v_{cap} > \sqrt{6}E_{L-N}rms \quad (44)$$

In the example of the operating point and trajectories illustrated in Figure 23, the operating point lies outside the hexagon and therefore v_{cap} is below the specified limit.

4.4.2.3 Maintainability Criteria Summary

The concept of maintainability has been introduced in order to select target operating points in the ($\underline{i}$, v_{cap}) space that allow stable control; specifically the value of i_d, which defines the magnitude of the target supply current vector. From the criteria for maintainability it has been shown that, if i_q is required to be zero, the maintainable operating points are those that are:

- on the line through the centre of the circular active mode trajectories in the ($Z_0 i_d$, v_{cap}) plane, and
- above the centre of the trajectories.

Therefore when choosing a target point given the required value of v_{cap}, the required target value of i_d is given by Equation 41 or graphically from the line of maintainable operating points shown below.

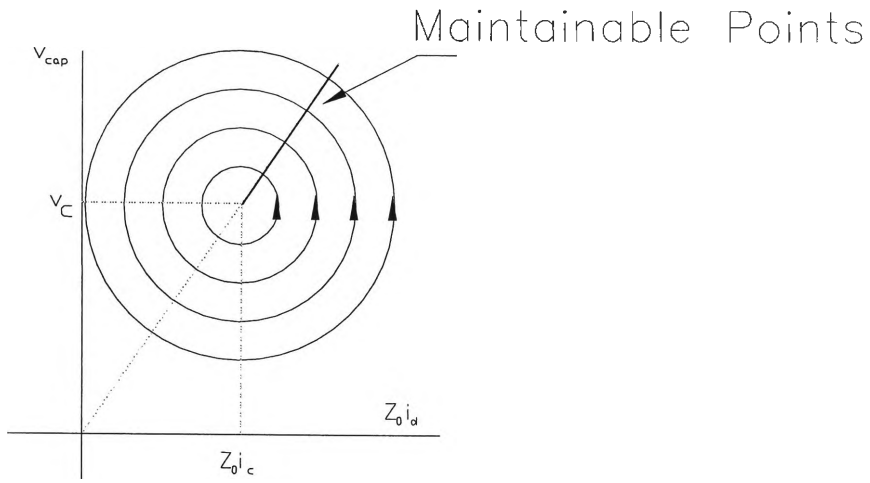

Figure 27 Line of maintainable points

These results are closely related to those discussed for the dc source circuit in Chapter 2. Using the same logic as Figure 7, for the three phase rectifier stable control of maintainable targets is possible due to the relative directions of the straight line and circular trajectories.

There is a relationship between points that do not meet the maintainability criteria and the rectifier trajectories in state space as summarised below:

In the 2-D ($Z_0 i_d$, v_{cap}) plane:		**In the 3-D ($\underline{i}$, v_{cap}) space:**
• The operating point is on the line through the centre of the circular trajectories, but is below the centre of the trajectories.	⇒	The operating point is on the plane defined by the trajectories but it is outside the region (hexagon) defined by them.
• The operating point is above the centre of the circular trajectories but not on the line through the centre of the trajectories.	⇒	The operating point is inside the region (hexagon) defined by the trajectories but not on the plane defined by them.

4.4.3 Relationship to Physical

An insight into why points on the line through the centre of the active mode trajectories are maintainable is gained by considering the power into and out of the dc bus capacitor. The equations for the power flows are given by:

$$\text{Power In} = \frac{2}{3}\underline{E}\cdot\underline{i} \tag{45}$$

$$\text{Power Out} = v_{cap} I_{out} \tag{46}$$

When there is a balance of power into and out of the capacitor:

$$\begin{aligned} v_{cap} &= \frac{2}{3}\frac{\underline{E}\cdot\underline{i}}{I_{out}} \\ &= \frac{2}{3}\frac{|\underline{E}| i_d}{I_{out}} \quad \text{when } i_q \text{ is zero.} \end{aligned} \tag{47}$$

This equation for power balance is the same as that defining the first criterion for

maintainability, and it defines the operating points on the line through the centre of the active mode trajectories. This line is referred to here as a 'line of power balance'. Therefore, for an operating point to be maintainable a balance of power must occur.

The second criterion for maintainability, that an operating point be above the centre of the active mode trajectories in order to be maintainable, relates to the level of capacitor voltage required for control as discussed in Section 4.4.4.

4.4.4 Comparison to Published Work

The limit on the value of the capacitor voltage that is specified by the maintainability criteria can be compared to limits published elsewhere.

The limit on v_{cap} is described by Equation 44, which is reproduced below.

$$v_{cap} > \frac{2}{\sqrt{3}}|\underline{E}|$$
$$v_{cap} > \sqrt{6}E_{L-N}rms \quad (48)$$

This limit is equal to the peak line-to-line voltage. This corresponds to work published by Wernekinck et al [12] which states that the dc output voltage must be larger than the peak line-to-line voltage to control the ac line current.

This limit was also described by Ooi et al [2], who referred to it as the 'current distortion limit'. This limit refers to the minimum level of capacitor voltage required to force the supply currents through the line inductances so as to follow the references.

Ooi also describes the loss of control limit [2] which refers to the minimum level

of capacitor voltage required to ensure that the free-wheeling diodes in the rectifier bridge are reverse biased. This limit is not considered here as, with supply currents flowing, the switching operation will ensure that the diodes will be reverse biased by the dc bus voltage.

4.4.5 Selection of Switching Modes

As discussed in Chapter 4.3, the trajectories that define a region enclosing a maintainable operating point are those that can be utilised to maintain the original operating conditions. Therefore, the position of a maintainable rectifier operating point in the hexagon defined by the trajectories will indicate the switching modes that can be utilised to achieve stable control. If $\underline{E}$ is aligned with a switching vector and the operating point is maintainable then (in the current plane) the operating point will be inside the hexagon and can be maintained using an active switching mode and a zero switching mode.

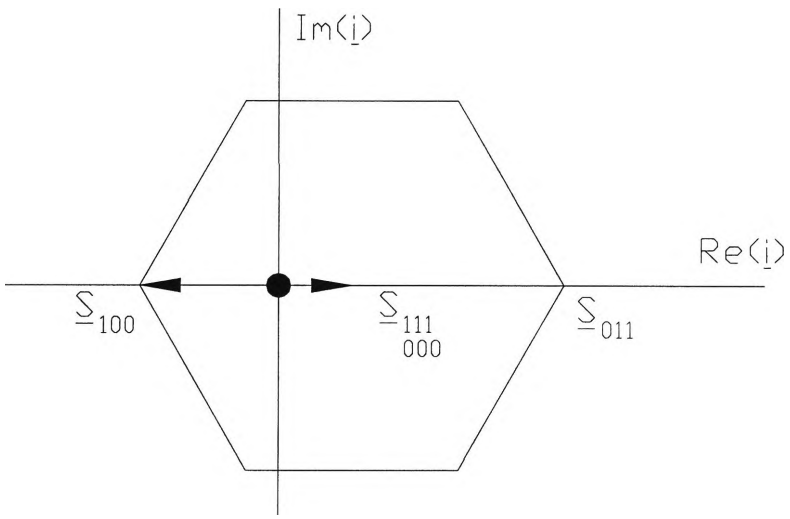

Figure 28 Selection of switching modes ($\underline{E}$ aligned with $\underline{S}$)

If $\underline{E}$ is not aligned with a switching vector and the operating point is maintainable then the operating point will be inside the hexagon and can be maintained using

two active switching modes and a zero switching mode. The switching modes with vectors adjacent to $\underline{E}$ are the modes that define the triangle that encloses the operating point.

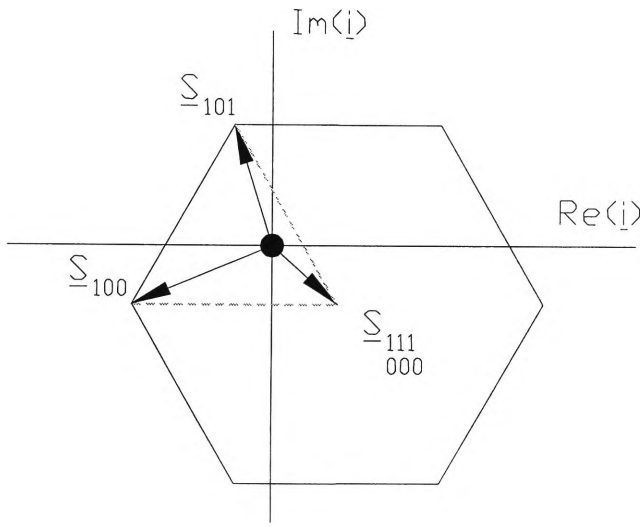

Figure 29 Selection of switching modes ($\underline{E}$ not aligned with $\underline{S}$)

If the operating point is not maintainable, the switching modes adjacent to $\underline{E}$ can be utilised to reach a maintainable operating point.

4.5 Summary

The rectifier target represents target values for the state variables; that is for the capacitor voltage and supply current. The target selected is required to meet the control aims of sinusoidal supply currents at unity power factor and also to allow stable control of the state variables. The target value of capacitor voltage is specified by the requirements of the system and is a constant. The target value of the out of phase current (i_q) is zero in order to achieve unity power factor. An assessment of the rectifier maintainability has been conducted to allow selection of target values for in phase current (i_d).

The operating points in the ($\underline{i}$, v_{cap}) space have been classified as maintainable or unmaintainable. The selection of a target operating point that is maintainable will allow stable control of the rectifier state variables. If the target selected is unmaintainable then it will not be possible to achieve stable control at that point.

Rectifier maintainability has been assessed based on the position of the operating points relative to the regions defined by the rectifier trajectories. The trajectories define a hexagon in a plane in the ($\underline{i}$, v_{cap}) space. When the criteria for maintainability are related to points in the ($Z_0 i_d$, v_{cap}) plane, it is shown that maintainable points are those on the line through the centre of the circular active mode trajectories and above the circle centre. The target value of i_d is thus selected to be a point on the line of maintainable points.

It is possible to achieve stable control at a maintainable operating point by switching between the two switching modes adjacent to the supply voltage vector (or a single mode if it is aligned with the supply voltage vector) and the zero switching mode. In the following chapter control rules are discussed which are used to select which of these modes to apply at each control instant.

CHAPTER 5

CONTROL OF THE HIGH-FREQUENCY RECTIFIER

5.1 Introduction

The control techniques reviewed in Chapter 1 tend to overlook the overall form of the switching trajectories and use target trajectories chosen without a close examination of the full capability of the system. In this chapter control strategies are presented that are based on the detailed examination presented in previous chapters.

Control of the rectifier involves measuring the actual supply currents and capacitor voltage, and comparing them to target values. A switching mode is then selected based on a set of rules to force the variables to reach the target and to follow the target as it moves. Important consideration must be given to the choice of target and the control rules used to reach and stay at the target.

The maintainability criteria can be used to choose a target that allows unity power factor and stable control to be achieved as discussed in Chapter 4. Stable control of the state variables at a maintainable target point is possible by utilising the shape of the system trajectories. In this chapter, four control strategies are presented which take advantage of the shape of the circular and straight line trajectories

The control rules that have been developed are described in this chapter and they are used for the selection of the switching mode to be applied in each control cycle. It was shown for the dc source circuit in Chapter 2 that stable control at certain operating points is possible using the shape of the active and zero mode trajectories. Similar trajectories are possible for the three-phase rectifier as shown in Chapter 3.4.3. This chapter thus considers control strategies which utilise the shape of the system trajectories.

Control of the rectifier under steady-state conditions (constant output current) is analysed, and the previous assumption that the rectifier output current is constant is removed to allow transient conditions (variable output current) to also be considered. Simulations allow the control strategies presented to be assessed on the basis of:

- variation of the state variables from the target values, particularly capacitor voltage;
- speed of response to changes in the target values under transient conditions.

The simulations presented are all conducted with a variable (rotating) supply voltage; that is, the assumption of constant supply voltage is removed.

The choice of rectifier target was discussed in Chapter 4 and a review is presented in this chapter which considers how the target is affected by variations in supply voltage and output current. The chapter then covers aspects of the rectifier control that are common to all of the strategies considered. An overview of each of the control strategies includes a description of the control rules applied, a selection of simulation results and an analysis of the control performance. Additional

simulations for each strategy are presented in Appendix E. The chapter concludes with a summary and comparison of performance.

5.2 Choice of Target

As discussed in Chapter 4, for a practical system the target values of the capacitor voltage and supply current will be given by:

- The capacitor voltage is given by the system. For example, the required dc bus voltage of the circuit might be specified as 700V.
- Since unity power factor is required, the component of the supply current out of phase with the supply voltage (i_q) is equal to zero.
- The component of the supply current in phase with the supply voltage (i_d) will be given by the maintainability criteria.

In previous chapters the supply voltage and output current have been assumed constant. In this chapter these assumptions are no longer applied. Under conditions of variable supply voltage and output current the capacitor voltage and out of phase current targets will remain constant, though the effect on the in phase current target must be considered.

The target value of i_d is given by Equation 41 which is reproduced below:

$$i_d = \frac{3}{2}\frac{v_{cap} i_{out}}{|\underline{e}|} \tag{49}$$

The above equation shows that the target value of i_d is unchanged by variations in the supply voltage, as the magnitude of the supply voltage vector ($|\underline{e}|$) is a constant.

For a given target v_{cap}, the target value of i_d changes with variations in the output current. The target value of i_d is given graphically by the line through the centre of the active mode trajectories (as discussed in Chapter 4.4.2.3) at a point corresponding to the given target v_{cap}. As the output current changes, the target value of i_d changes also, as shown in the example in Figure 30.

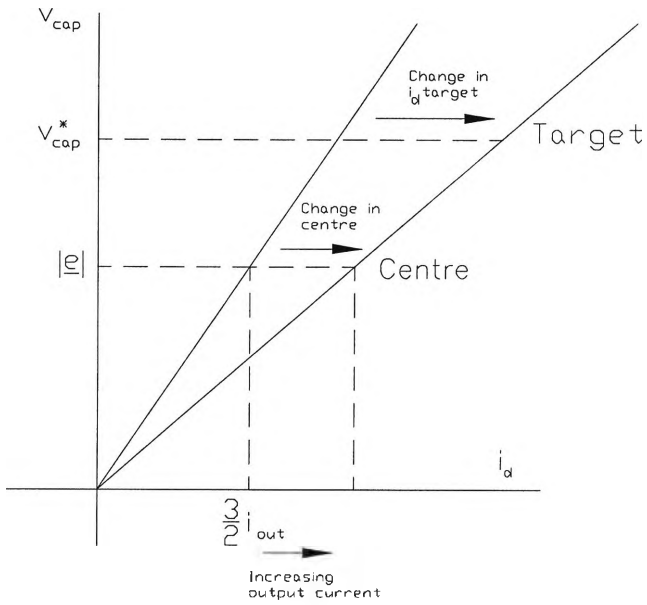

Figure 30 Change in target with variable output current

5.3 Overview of Control

A number of different control strategies have been developed and these are discussed in Chapters 5.4 to 5.7. All of these strategies are based around the concept of using the shape of the circular and straight line trajectories to achieve stable control. The trajectories also provide the means for defining control rules in the form of switching boundaries that are straight-forward to apply and easy to represent graphically. Since the aim is to control i_q equal to zero, the focus of the following chapters is on the ($Z_0 i_d$, v_{cap}) plane. In all of the discussions the active mode trajectories are presented as circles, though they may represent a

combination of trajectories from two adjacent active modes.

There are two aspects to the rectifier control implementation:

1. When the operating point is at the target and there is no change in i_{out} it is necessary to maintain the values of the state variables as closely as possible to the target values. This control phase is referred to here as operating under steady-state conditions, although there will be some variation in the state variables with the switching operation.

2. When a change in output current occurs it is necessary to quickly reach a new maintainable target point while minimising capacitor voltage variation. This control phase is referred to here as operating under transient conditions.

In all further discussions for the rectifier circuit, transient conditions refer to changes in output current. When the supply voltage is variable, the target supply current vector rotates with the supply voltage vector. Therefore even under steady state conditions the supply current vector target in the stationary reference frame changes slowly with time.

The discussion of the selection of switching modes in Chapter 4.4.5 showed that under steady state conditions it is possible to remain close to a maintainable operating point using a combination of active and zero switching modes. The modes selected are those for which the trajectories define a region enclosing the operating point. When the supply voltage is aligned with an active mode switching vector the operating point is maintained using the active mode and a zero mode. When the supply voltage is not aligned with a switching vector the operating point is maintained using the zero mode and the active modes adjacent

to the supply voltage vector. The rectifier control strategies presented provide sets of rules that can be applied to determine whether to apply an active switching mode or a zero switching mode at each switching instant.

When it is determined that an active mode should be applied, the actual mode utilised will be the one adjacent to $\underline{e}$ which drives i_q towards its target value of zero. This selection of active mode is summarised graphically in Figure 31. Once the segment in which $\underline{e}$ lies is identified, the control strategies select the required active mode based on the sign of i_q. The resultant trajectory will be a weighted combination of trajectories with zero nett drift of i_q (under steady state conditions).

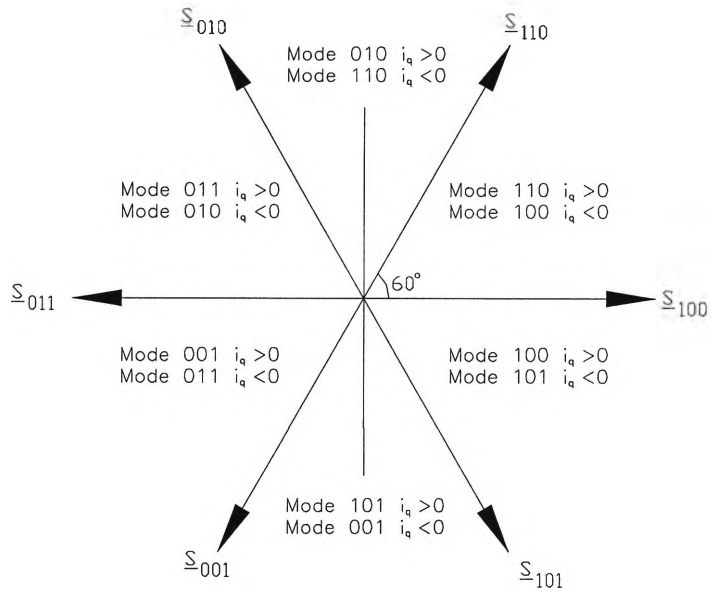

Figure 31 Active switching mode selection

Simulation results for each control strategy are presented in this chapter for the following scenarios:

- Steady state operation with full rectifier output current.
- Transient operation for a step change in output current from zero to full

current.

Though the rectifier output current is intended to represent the current drawn in the converter by an inverter bridge and load, it is unlikely that the actual current would be a constant at full current or a step from no load to full load. These scenarios have been considered because they allow the rectifier performance to be assessed under relatively extreme operating conditions.

The characteristics of the system simulated are discussed in full in Appendix E. In summary, the system has a switching frequency of 10kHz, a dc bus voltage of 700V and a very small dc bus capacitor (20μF). The simulations have been based on the rectifier equations presented in Appendix C to give the change in capacitor voltage and supply currents over each control cycle. While the supply voltage vector is advanced at the start of each control cycle, the use of these equations assumes that the supply voltage is constant during each cycle. While this assumption is not strictly true, as discussed in Chapter 3.4 the supply voltage changes little (1.8°) in a control cycle and the use of these equations simplifies the simulation somewhat.

5.4 Method 1: Optimal Control Strategy

The optimal control strategy is represented by the switching boundaries illustrated in Figure 32. Variables labelled with * represent target values.

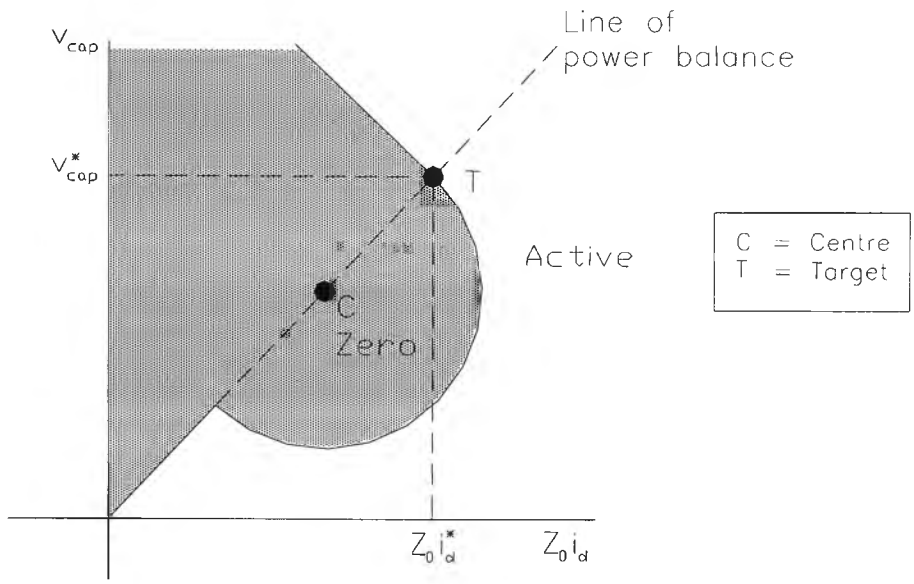

Figure 32 Optimal control switching boundaries

As indicated by the key in Figure 32, the point labelled 'T' represents the target values of v_{cap} and $Z_0 i_d$. The point labelled 'C' represents the centre of the active mode trajectories.

The target is a point on the line of power balance, above the centre of the active mode trajectories. The switching boundaries are given by the active and zero mode trajectories that pass through the target point. Below the line of power balance the active mode trajectory forms the boundary; if the operating point is inside the semi-circle the zero mode is applied, if it is outside an active mode is applied. Above the line of power balance the zero mode trajectory forms the boundary; if the operating point is below the boundary the zero mode is applied, if it is above an active mode is applied. As a result of these rules, the operating point will generally either follow a circular path until the target can be reached on a straight line trajectory, or follow a straight line trajectory until the target can be reached on a circular path.

Assuming that the state variables are initially at the target values, under steady

state conditions it is desirable that the net change of power during operation is zero and so it is necessary to spend similar amounts of time on either side of the line of power balance.

Figure 33 shows how the shape of the trajectories allows stable control during steady-state operation. The amount of deviation of the state variables from the target depends on the switching frequency and the initial conditions.

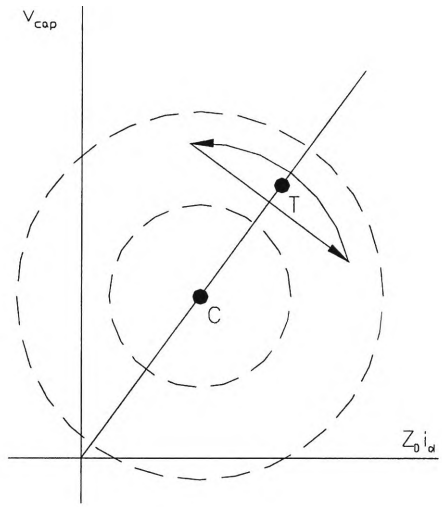

Figure 33 Optimal control steady-state operation

Transient conditions occur when the output current changes and the aim is to move to a new maintainable target. It is generally necessary to either put energy into or take energy out of the system and, as a result, the control strategy will result in the operating point being mainly on one side of the line of power balance or the other until the target is reached.

Under transient conditions the control strategy also uses the switching boundaries shown in Figure 32. Examples of the resultant trajectories are shown in Figure 34.

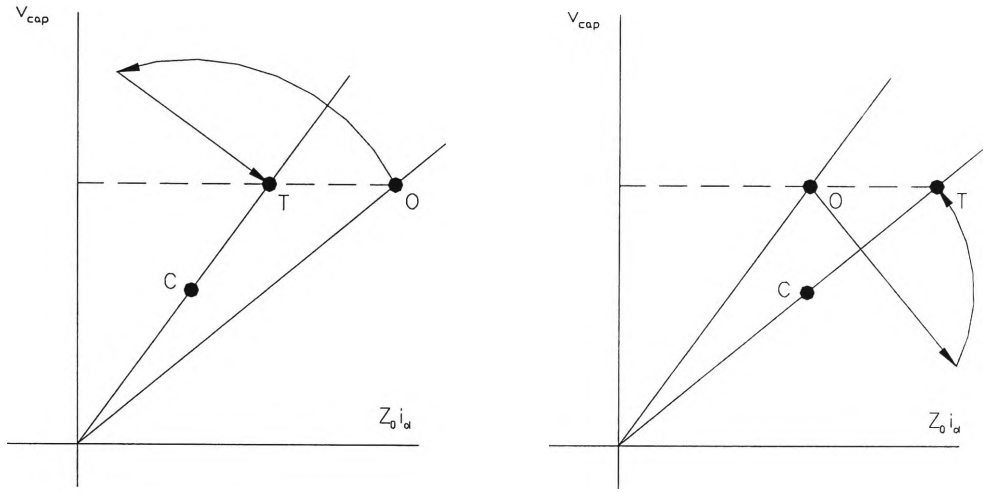

Figure 34 Optimal control transient operation

(a) output current decrease, (b) output current increase

For the examples presented in Figure 34, the points labelled 'O' represent the initial operating point (or original target) and the points labelled 'T' represent the new target values of v_{cap} and $Z_0 i_d$. Figure 34 shows that the operating point follows a circular path until the target can be reached on a straight line trajectory (example (a)), and follows a straight line trajectory until the target can be reached on a circular path (example (b)).

5.4.1 Simulations

Matlab simulations have been conducted for a number of scenarios of steady state and transient operation. These are presented in detail in Appendix E. Examples are presented in Figures 35 and 36.

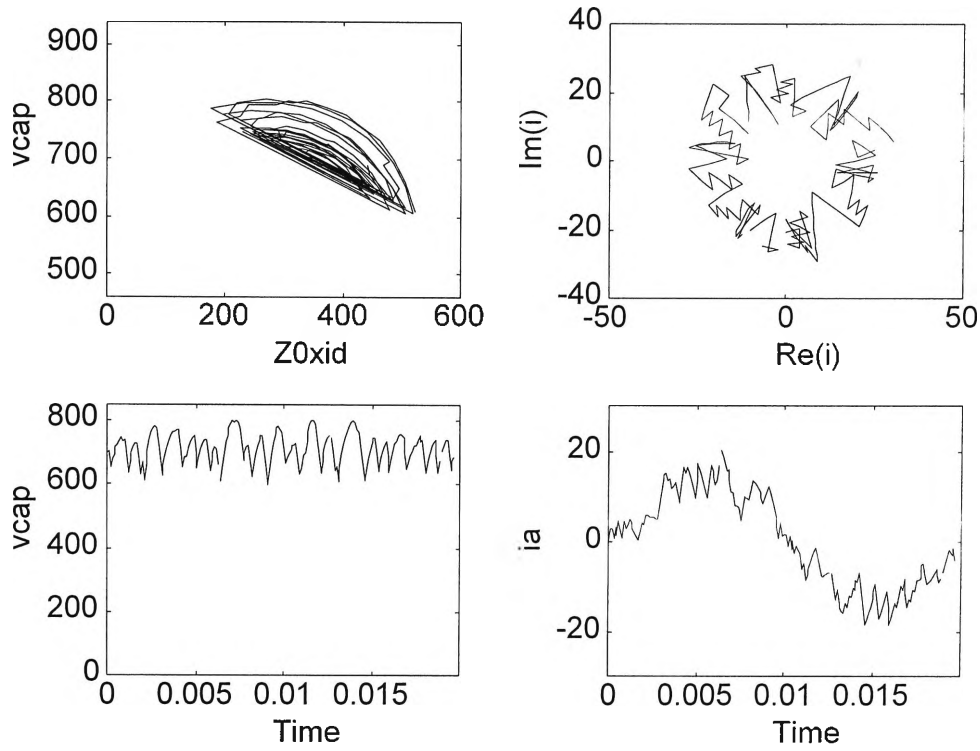

Figure 35 Optimal control simulation – steady state conditions - full load

(a) Graph of v_{cap} versus $Z_0 i_d$ (b) Graph of Re(i) versus Im(i)
(c) Graph of v_{cap} versus time (d) Graph of i_a versus time

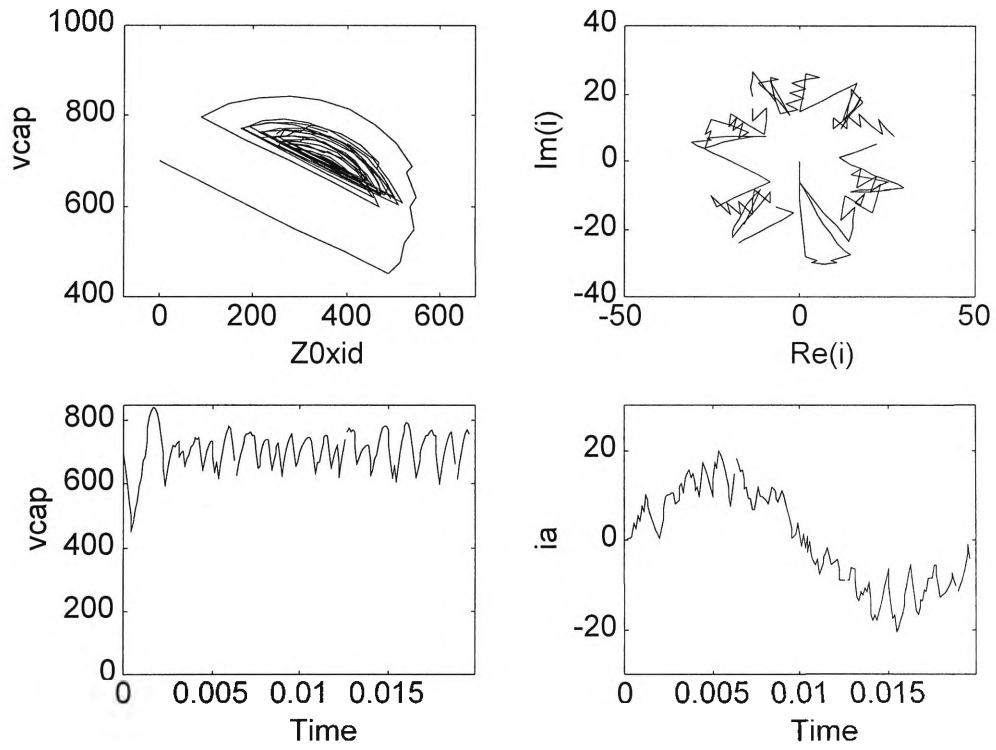

Figure 36 Optimal control simulation – transient conditions – output current stepping up

(a) Graph of v_{cap} versus $Z_0 i_d$ (b) Graph of Re(i) versus Im(i)
(c) Graph of v_{cap} versus time (d) Graph of i_a versus time

The simulations show that under steady state conditions the average value of the variables v_{cap}, i_d and i_q are equal to the target. This confirms that the target point is maintainable and that stable control is possible. It can be seen in Figure 35(a) that the shape of the trajectories is being utilised to maintain the state variables close to the target values. In this example the output current is large and therefore it represents the worst case performance in terms of capacitor voltage variation at steady state. For the example presented in Figure 35 the capacitor voltage varies from the target by approximately ±100V. Figure 35(b) shows that the supply current vector is rotating in order to keep the supply currents in phase with the supply voltages.

Under transient conditions a new target value of i_d is calculated when a change in output current occurs and the control strategy aims to reach the new target. In the example shown in Figure 36 the output current steps from 0A to 10A in a single cycle. Therefore the target in the ($Z_0 i_d$, v_{cap}) plane moves from the point (0,700) to (357,700) and the state variables move from the original target to the new one in approximately 22 switching periods (2.2ms). The minimum capacitor voltage reached during the transient phase of operation is 450V.

This review of the performance of the optimal control strategy highlights that this method of control has advantages and disadvantages. It is referred to here as an optimal control strategy as it has a very high speed of response, but it can be seen in Figures 35 and 36 that the speed of response is achieved at the expense of capacitor voltage and in phase current variation. There is a trade-off involved and if tighter voltage and current control is required then a decrease in the speed of response will result.

For a given capacitor value, the amount of deviation of the capacitor voltage from the target under steady state conditions depends on the output current and the switching frequency. The capacitor voltage reached under transient conditions also varies with the output current.

It is possible to apply weighting factors to the capacitor voltage and supply currents to reduce the variation of one at the expense of the other. By doing this the advantage of easy computations due to the shape of the circular trajectories is lost.

5.5 Method 2: Hysteresis Control

It is possible to improve the performance of the optimal control scheme, in terms of reducing variations in capacitor voltage and supply currents, by modifying the switching boundaries. At some operating points in the ($Z_0 i_d$, v_{cap}) plane the optimal control strategy would apply a zero switching mode when it would be better if an active mode were applied instead, and vice versa. In the example shown in Figure 37, at operating point 'A' the optimal control strategy would select a zero switching mode (to B1), when applying an active switching mode would drive the state variables closer to the target (to B2).

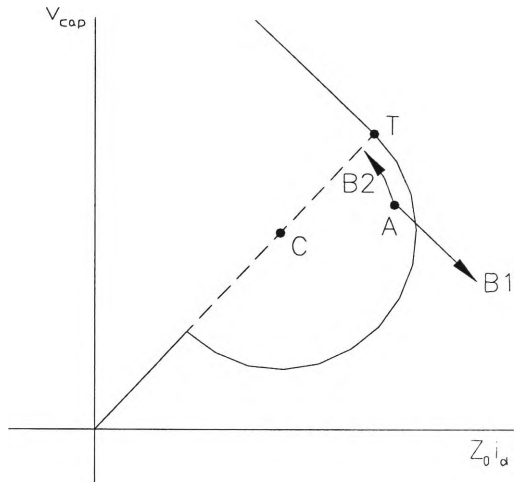

Figure 37 Possible trajectories

By including 'negative' hysteresis bands on the boundaries the variation of the state variables is reduced. The hysteresis bands are shown in Figure 38 below. The boundaries have been moved by half the distance travelled in a single cycle.

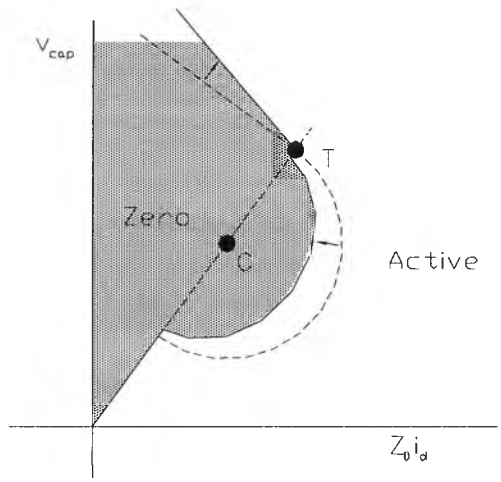

Figure 38 Hysteresis bands

The change in the state variables in a single control cycle is much greater on application of a zero switching mode than it is for an active switching mode. (Note that Figure 38 is not drawn to scale). As a result it is sufficient to include a hysteresis band only when switching from zero switching modes to active switching modes. Also, for ease of computations, the hysteresis band is assumed to be circular. The modified switching boundaries are shown in Figure 39.

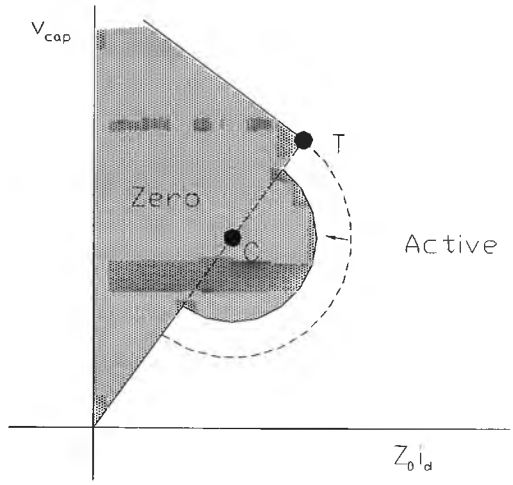

Figure 39 Modified switching boundaries

The radius of the boundary has been reduced by half of the distance travelled in a single zero mode switching cycle:

$$\Delta Radius = \frac{1}{2}\sqrt{dv_{cap}^2 + \left(Z_0 di_d^2\right)} \tag{50}$$

5.5.1 Simulations

Matlab simulations have been conducted for a number of scenarios of steady state and transient operation. These are presented in detail in Appendix E. Examples are presented in Figures 40 and 41.

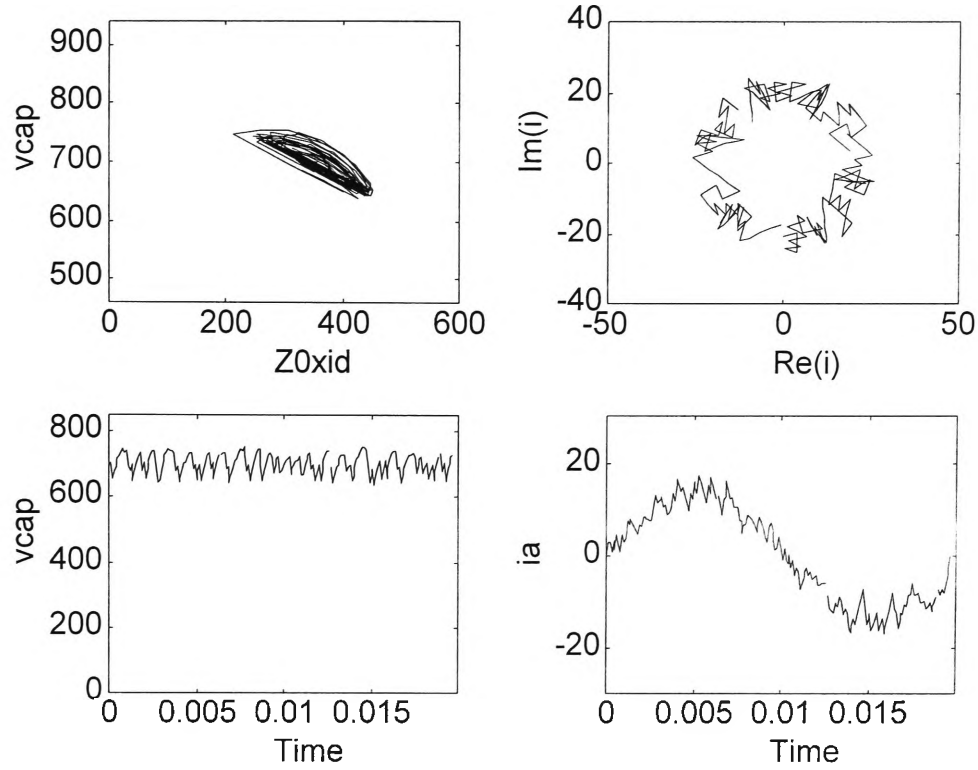

Figure 40 Hysteresis control simulation – steady state conditions - full load

(a) Graph of v_{cap} versus $Z_0 i_d$ (b) Graph of Re(i) versus Im(i)
(c) Graph of v_{cap} versus time (d) Graph of i_a versus time

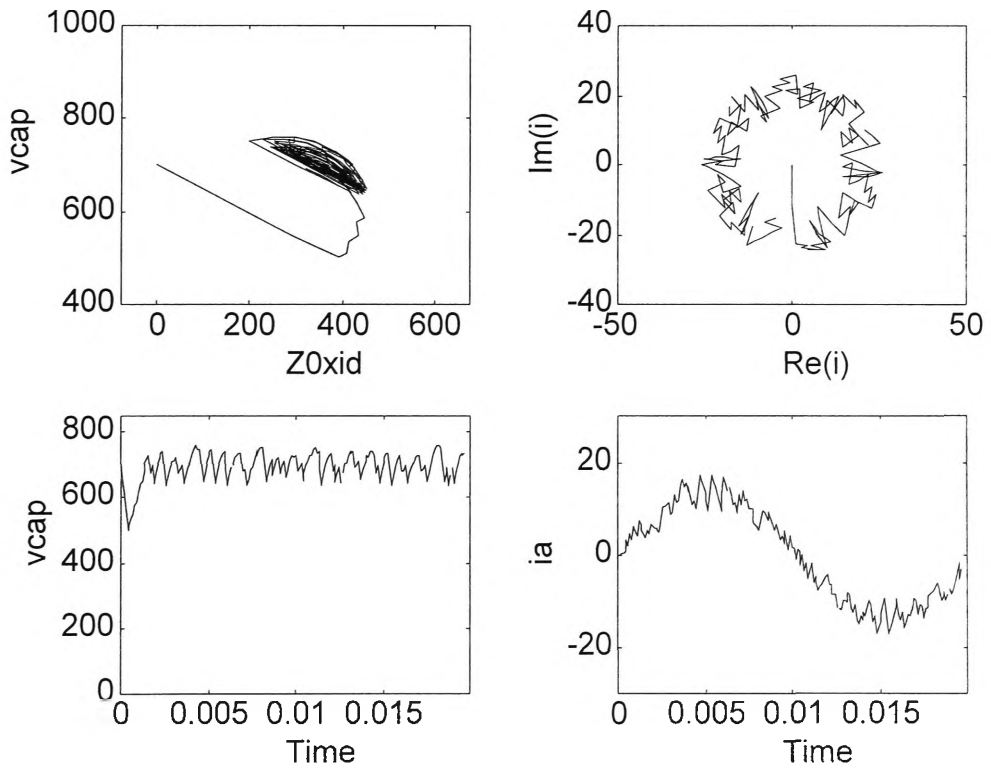

Figure 41 Hysteresis control simulation – transient conditions – output current stepping up

(a) Graph of v_{cap} versus $Z_0 i_d$ (b) Graph of Re(i) versus Im(i)
(c) Graph of v_{cap} versus time (d) Graph of i_a versus time

The simulations show that, in terms of variation in capacitor voltage and supply current, the hysteresis control strategy performs better than the optimal strategy. The improvement in performance is particularly clear when the results for the example of transient conditions (Figures 36 and 41) are compared.

Under steady state conditions the average value of the variables v_{cap}, i_d and i_q are equal to the target. The capacitor voltage varies from the target by approximately ±60V, or less than ±10% of the target value.

Under transient conditions the output current undergoes a step change of 10A in a single cycle and the state variables move from the original target to the new one in 14 switching periods (1.4ms). In this example the hysteresis control strategy shows a significant improvement in speed of response compared to the optimal strategy due to the improved accuracy in reaching the new target. The minimum capacitor voltage reached during the transient phase of operation is 500V.

5.6 Method 3: Chatter Control

The two control methods described previously result in large variations in the state variables and fast response under transient conditions. It is possible to achieve smaller variations in the state variables if a slower speed of response can be tolerated. Chatter control is a strategy which results in a trade off between the two extremes.

For the chatter control strategy, either a circular path or a straight line trajectory is followed until the line of power balance is reached. A combination of straight and circular trajectories are then used to "chatter" down one side of the line of power

balance. Control under transient conditions is illustrated in Figure 42.

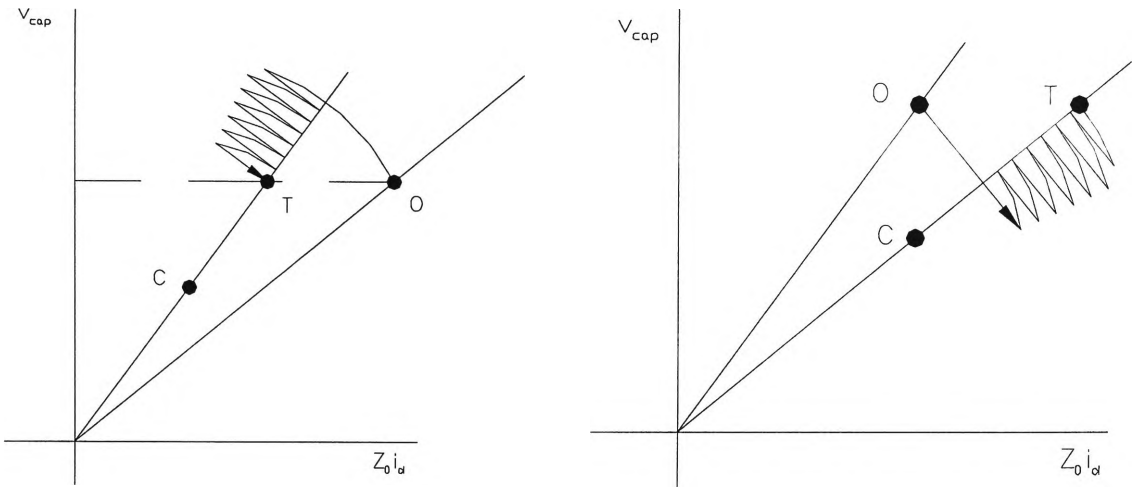

(a) output current decrease (b) output current increase

Figure 42 Chatter control transient operation

Since a change in power into/out of the capacitor is occurring during the transient phase, the operating point moves down one side of the line of power balance to decrease i_d, and up the other side to increase i_d (put power in).

This control strategy uses the speed of the optimal control strategy to reach the line of power balance.

The chatter control strategy is represented by the switching boundaries illustrated in Figure 43.

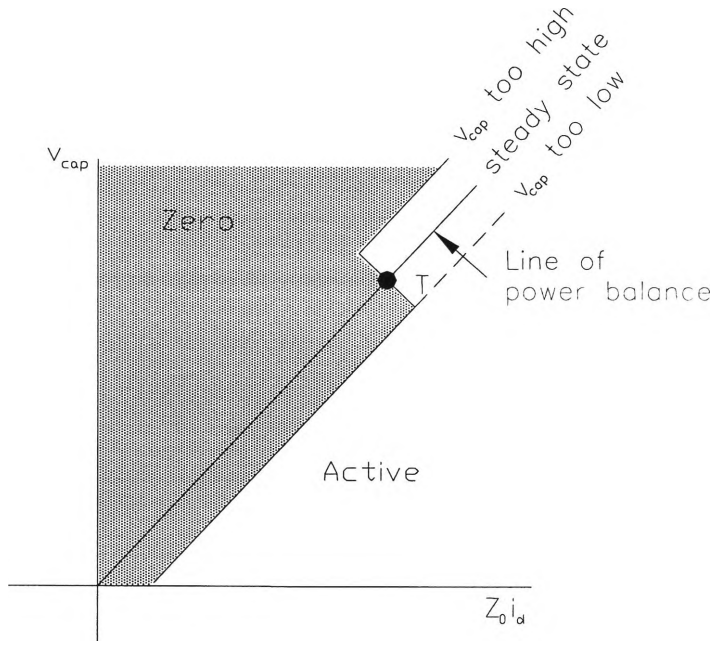

Figure 43 Chatter control switching boundaries

The point labelled 'T' represents the target values of v_{cap} and $Z_0 i_d$.

The target is a point on the line of power balance, above the centre of the active mode trajectories. The switching boundary is a line parallel to the line of power balance and offset by an amount that depends on the value of v_{cap} compared to the target. As shown in Figure 43, if v_{cap} is too high compared to the target then the switching boundary is moved up, and the resultant trajectory chatters above the line of power balance, reducing v_{cap}. If v_{cap} is too low compared to the target then the switching boundary is moved down, and the resultant trajectory chatters below the line of power balance, increasing v_{cap}. Under steady state conditions, when v_{cap} is close to the target, the switching boundary is such that stable control at the target is possible.

As discussed in Chapter 5.5, the change in the state variables in a single control cycle is greater on application of a zero switching mode than it is for an active mode. Therefore the switching boundaries are offset to take into account

hysteresis. The modified switching boundaries are illustrated in Figure 44.

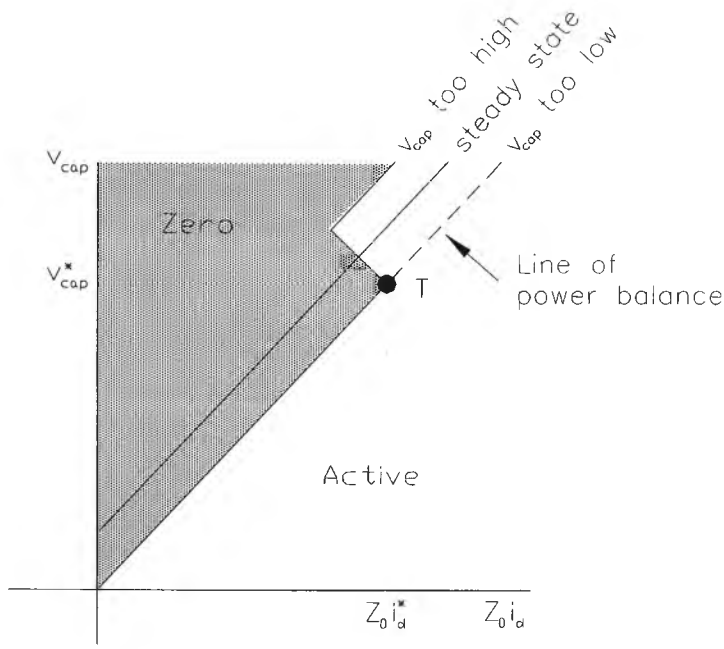

Figure 44 Chatter control switching boundaries with hysteresis

Due to the simple nature of the switching boundaries this control strategy is straight-forward and computationally efficient to implement.

5.6.1 Simulations

Matlab simulations have been conducted for a number of scenarios of steady state and transient operation. These are presented in detail in Appendix E. Examples are presented in Figures 45 and 46.

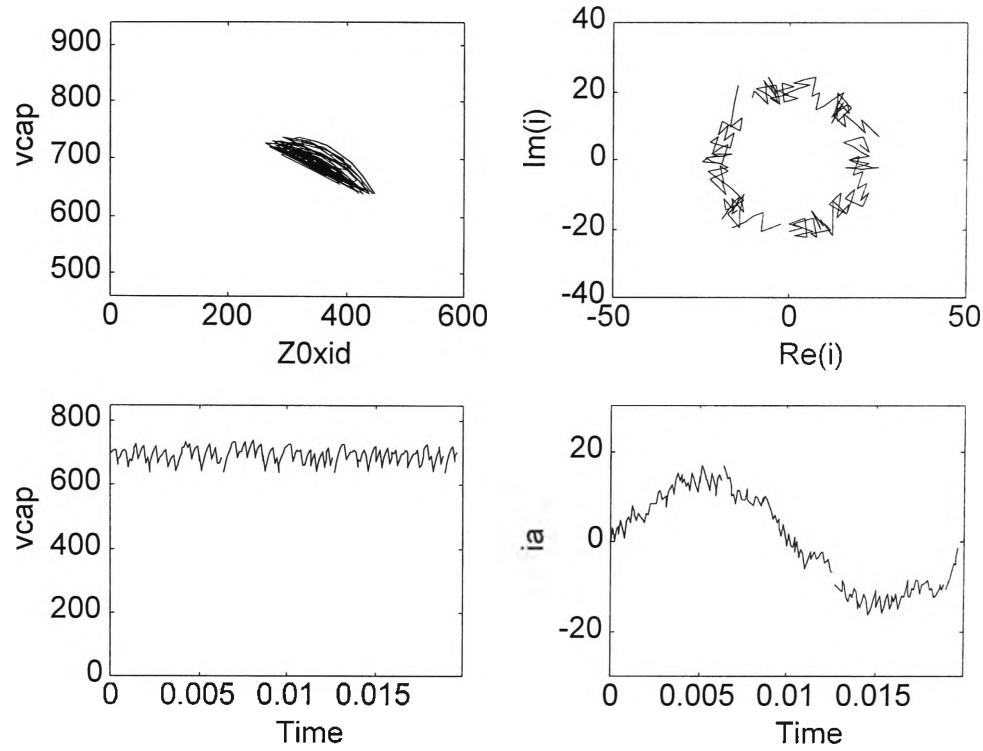

Figure 45 Chatter control simulation – steady state conditions - full load

(a) Graph of v_{cap} versus $Z_0 i_d$ (b) Graph of Re(i) versus Im(i)
(c) Graph of v_{cap} versus time (d) Graph of i_a versus time

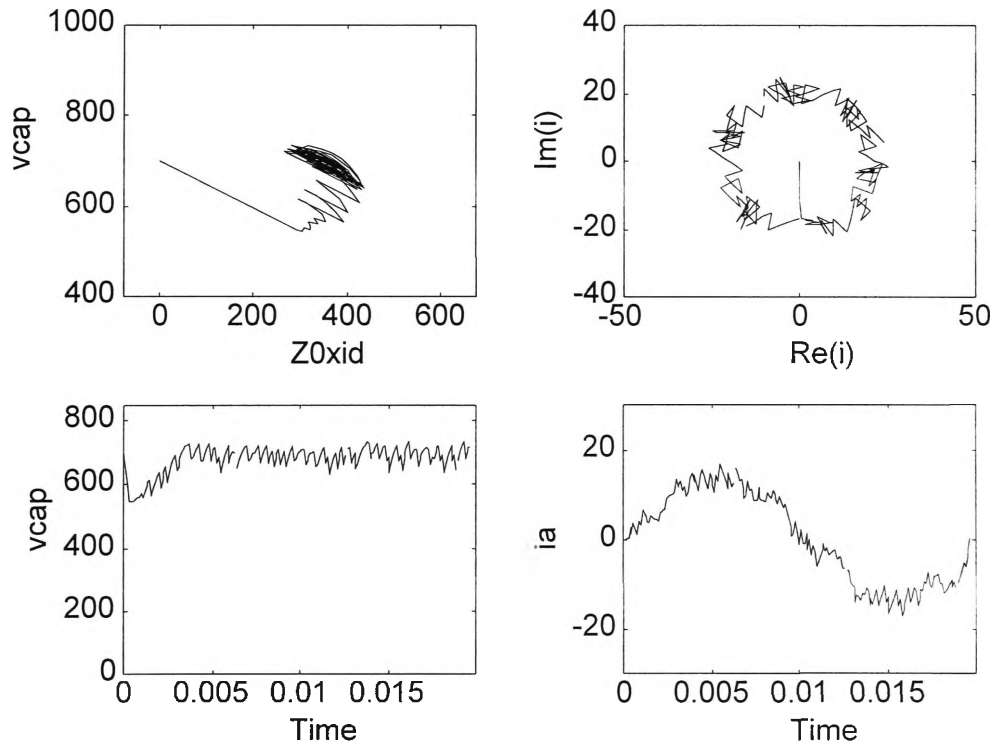

Figure 46 Chatter control simulation – transient conditions – output current stepping up

(a) Graph of v_{cap} versus $Z_0 i_d$ (b) Graph of Re(i) versus Im(i)
(c) Graph of v_{cap} versus time (d) Graph of i_a versus time

The simulations show that, in terms of variation in capacitor voltage and supply current, the chatter control strategy is capable of improved performance compared to the previously discussed strategies.

Under steady state conditions the average value of the variables v_{cap}, i_d and i_q are approximately equal to the target. The capacitor voltage varies from the target by approximately +40V and -60V, or less than ±10% of the target value.

Under transient conditions the output current undergoes a step change of 10A in a single cycle and the state variables move from the original target to the new one in 28 switching periods (2.8ms). The minimum capacitor voltage reached during the transient phase of operation is 546V.

The chatter control strategy has a slower speed of response than the strategies presented previously, but the variation in the state variables is considerably less. For example, the deviation of the capacitor voltage from the target during the transient was almost 50V less than for the hysteresis strategy.

5.7 Method 4: Simple Control Strategy

The simple control strategy has been derived from the optimal control strategy. The semi-circular switching boundary has been removed and therefore an active switching mode is selected whenever the operating point is below the line of power balance. The simple control strategy is represented by the switching boundaries illustrated in Figure 47.

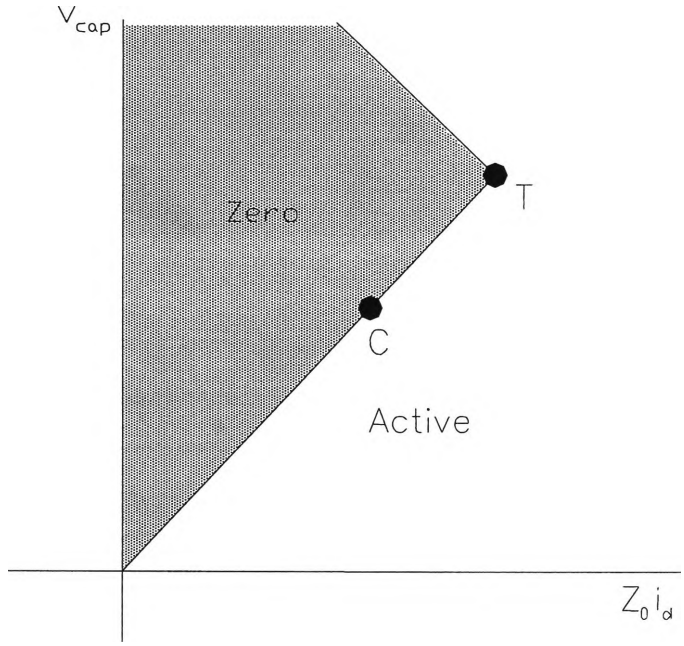

Figure 47 Simple control switching boundaries

Due to the simple nature of the switching boundaries this control strategy is straight-forward to implement.

5.7.1 Simulations

Matlab simulations have been conducted for a number of scenarios of steady state and transient operation. These are presented in detail in Appendix E. Examples are presented in Figures 48 and 49.

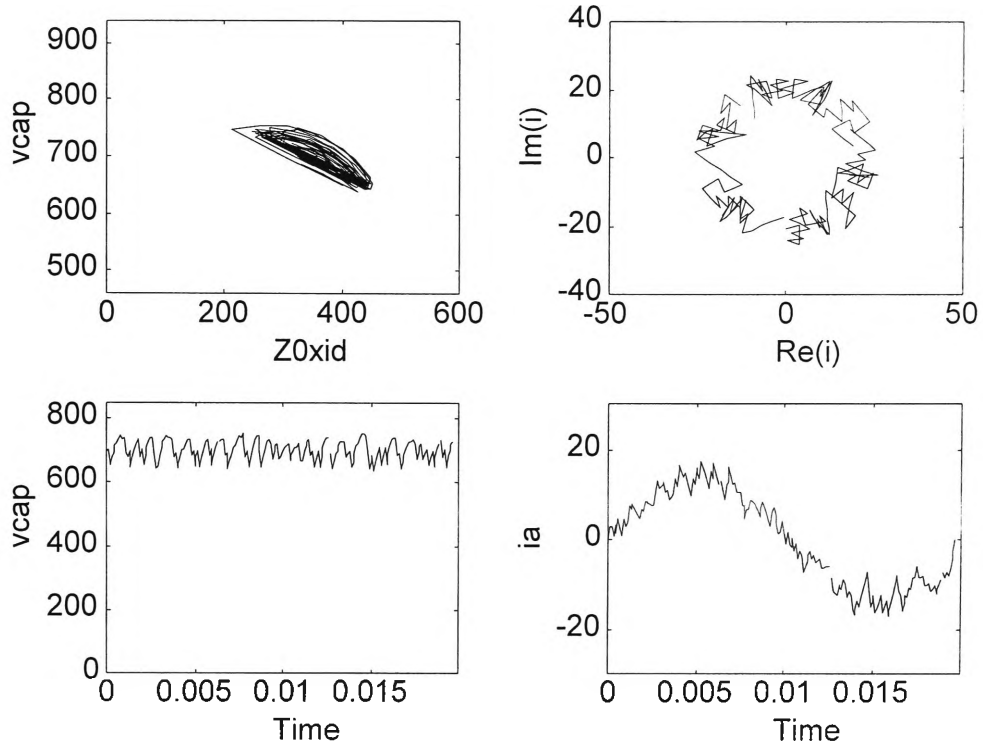

Figure 48 Simple control simulation – steady state conditions - full load

(a) Graph of v_{cap} versus $Z_0 i_d$ (b) Graph of Re(i) versus Im(i)
(c) Graph of v_{cap} versus time (d) Graph of i_a versus time

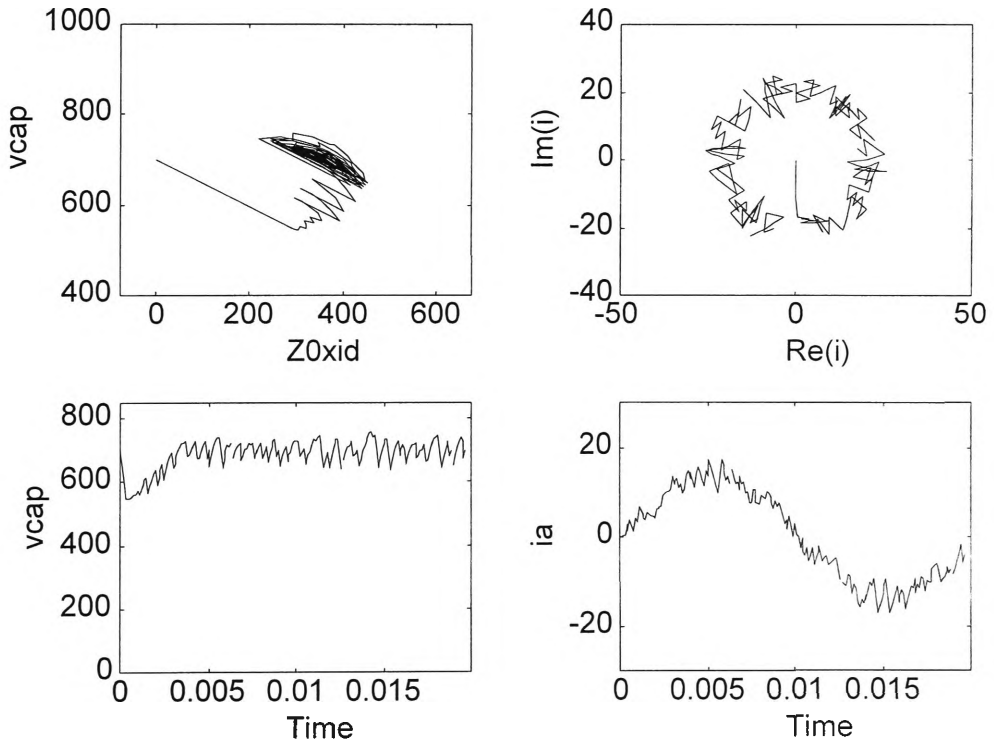

Figure 49 Simple control simulation – transient conditions – output current stepping up

(a) Graph of v_{cap} versus $Z_0 i_d$ (b) Graph of Re(i) versus Im(i)
(c) Graph of v_{cap} versus time (d) Graph of i_a versus time

The simulations show that, in terms of variation in capacitor voltage and supply current, the simple control strategy performs as well or better than the hysteresis strategy.

Under steady state conditions the average value of the variables v_{cap}, i_d and i_q are approximately equal to the target. The capacitor voltage varies from the target by approximately +55V and –60V, or less than ±10% of the target value.

Under transient conditions the output current undergoes a step change of 10A in a single cycle and the state variables move from the original target to the new one in 28 switching periods (2.8ms). The minimum capacitor voltage reached during the transient phase of operation is 546V.

The simple control strategy gives results similar to those for hysteresis control but the strategy is much simpler to implement.

5.8 Comparison

A comparison of the performance of the four control strategies under steady state conditions with full load is presented in Table 1. The comparison is based on the variation from the target of the capacitor voltage and supply current.

Control Strategy	v_{cap} variation	i_d variation
Optimal	± 100 V	± 10 A
Hysteresis	± 60 V	+ 5A and – 8 A
Chatter	+40 V and –60 V	± 5 A
Simple	+55 V and –60 V	+ 5A and – 8 A

Table 1 Comparison – steady state conditions - full load

A comparison of the performance of the control strategies under transient conditions for a step increase in output current is presented in Table 2. The comparison is based on the maximum deviation of the capacitor voltage from the target during the transient phase of operation and the response time.

Control Strategy	Maximum v_{cap} deviation during transient	Response Time
Optimal	250 V	2.2ms
Hysteresis	200 V	1.4 ms
Chatter	154 V	2.8 ms
Simple	154 V	2.8 ms

Table 2 Comparison – transient conditions – output current stepping up

The optimal control strategy results in a large variation of the state variables from the target. The speed of response to a transient is good though additional cycles can be needed to achieve the state variables close to the target values.

The hysteresis strategy is a modified version of the optimal strategy where the speed of response to a transient is maintained, and actually improved by improving the ability of the strategy to closely reach the target. This also leads to a reduction in variation of state variables. When comparing the position of the operating point to the switching boundaries, the hysteresis strategy is computationally more difficult.

The above results indicate that the chatter control strategy performs best in terms of variation of the state variables from the target. The trade-off is an increase in the speed of response. When compared to the hysteresis strategy, the speed of response of the chatter strategy has doubled for the large step change in output

current. The chatter strategy is straight-forward to implement.

The simple control strategy produces similar results to the chatter strategy during transient conditions and similar results to the hysteresis strategy during steady state conditions. This strategy is the simplest to implement.

Further consideration of the chatter control strategy for rectifier control is given here due to the superior performance under steady state conditions and the ease of implementation. While the performance under transient conditions is also important, as shown in the following chapter the average rectifier output current under typical operating conditions more closely resemble the steady state operation. Additional simulation results for the chatter strategy for steady state full load operation are presented below. Figures 50 and 51 are graphs of the supply currents and supply voltages versus time which show that the supply currents are controlled to be in phase with the supply voltages as required.

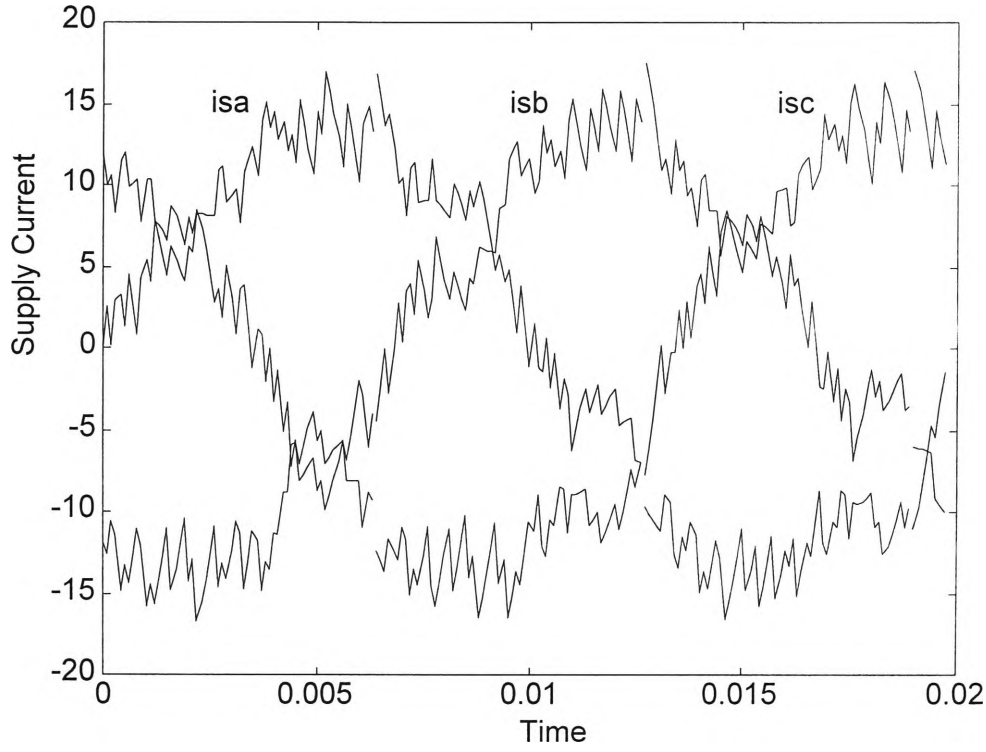

Figure 50 Chatter control simulation – supply currents

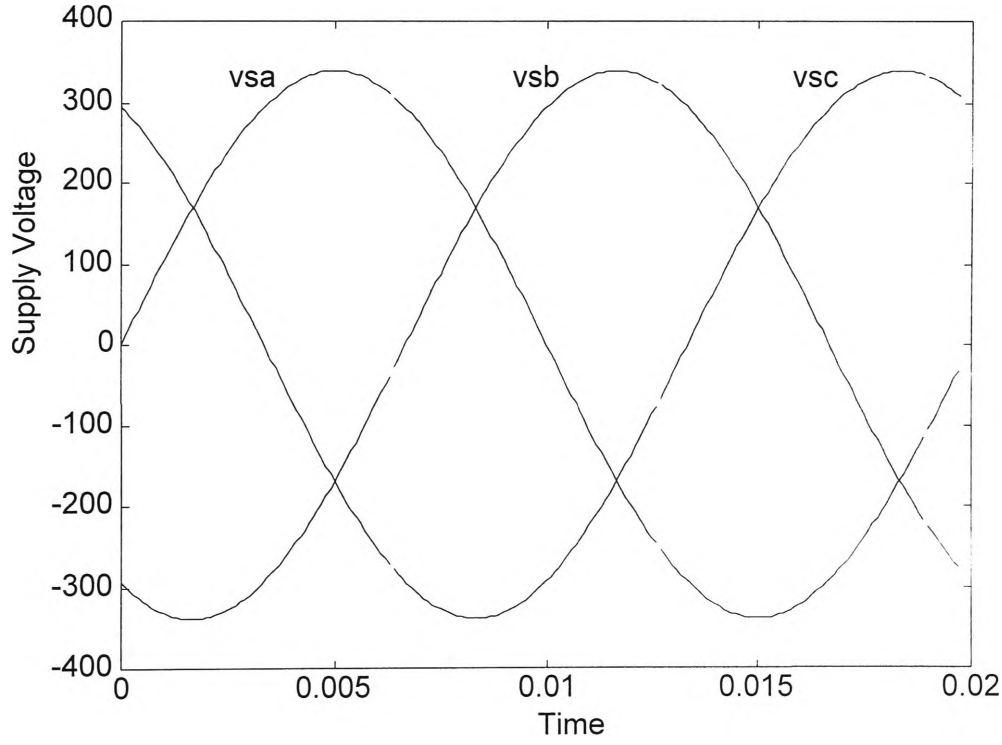

Figure 51 Chatter control simulation – supply voltages

Figure 52 shows a graph of the capacitor voltage versus time as well as a harmonic spectrum for the waveform. The spectrum shows the large dc component of the capacitor voltage waveform.

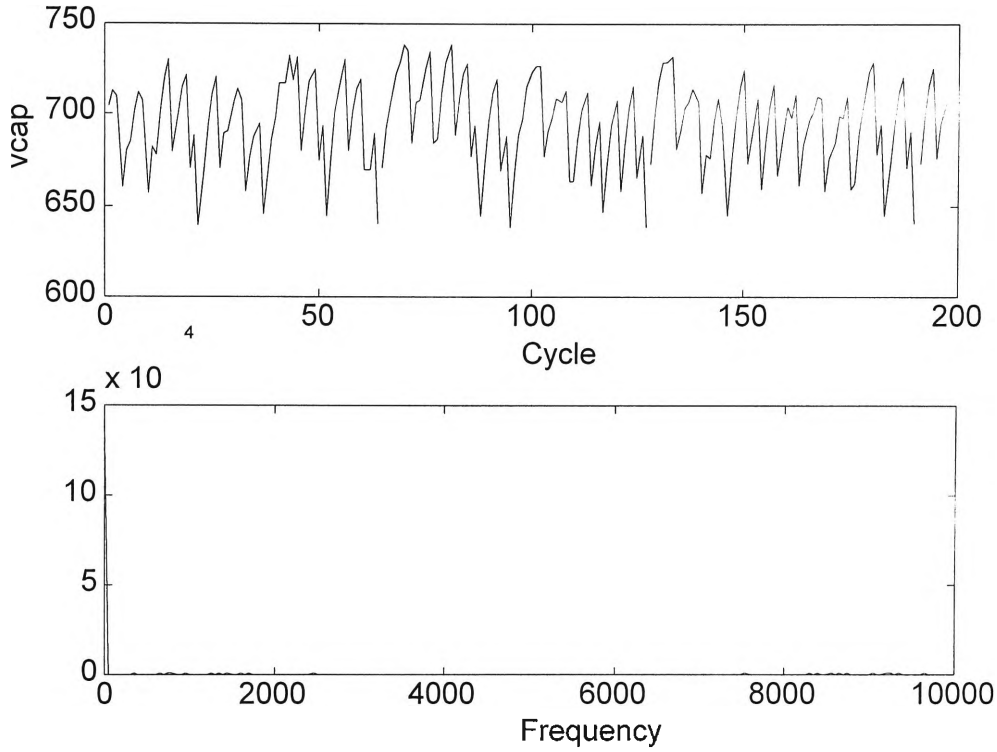

Figure 52 Chatter control simulation

(a) Graph of v_{cap} versus cycle

(b) Harmonic spectrum – capacitor voltage

Figure 53 shows a graph of one of the supply currents versus time and a harmonic spectrum for the waveform which shows the 50Hz supply frequency and 10kHz switching frequency components.

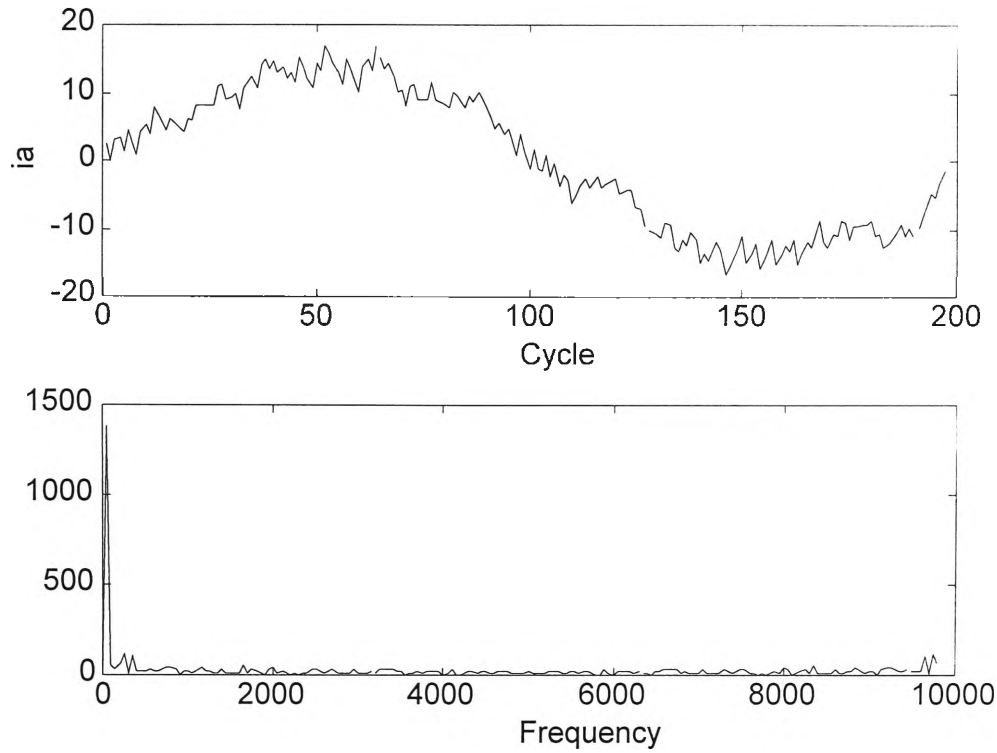

Figure 53 Chatter control simulation

(a) Graph of i_a versus cycle

(b) Harmonic spectrum – supply current

As mentioned, a tradeoff exists between the performance under transient conditions (speed of response) and under steady state conditions (variation of state variables). The optimal control strategy has been presented as a control strategy capable of a very high speed of response. Though these modifications have not been considered in this report, it is possible to increase further the speed of response under transient conditions if variations of the out of phase current (i_q) from the target can be tolerated. One such strategy, which utilises space vector control, has been presented by Choi and Sul [16] and is called minimum time current control. This control strategy determines the optimal voltage to drive the supply current vector to the reference in the minimum amount of time.

5.9 Summary

It can be seen in the examples presented that the control strategies developed utilise the shape of the rectifier trajectories to maintain the state variables close to the target values during steady state conditions, and to reach the target under transient conditions. For the chatter control strategy the maximum variation in capacitor voltage is less than ±10% of the target value for steady state conditions at full load. This example represents the worst case performance in terms of capacitor voltage variation under steady state conditions. As an example of control under transient conditions, a step change in the output current is considered. The chatter control strategy is shown to have a slower speed of response than other strategies considered though the variation in the state variables is reduced under these conditions also.

The examples presented show that the supply current vector rotates in order to keep the supply currents in phase with the supply voltages.

By comparing the various control strategies developed, it can be seen that a fast speed of response is achieved at the expense of capacitor voltage and in phase current variation. There is a trade-off involved and if tighter voltage and current control is required then a decrease in the speed of response will result.

In the following chapter the chatter control strategy is applied to a rectifier which forms part of a full ac/dc/ac converter.

CHAPTER 6

CONTROL OF THE HIGH-FREQUENCY CONVERTER

6.1 Introduction

The rectifier control strategies presented in Chapter 5 can be incorporated into the control of the high-frequency converter. The rectifier control strategy is used to control the switching operations of the rectifier bridge in order to control the supply currents and the dc bus voltage. Standard inverter control can be used to control the inverter bridge and load currents.

In this chapter the converter control is discussed and the results of simulations under steady state and transient conditions are presented based on a simplified converter circuit.

6.2 Converter Circuit

The three phase ac/dc/ac converter considered was illustrated in Figure 4. In order to simulate the operation of this system, the converter circuit is simplified by representing the three phase induction motor as a balanced three phase RL load as shown in Figure 54.

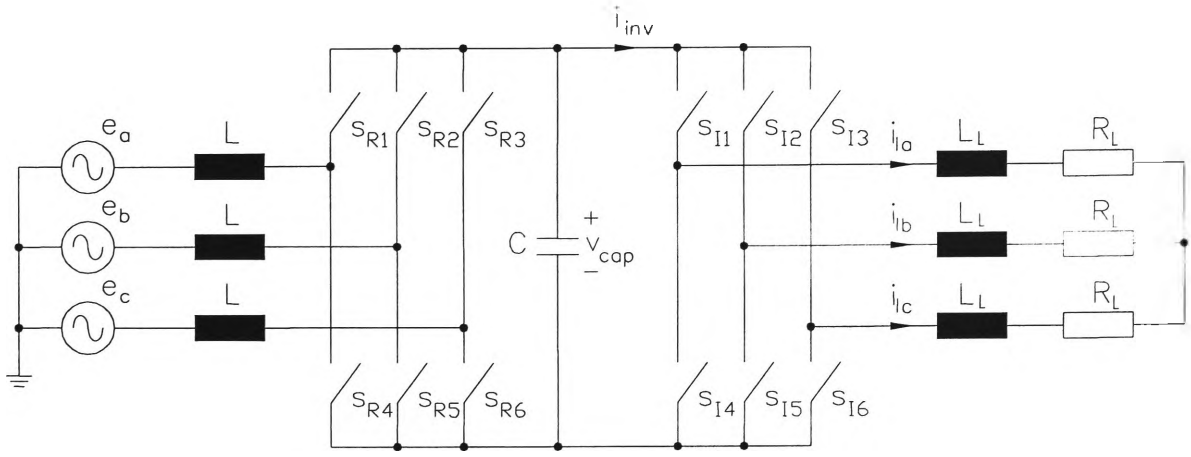

Figure 54 Simplified three phase converter

Control of the rectifier bridge is based on the chatter control strategy presented in Chapter 5.6. In the discussion of the rectifier control presented earlier, the rectifier output current was represented by a current source (Figure 8). In the simulations presented this current was either a constant, a ramp or a step.

In the high-frequency converter the rectifier output current is the current drawn by the inverter bridge and load which will generally not be a constant, a ramp or a step due to the switching action of the inverter bridge. The simulations presented here demonstrate that the rectifier control strategy produces stable control under realistic operating conditions.

Control of the inverter bridge is discussed below.

6.3 Inverter Control

Like the switched rectifier, the switched inverter has eight possible switching modes. For each mode the voltage applied by the inverter to the load can be represented by a voltage vector as illustrated in Figure 55.

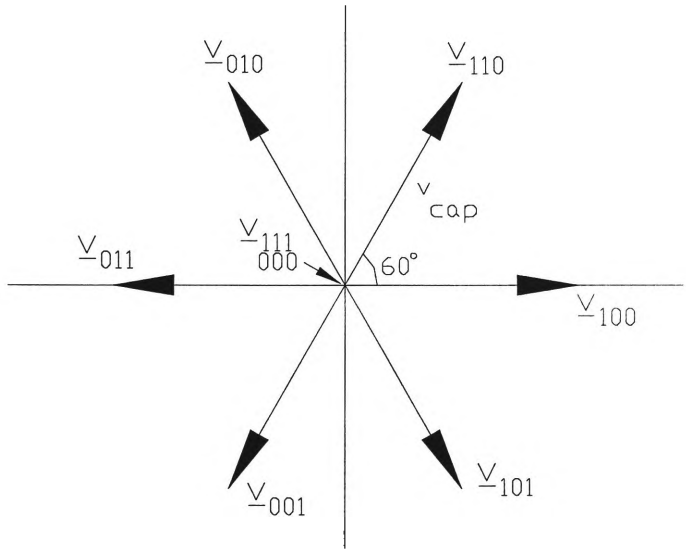

Figure 55 Inverter switching vectors

The inverter is controlled to produce the required current through the load. In order to do this the load current is measured and compared to a reference value. The inverter voltage vector $\underline{V}$ that will produce the required change in current is calculated using the equation below.

$$\underline{V} = L_L \frac{d\underline{i}_{LL}}{dt} + R_L \underline{i}_{LL} \tag{51}$$

where

L_L = load inductance

$\underline{i}_{LL}$ = load current vector

$$= i_{la} + i_{lb} e^{j(2\pi/3)} + i_{lc} e^{j(4\pi/3)}$$

R_L = load resistance

dt = switching time

The resultant vector is compared to the available inverter voltage vectors and the

inverter switching mode applied is that for which the voltage vector is closest to the required vector (given by Equation 51).

6.4 Converter Control

The converter control incorporates the inverter and rectifier control strategies discussed above. The sequence of control is as follows:

- The inverter switching mode is selected based on the required change in load current;
- The rectifier output current is calculated;
- The rectifier switching mode is selected based on the required supply currents and dc bus voltage.

The inverter switching mode is selected to minimise the error between the current reference and the load current feedback. The rectifier switching mode is selected based on the rectifier output current (or link current to the inverter) which depends on the load currents and the inverter switching state:

$$i_{inv} = S_a i_{la} + S_b i_{lb} + S_c i_{lc} \tag{52}$$

As the inverter switching mode can change at each switching instant, the link current can change also. The control of the rectifier is based on the average link current over a number of cycles (ten cycles for the simulations presented). This becomes the rectifier output current for the rectifier control strategy.

DC bus voltage fluctuations will result in variations in the length of the inverter switching vectors which were illustrated in Figure 55. In order to simplify the

simulation, the calculation of the inverter currents each cycle are based on the dc bus voltage at the beginning of the cycle.

6.4.1 Simulations

Simulations have been performed for the system illustrated in Figure 54 and described in the table below.

Supply	
Supply voltage	Sinusoidal 240 Vrms L-N
Supply voltage frequency	50 Hz
Supply inductance (L)	9 mH
DC link capacitor (C)	20 μF
Capacitor voltage target	700 V
Load	
Load current reference	Sinusoidal 10 A peak
Load current frequency	75 Hz
Load inductance (L_L)	33 mH
Load resistance (R_L)	34 Ω

Table 3 Characteristics of three phase converter simulation circuit

Matlab simulations have been conducted for both steady state and transient conditions. In this case transient conditions refers to a change in the load current reference.

Steady State Conditions

Under steady state conditions the load current reference is a sinusoidal waveform with a constant magnitude. The waveforms for the supply side and the rectifier are illustrated in Figure 56 as described below:

(a) Capacitor voltage versus in phase current (which has been scaled by Z_0)

(b) In phase current versus time

(c) Supply current vector

(d) Supply current (a-phase) versus time

Figure 57 is a graph of dc bus voltage versus time.

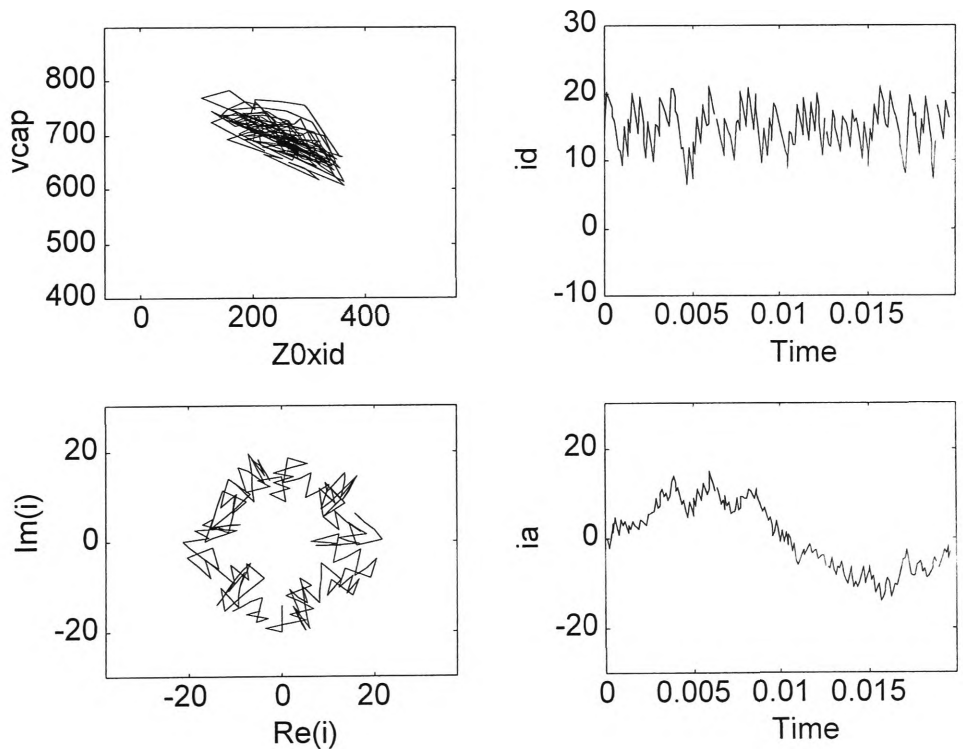

Figure 56 Converter control simulation – Steady state – supply/rectifier waveforms

(a) Graph of v_{cap} versus $Z_0 i_d$ (b) Graph of i_d versus time
(c) Graph of Re(i) versus Im(i) (d) Graph of i_a versus time

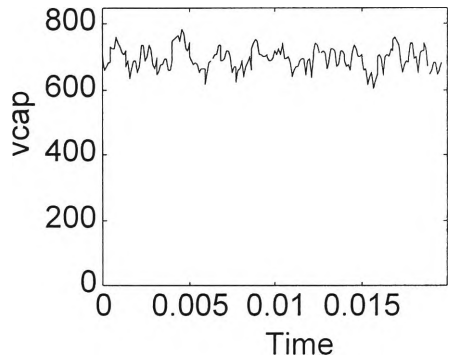

Figure 57 Converter control simulation – Steady state – Graph of v_{cap} versus time

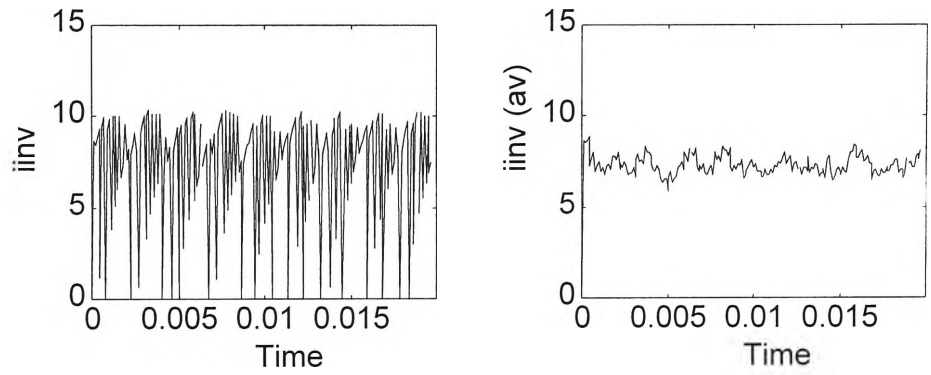

Figure 58 Converter control simulation – Steady state – link current waveforms

(a) Graph of inverter link current versus time
(b) Graph average inverter link current versus time

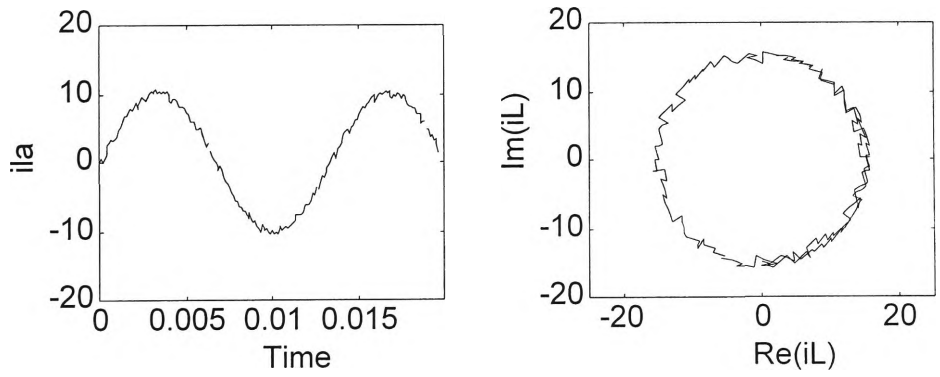

Figure 59 Converter control simulation – Steady state – inverter/load waveforms

(a) Graph of i_{la} versus time (b) Graph of Re(i_L) versus Im(i_L)

The rectifier output current versus time is plotted in Figure 58(a), and the averaged current, which is used by the rectifier control strategy, is plotted in Figure 58(b).

The load side waveforms are plotted in Figure 59; these are the load current (a-phase) versus time and the load current vector.

The results show that the rectifier control scheme maintains the dc bus voltage close to the target value and the in phase supply current is controlled to match the *average* current into and out of the dc bus capacitor. The inverter is being switched to produce sinusoidal load current waveforms. The load current waveforms are smoother than the supply current waveforms due to the relative size of the line inductances. The supply inductance is smaller than the load inductance and as a result the supply currents react faster than the load currents. Some distortion of the supply current is indicated in Figure 56(d). This is due to the application of a zero switching mode when the operating point is close to the target. By modifying the rectifier switching boundaries to incorporate hysteresis when the capacitor voltage is below the target it is possible to minimise this occurrence.

Transient Conditions – Load Current Increase

The same set of waveforms are presented for the simulation of transient conditions whereby the load current reference magnitude undergoes a step change from 0A to 10A.

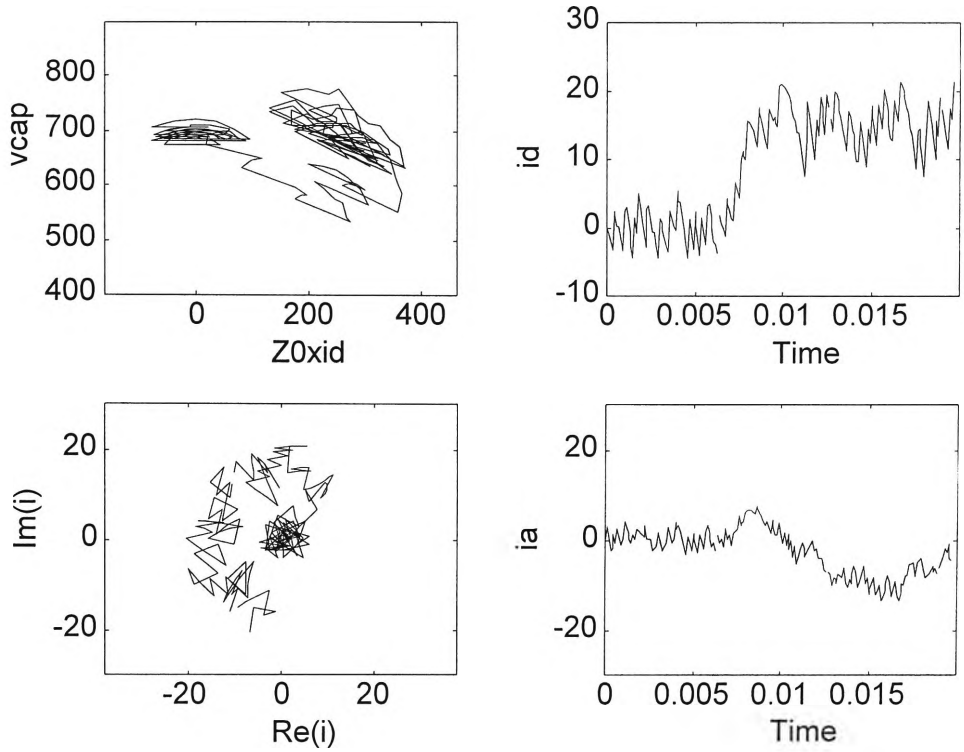

Figure 60 Converter control simulation – Transient – supply/rectifier waveforms

(a) Graph of v_{cap} versus $Z_0 i_d$ (b) Graph of i_d versus time
(c) Graph of Re(i) versus Im(i) (d) Graph of i_a versus time

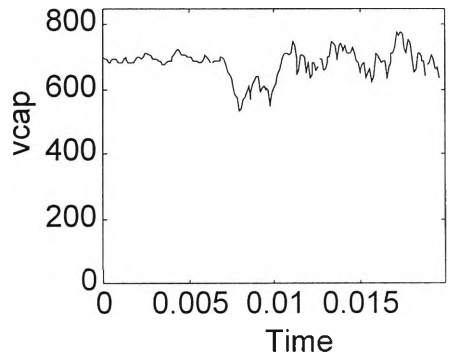

Figure 61 Converter control simulation – Transient – Graph of v_{cap} versus time

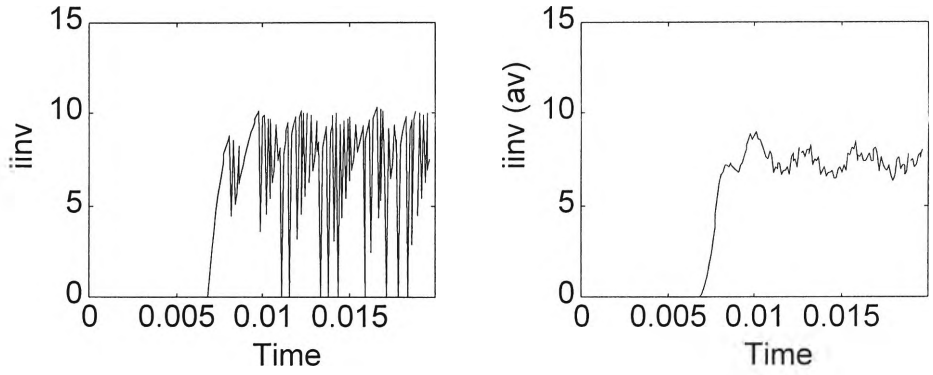

Figure 62 Converter control simulation – Transient – link current waveforms

(c) Graph of inverter link current versus time
(d) Graph average inverter link current versus time

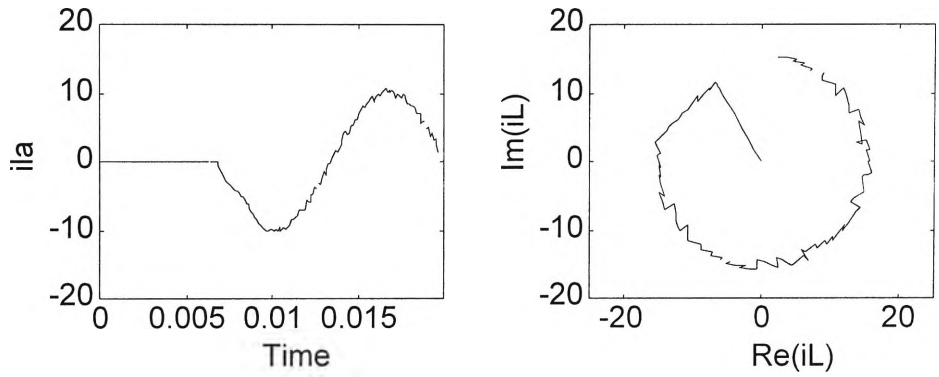

Figure 63 Converter control simulation – Transient – inverter/load waveforms

(a) Graph of i_{la} versus time (b) Graph of Re($\underline{i_L}$) versus Im($\underline{i_L}$)

When the transient occurs the dc bus voltage drops to a minimum of 167V below the target. The dc bus voltage and supply currents reach the new target in approximately 37 cycles (3.7mS).

Transient Conditions – Load Current Decrease

The same set of waveforms are presented for the simulation of transient conditions whereby the load current reference magnitude is halved.

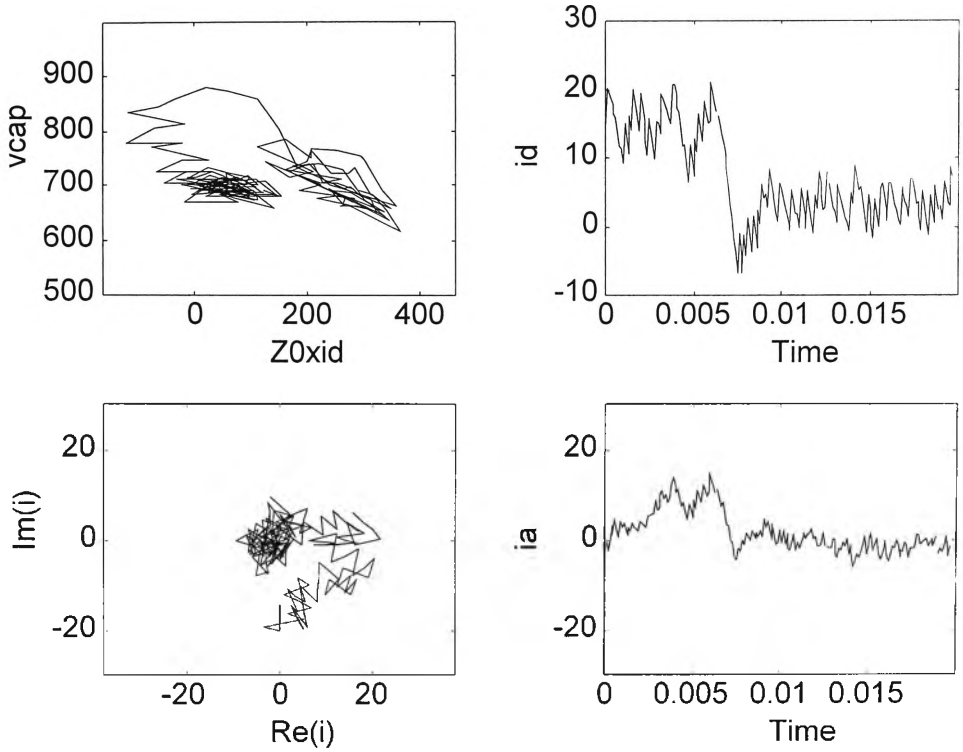

Figure 64 Converter control simulation – Transient – supply/rectifier waveforms

(a) Graph of v_{cap} versus $Z_0 i_d$
(b) Graph of i_d versus time
(c) Graph of Re(i) versus Im(i)
(d) Graph of i_a versus time

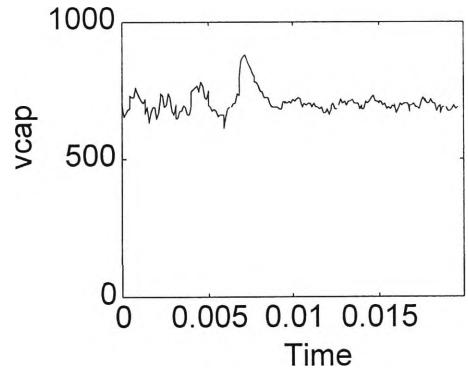

Figure 65 Converter control simulation – Transient – Graph of v_{cap} versus time

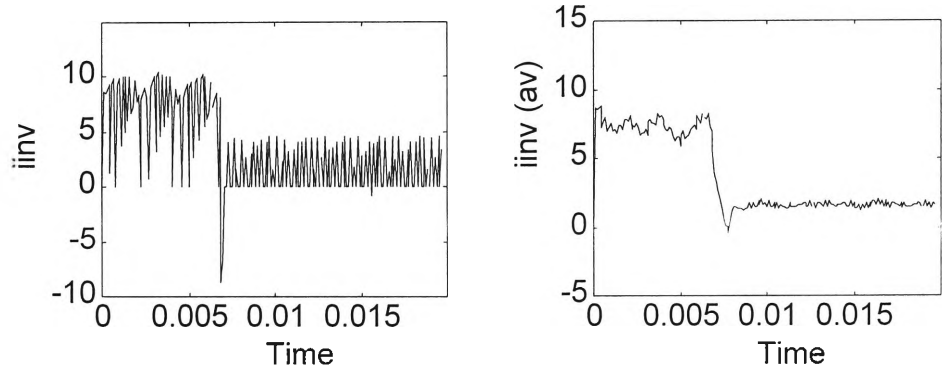

Figure 66 Converter control simulation – Transient – link current waveforms

(e) Graph of inverter link current versus time
(f) Graph average inverter link current versus time

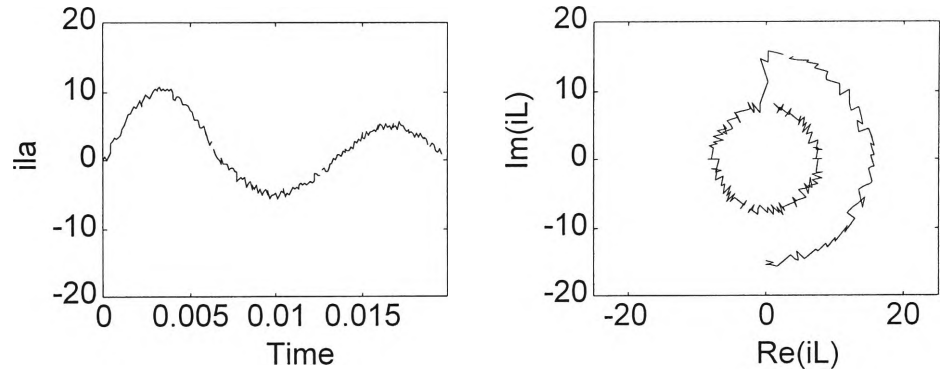

Figure 67 Converter control simulation – Transient – inverter/load waveforms

(a) Graph of i_{la} versus time (b) Graph of $Re(\underline{i}_L)$ versus $Im(\underline{i}_L)$

The results show that due to the transient the dc bus voltage deviates from the target, peaking at 180V above the target. The fast speed of response of the rectifier brings the dc bus voltage and supply currents back to the target in approximately 18 cycles (1.8mS).

As mentioned earlier, the steady state variation in dc bus voltage depends on the rectifier output current. This is illustrated clearly in Figure 65 where the voltage ripple is greater before the transient than it is after.

6.5 Conclusion

Simulations have been presented which show that the chatter rectifier control strategy can be incorporated into the control of a full ac/dc/ac converter. Stable control of the state variables under steady state conditions has been achieved with the dc bus voltage remaining within ±14% of the target for a very small (20μF) bus capacitor.

Under transient conditions the simulations have shown that the control strategy quickly moves the state variables to the new target. For the transient conditions considered, the speed of response was in the order of just a few milliseconds.

A simple vector based control strategy has been implemented for the inverter control which is switched to produce sinusoidal load current waveforms. The load current waveforms are smoother than the supply current waveforms due to the relative size of the line inductances.

CHAPTER 7
CONCLUSION

An analysis of the three phase switched rectifier has allowed the development of rectifier control strategies that utilise the shape of the system trajectories to achieve stable control at the target.

The analysis of the trajectories for the state variables and application of them to control were introduced for a simple dc source circuit in Chapter 2. In this case the active mode trajectories were found to be circular and the zero mode trajectories straight lines. A balance of power occurs on the line through the origin and the centre of the circular trajectory. For operating points on the line of power balance and above the centre of the circular trajectories stable control is possible by taking advantage of the shape of the circular and straight line trajectories.

An analysis of the three phase ac/dc rectifier, which was based on a simplified circuit with constant supply voltage and output current, showed that the active mode trajectories for the rectifier state variables are helical. The direction and rate of drift for the helices is proportional to the component of the supply current vector perpendicular to the supply voltage vector. The height of the centre of the trajectory above the current plane is proportional to the component of the supply current vector parallel to the supply voltage vector.

For the case where the supply voltage vector is aligned with a rectifier switching vector, the drift of the trajectory is zero and the trajectory becomes a circle in the dc bus voltage and in phase current plane. It has also been shown that it is possible to achieve circular trajectories for any position of the supply voltage vector by using a combination of the switching modes adjacent to the supply voltage vector.

The zero mode trajectories have been shown to be straight lines perpendicular to the line through the centre of the active mode trajectories.

Rectifier control strategies have been developed which take advantage of the shape of the circular and straight line trajectories.

The first stage of the control has involved the selection of target values for the state variables; that is for the capacitor voltage and supply current. The selection of the target has been based on the control aims which include unity power factor and stable control of the state variables. The target value of capacitor voltage is specified by the requirements of the system and is a constant. The target value of the out of phase current (i_q) is zero in order to achieve unity power factor. An assessment of the rectifier maintainability has been conducted to allow selection of target values for the in phase current (i_d) which represents the magnitude of the supply current vector reference. Maintainability has been presented as a method of identification of target points which allow stable control. Rectifier maintainability has been assessed based on the position of the operating points relative to the regions defined by the rectifier trajectories. These regions have been shown to be hexagons in a plane in the ($\underline{i}$, v_{cap}) space. When the

maintainable operating points are related to the rectifier trajectories, they are shown to be those on the line through the centre of the circular active mode trajectories and above the circle centre.

Several control strategies which take advantage of the shape of the rectifier trajectories to achieve stable control at maintainable points have been presented. These strategies are used to select the switching mode to be applied at each switching interval. Simulations have been presented which show that the strategies are capable of stable control of the rectifier both as a stand-alone unit and also as the input stage of an ac/dc/ac converter under steady state and transient conditions.

The control strategies presented have been assessed based on a fixed switching frequency which allows these techniques to be applied to the control of a converter employing a resonant dc link.

PUBLICATIONS OF WORK PERFORMED AS PART OF THIS THESIS

[1] **Murdoch, L.J., Platt, D, Gosbell, V.J.,** "*Dynamic behaviour of a high-frequency switched rectifier*", AUPEC, Vol. 3, September 1994, pp. 536-541.

[2] **Murdoch, L.J., Gosbell, V.J., Platt, D,** "*Dynamic behaviour and control of a high-frequency switched rectifier*", AUPEC, Vol. 1, October 1996, pp. 157-162.

REFERENCES

[1] **Ooi, B.T., Salmon, J.C., Dixon, J.W., Kulkarni, A.B.**, "*A 3-phase controlled current PWM converter with leading power factor*", IEEE Industry Applications Society Annual Meeting Conference Record, October 1985, pp. 1008-1014.

[2] **Ooi, B.T., Dixon, J.W., Kulkarni, A.B., Nishimoto, M.**, "*An integrated ac drive system using a controlled-current PWM rectifier/inverter link*", IEEE Power Electronics Specialists Conference, June 1986, pp. 494-501.

[3] **Dixon, J.W., Kulkarni, A.B., Nishimoto, M., Ooi, B.T.**, "*Characteristics of a controlled-current PWM rectifier-inverter link*", IEEE Industry Applications Society Annual Meeting Conference Record, October 1986, pp. 685-691.

[4] **Nishimoto, M., Dixon, J.W., Kulkarni, A.B., Ooi, B.T.**, "*An integrated controlled-current PWM rectifier chopper link for sliding mode position control*", IEEE Industry Applications Society Annual Meeting Conference Record, October 1986, pp. 752-757.

[5] **Wu, R., Dewan, S.B., Slemon, G.R.**, "*A PWM ac-to-dc converter with fixed switching frequency*", IEEE Transactions on Industy Applications, Vol. 26, No. 5, September/October 1990, pp. 880-885.

[6] **Wu, R., Dewan, S.B., Slemon, G.R.**, "*Analysis of a PWM ac to dc voltage source converter under the predicted current control with a fixed switching frequency*", IEEE Transactions on Industy Applications, Vol. 27, No. 4, July/August 1991, pp. 756-764.

[7] **Chen, L., Blaabjerg, F.**, "*A three-phase predictive PWM ac/dc converter with phase compensation and space vector control*", IEEE Applied Power Electronics Conference, Vol. 2, 1995, pp. 863-869.

[8] **Habetler, T.G.**, "*A space vector-based rectifier regulator for ac/dc/ac converters*", IEEE Transactions on Power Electronics, Vol. 8, No. 1, January 1993, pp. 30-36.

[9] **Kim, J.S., Sul, S.K.**, "*New control scheme for ac-dc-ac converter without dc link electrolytic capacitor*", IEEE Power Electronics Specialists Conference, 1993, pp. 300-306.

[10] **Malesani, L., Rossetto, L., Tenti, P., Tomasin, P.**, "*AC/DC/AC PWM converter with reduced energy storage in the dc link*", IEEE Transactions on Industy Applications, Vol. 31, No. 2, March/April 1995, pp. 287-292.

[11] **Dixon, J.W., Ooi, B.T.**, "*Indirect current control of a unity power factor sinusoidal current boost type three-phase rectifier*", IEEE Transactions on Industrial Electronics, Vol. 35, No. 4, November 1988, pp. 508-515.

[12] **Wernekinck, E., Kawamura, A., Hoft, R.**, "*A high frequency ac/dc converter with unity power factor and minimum harmonic distortion*", IEEE Transactions on Power Electronics, Vol. 6, No. 3, July 1991, pp. 364-370.

[13] **Wu, R., Dewan, S.B., Slemon, G.R.**, "*Analysis of an ac-to-dc voltage source converter using PWM with phase and amplitude control*", IEEE Transactions on Industy Applications, Vol. 27, No. 2, March/April 1991, pp. 355-364.

[14] **Divan, D.M.**, "*The resonant dc link converter-A new concept in static power conversion*", IEEE Transactions on Industy Applications, Vol. 25, No. 2, March/April 1989, pp. 317-325.

[15] **Habetler, T.G., Divan, D.M.**, "*Angle controlled current regulated rectifiers for ac/ac converters*", IEEE Transactions on Power Electronics, Vol. 6, No. 3, July 1991, pp. 463-469.

[16] **Choi, J.W., Sul, S.K.**, "*New current control concept-Minimum time current control in the three-phase PWM converter*", IEEE Transactions on Power Electronics, Vol. 12, No. 1, January 1997, pp. 124-131.

APPENDIX A

DERIVATION OF RECTIFIER EQUATIONS

The equations for the rectifier state variables are reproduced below.

$$\frac{\mathrm{d}\underline{i}}{\mathrm{dt}} = \frac{1}{L}\left(\underline{e} - \underline{S}v_{cap}\right) \tag{A1}$$

$$\frac{\mathrm{d}v_{cap}}{\mathrm{dt}} = \frac{1}{C}\left(\frac{2}{3}\underline{S}\cdot\underline{i} - i_{out}\right) \tag{A2}$$

The derivation of these equations is based on Kirchhoff's Voltage Law:

$$e_a = L\frac{\mathrm{d}i_a}{\mathrm{dt}} + s_a v_P + \left(1 - s_a\right)v_N \tag{A3}$$

Similarly for e_b and e_c:

$$e_b = L\frac{\mathrm{d}i_b}{\mathrm{dt}} + s_b v_P + \left(1 - s_b\right)v_N \tag{A4}$$

$$e_c = L\frac{\mathrm{d}i_c}{\mathrm{dt}} + s_c v_P + \left(1 - s_c\right)v_N \tag{A5}$$

Since

$$\begin{aligned} e_a &= e_{ab} + e_b \\ &= e_c - e_{ca} \end{aligned}$$

substitute in for e_a, e_b and e_c from Equations A3, A4 and A5:

$$L\frac{di_a}{dt} + s_a v_P + \left(1 - s_a\right)v_N = e_{ab} + L\frac{di_b}{dt} + s_b v_P + \left(1 - s_b\right)v_N$$

$$L\frac{di_a}{dt} + s_a v_P + (1 - s_a)v_N = L\frac{di_c}{dt} + s_c v_P + (1 - s_c)v_N - e_{ca}$$

Adding:

$$e_{ab} - e_{ca} = L\frac{d}{dt}(2i_a - i_b - i_c) + v_P(2s_a - s_b - s_c) - v_N(2s_a - s_b - s_c) \quad \text{(A6)}$$

From Kirchhoff's Current Law:

$$i_a + i_b + i_c = 0$$

Therefore

$$(-i_b - i_c) = i_a$$

Substitute into Equation A6:

$$(e_{ab} - e_{ca}) = 3L\frac{di_a}{dt} + (v_P - v_N)(2s_a - s_b - s_c) \quad \text{(A7)}$$

But

$$(v_p - v_N) = v_{cap}$$

and

$$\frac{di_a}{dt} = \frac{2}{3}\frac{di_\alpha}{dt}$$

So Equation A7 becomes

$$(e_{ab} - e_{ca}) = 2L\frac{di_\alpha}{dt} + v_{cap}(2s_a - s_b - s_c)$$

Rearranging gives

$$\frac{di_\alpha}{dt} = \frac{1}{2L}\left(e_{ab} - e_{ca}\right) - \frac{v_{cap}}{2L}\left(2s_a - s_b - s_c\right) \tag{A8}$$

Subtract Equations A4 and A5:

$$e_b - e_c = L\frac{d}{dt}\left(i_b - i_c\right) + v_P\left(s_b - s_c\right) - v_N\left(s_b - s_c\right) \tag{A9}$$

Since

$$e_b - e_c = e_{bc}$$

and

$$\left(v_p - v_N\right) = v_{cap}$$

Equation A9 becomes:

$$e_{bc} = L\frac{d}{dt}\left(i_b - i_c\right) + v_{cap}\left(s_b - s_c\right)$$

Since

$$\frac{d}{dt}\left(i_b - i_c\right) = \frac{2}{\sqrt{3}}\frac{di_\beta}{dt}$$

$$e_{bc} = \frac{2L}{\sqrt{3}}\frac{di_\beta}{dt} + v_{cap}\left(s_b - s_c\right)$$

Rearranging gives

$$\frac{di_\beta}{dt} = \frac{\sqrt{3}}{2L}e_{bc} - \frac{\sqrt{3}}{2L}v_{cap}\left(s_b - s_c\right) \tag{A10}$$

Equations A8 and A10 can be combined:

$$\begin{aligned}\frac{d\underline{i}}{dt} &= \frac{di_\alpha}{dt} + j\frac{di_\beta}{dt} \\ &= \frac{1}{2L}\left(e_{ab} - e_{ca}\right) - \frac{v_{cap}}{2L}\left(2s_a - s_b - s_c\right) + j\frac{\sqrt{3}}{2L}e_{bc} - j\frac{\sqrt{3}}{2L}v_{cap}\left(s_b - s_c\right)\end{aligned} \tag{A11}$$

Let

$$\begin{aligned}\underline{e} &= e_\alpha + je_\beta \\ &= e_a + e_b e^{j\frac{2\pi}{3}} + e_c e^{j\frac{4\pi}{3}} \\ &= \frac{3}{2}e_a + j\frac{\sqrt{3}}{2}\left(e_b - e_c\right) \\ &= \frac{1}{2}\left(e_{ab} - e_{ca}\right) + j\frac{\sqrt{3}}{2}e_{bc}\end{aligned}$$

$$\begin{aligned}\underline{S} &= s_\alpha + js_\beta \\ &= s_a + s_b e^{j\frac{2\pi}{3}} + s_c e^{j\frac{4\pi}{3}} \\ &= \frac{1}{2}\left(2s_a - s_b - s_c\right) + j\frac{\sqrt{3}}{2}\left(s_b - s_c\right)\end{aligned}$$

Applying a vector transformation, Equation A11 becomes:

$$\frac{d\underline{i}}{dt} = \frac{1}{L}\left(\underline{e} - \underline{S}v_{cap}\right)$$

as required.

From Kirchhoff's Current Law:

$$i_{cap} = C\frac{\mathrm{d}v_{cap}}{\mathrm{dt}} = s_a i_a + s_b i_b + s_c i_c - i_{out} \tag{A12}$$

Since:

$$i_a = \frac{2}{3} i_\alpha$$

$$i_b = -\frac{i_\alpha}{3} + \frac{i_\beta}{\sqrt{3}}$$

$$i_c = -\frac{i_\alpha}{3} - \frac{i_\beta}{\sqrt{3}}$$

Substitution into Equation A12 gives

$$\begin{aligned} C\frac{\mathrm{d}v_{cap}}{\mathrm{dt}} &= \left(\frac{2}{3}s_a - \frac{s_b}{3} - \frac{s_c}{3}\right)\mathrm{Re}(\underline{i}) + \left(\frac{s_b}{\sqrt{3}} - \frac{s_c}{\sqrt{3}}\right)\mathrm{Im}(\underline{i}) - i_{out} \\ &= \frac{2}{3}\left\{\mathrm{Re}(\underline{S}) \times \mathrm{Re}(\underline{i}) + \mathrm{Im}(\underline{S}) \times \mathrm{Im}(\underline{i})\right\} - i_{out} \\ &= \frac{2}{3}\underline{S} \cdot \underline{i} - i_{out} \end{aligned}$$

Rearranging:

$$\frac{\mathrm{d}v_{cap}}{\mathrm{dt}} = \frac{1}{C}\left(\frac{2}{3}\underline{S} \cdot \underline{i} - i_{out}\right)$$

as required.

APPENDIX B

DERIVATION OF RECTIFIER DECOUPLED EQUATIONS

The decoupled equations for the rectifier state variables are reproduced below.

$$LC\frac{\mathrm{d}^2 i_{par}}{\mathrm{dt}^2} = C\frac{\mathrm{d}e_{par}}{\mathrm{dt}} - \left(\frac{2}{3}i_{par} - i_{out}\right) \tag{B1}$$

$$LC\frac{\mathrm{d}^2 v_{cap}}{\mathrm{dt}^2} = \frac{2}{3}\left(e_{par} - v_{cap}\right) - L\frac{\mathrm{d}i_{out}}{\mathrm{dt}} \tag{B2}$$

$$\frac{\mathrm{d}i_{perp}}{\mathrm{dt}} = \frac{e_{perp}}{L} \tag{B3}$$

The derivation of these equations is given below. From Appendix A:

$$\frac{\mathrm{d}\underline{i}}{\mathrm{dt}} = \frac{1}{L}\left(\underline{e} - \underline{S}v_{cap}\right)$$

$$\frac{\mathrm{d}v_{cap}}{\mathrm{dt}} = \frac{1}{C}\left(\frac{2}{3}\underline{S}\cdot\underline{i} - i_{out}\right)$$

These equations can be expressed in terms of the projections of $\underline{S}$, $\underline{i}$ and $\underline{e}$ parallel and perpendicular to $\underline{S}$:

$$\frac{\mathrm{d}i_{par}}{\mathrm{dt}} = \frac{1}{L}\left(e_{par} - v_{cap}\right) \tag{B4}$$

$$\frac{\mathrm{d}i_{perp}}{\mathrm{dt}} = \frac{e_{perp}}{L} \tag{B5}$$

$$\frac{dv_{cap}}{dt} = \frac{1}{C}\left(\frac{2}{3}i_{par} - i_{out}\right) \tag{B6}$$

Differentiate Equation B4:

$$\frac{d^2 i_{par}}{dt^2} = \frac{1}{L}\left(\frac{de_{par}}{dt} - \frac{dv_{cap}}{dt}\right)$$

Substitute Equation B6:

$$\frac{d^2 i_{par}}{dt^2} = \frac{1}{L}\left(\frac{de_{par}}{dt} - \frac{1}{C}\left(\frac{2}{3}i_{par} - i_{out}\right)\right)$$

Rearrange:

$$LC\frac{d^2 i_{par}}{dt^2} = C\frac{de_{par}}{dt} - \left(\frac{2}{3}i_{par} - i_{out}\right)$$

Equation B5 is already decoupled:

$$\frac{di_{perp}}{dt} = \frac{e_{perp}}{L}$$

Differentiate Equation B6:

$$\frac{d^2 v_{cap}}{dt^2} = \frac{1}{C}\left(\frac{2}{3}\frac{di_{par}}{dt} - \frac{di_{out}}{dt}\right)$$

Substitute Equation B4:

$$\frac{d^2 v_{cap}}{dt^2} = \frac{1}{C}\left(\frac{2}{3}\frac{1}{L}\left(e_{par} - v_{cap}\right) - \frac{di_{out}}{dt}\right)$$

Rearrange:

$$LC\frac{\mathrm{d}^2 v_{cap}}{\mathrm{dt}^2} = \frac{2}{3}\left(e_{par} - v_{cap}\right) - L\frac{\mathrm{d}i_{out}}{\mathrm{dt}}$$

APPENDIX C

RECTIFIER EQUATIONS

If it is assumed that:

- the supply voltage is constant ($\underline{E}$)
- the output current is constant (I_{out})
- the supply is balanced

Then equations for the state variables for the active switching modes are given by:

$$i_1(t) = \frac{(E_1 - E_2)t}{2L} + \frac{(i_{10} - i_{20})}{2} - \frac{3E_3}{4Z}\sin\omega t - \frac{i_{30}}{2}\cos\omega t + S\frac{v_{cap0}}{2Z}\sin\omega t - S\frac{I_{out}}{2}(1 - \cos\omega t)$$

$$i_2(t) = \frac{(E_2 - E_1)t}{2L} + \frac{(i_{20} - i_{10})}{2} - \frac{3E_3}{4Z}\sin\omega t - \frac{i_{30}}{2}\cos\omega t + S\frac{v_{cap0}}{2Z}\sin\omega t - S\frac{I_{out}}{2}(1 - \cos\omega t)$$

$$i_3(t) = \frac{3E_3}{2Z}\sin\omega t + i_{30}\cos\omega t - S\frac{v_{cap0}}{Z}\sin\omega t + SI_{out}(1 - \cos\omega t)$$

$$v_{cap}(t) = S\frac{3E_3}{2}(1 - \cos\omega t) + SZi_{30}\sin\omega t + v_{cap0}\cos\omega t - ZI_{out}\sin\omega t$$

where

$$\omega = \sqrt{\frac{2}{3LC}} \text{ and } Z = \sqrt{\frac{3L}{2C}} \text{ and}$$

Switching Mode		i_1	i_2	i_3	E_1	E_2	E_3
001	110	i_a	i_b	i_c	E_a	E_b	E_c
010	101	i_a	i_c	i_b	E_a	E_c	E_b
100	011	i_b	i_c	i_a	E_b	E_c	E_a
S=1	S=-1						

For the zero switching modes the state variables are given by:

$$i_a(t) = \frac{E_a t}{L} + i_{a0}$$

$$i_b(t) = \frac{E_b t}{L} + i_{b0}$$

$$i_c(t) = \frac{E_c t}{L} + i_{c0}$$

$$v_{cap}(t) = -\frac{I_{out} t}{C} + v_{cap0}$$

APPENDIX D

TRAJECTORIES FOR VARIABLE SUPPLY

The trajectories for the high-frequency rectifier that are presented in Chapter 3 are based on a constant supply voltage. In this appendix, an example of the rectifier trajectories for a variable supply voltage are presented and discussed.

It was shown in Chapter 3 that, when the supply voltage is assumed constant, the active mode trajectories are helical in the ($\underline{i}$, v_{cap}) space. For a particular active switching mode, the value of the capacitor voltage along the longitudinal axis of the helix is equal to E_{par}; the component of the supply voltage vector parallel to the switching vector. The rate of progression of the helix is proportional to E_{perp}; the perpendicular component.

When the supply voltage is variable, E_{par} and E_{perp} vary with time. For example, when the supply voltage is aligned with the switching vector, E_{par} is a maximum (equal to the magnitude of the supply voltage vector) and E_{perp} is equal to zero. As E_{par} changes, the centre of the helix for the active mode oscillates up and down. The changes in E_{perp} result in changes in the rate and direction of progression of the helix.

Figure D-1 shows an example of the active mode trajectories for modes 011 and 100. As the centre of one trajectory is raising, the centre of the complementary mode is falling. The helices progress in one direction and then reverse. The trajectory for the active mode 011 is shown in additional detail in the two-

dimensional projections in Figure D-2.

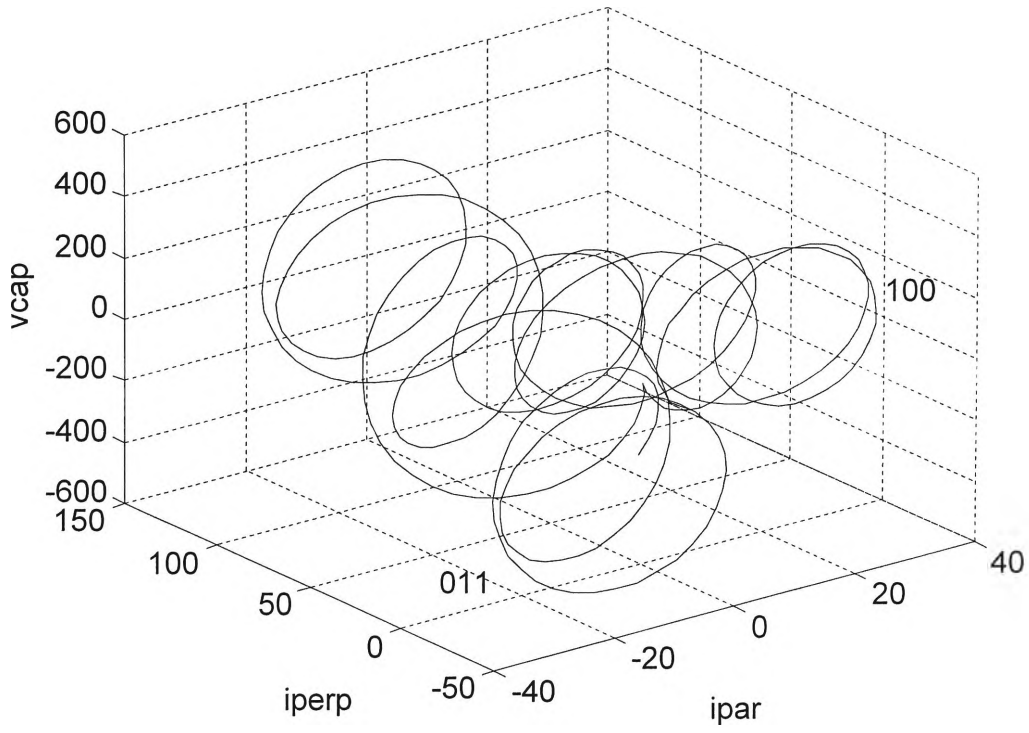

Figure D-1 Trajectories for modes 011 and 100 for variable supply

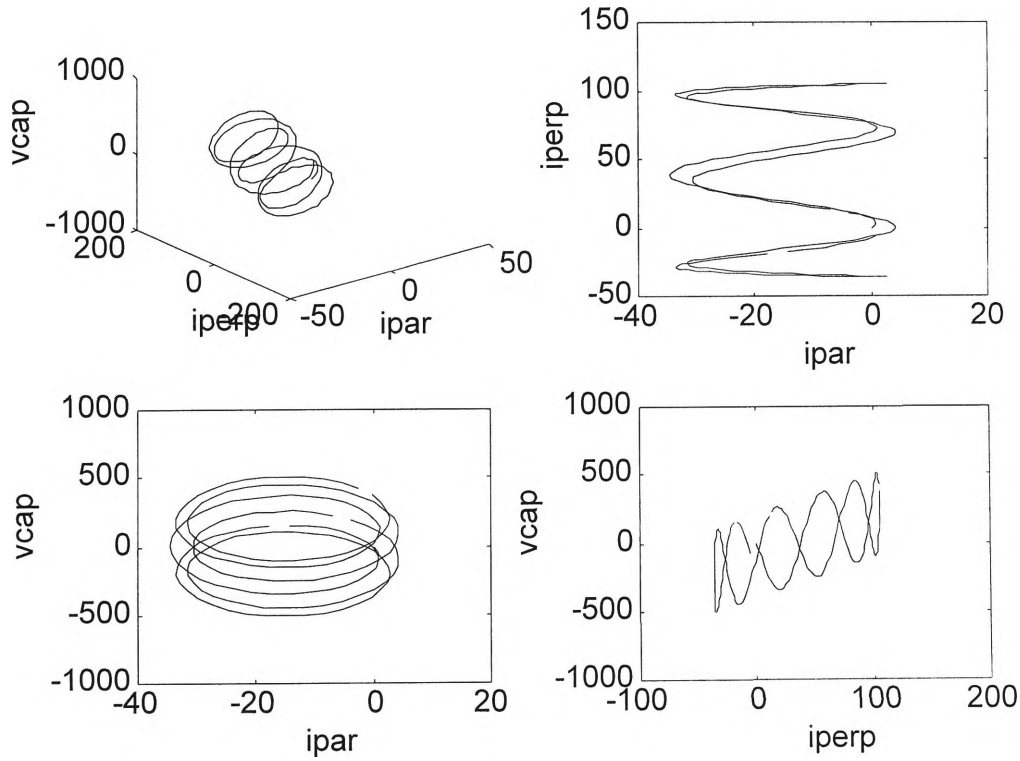

Figure D-2 Active mode trajectory for mode 011 with variable supply

When the supply voltage is assumed constant, the zero mode trajectories are straight lines. With a variable supply voltage the change in supply current for a zero mode is proportional to the supply voltage. As a result, the zero mode trajectories become helices; the plane of oscillation is the current plane, and the helices progress in the $-v_{cap}$ direction at a rate proportional to the rectifier output current. An example of the trajectories for a zero mode are shown in Figure D-3.

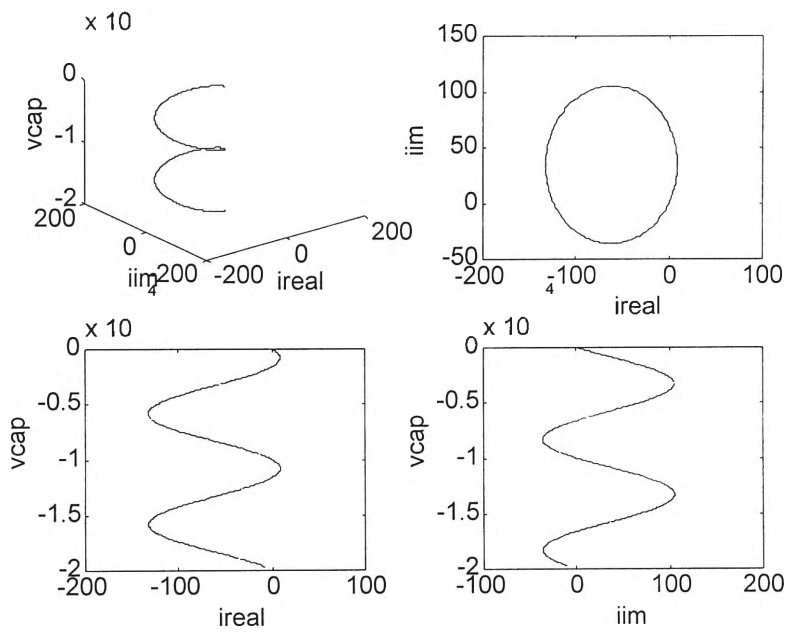

Figure D-3 Zero mode trajectory with variable supply

APPENDIX E

RECTIFIER SIMULATION RESULTS

E.1 Introduction

The results presented in this chapter are the results of Matlab simulations. For each of the control strategies presented in Chapter 5 the following conditions have been studied:

- Steady state conditions with no output current.
- Steady state conditions with full output current.
- Transient conditions with the output current ramping up and down.
- Transient conditions with a step increase and step decrease in the output current.

In all of the simulations the supply is a variable 50 Hz three phase waveform.

The results presented include graphs of capacitor voltage and supply currents. For each scenario a table summarises the performance of the control in terms of the maximum capacitor voltage and in phase supply current reached. For the cases where the output current undergoes a step change the time taken to reach the vicinity of the target is presented.

E.2 Model Characteristics

The characteristics of the variable supply model are described in Table E-1.

L	9mH
C	20μF
Capacitor voltage target	700V
Supply voltage	240Vrms L-N
Supply frequency	50Hz
Switching frequency	Fixed at 10kHz

Table E-1 Rectifier operating conditions – variable supply

For the transient scenarios with a ramping output current, the rate of change of output current is 5A/ms.

E.3 Steady State Conditions (Zero Load)

Optimal Control (Zero Load)

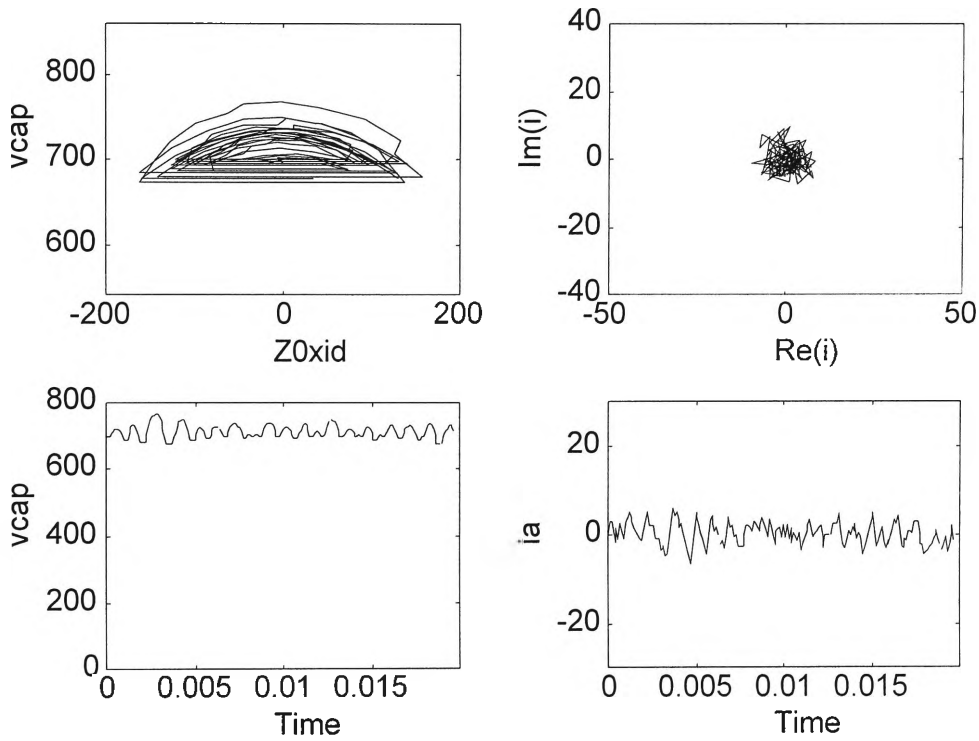

Figure E-1 – Optimal control simulation - zero load

(a) Graph of v_{cap} versus $Z_0 i_d$

(b) Graph of i_α versus i_β

(c) Graph of v_{cap} versus time

(d) Graph of i_a versus time

v_{cap} maximum	768.3	i_d maximum	9.1
v_{cap} minimum	673.4	i_d minimum	-9.4

Table E-2 Results

Hysteresis Control (Zero Load)

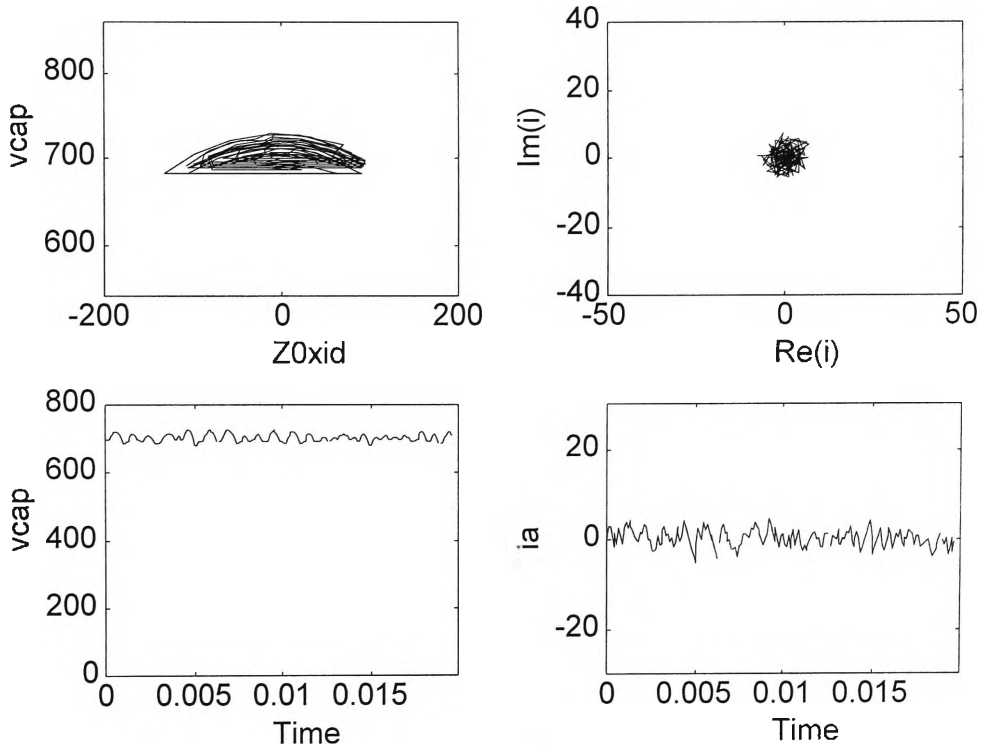

Figure E-2 – Hysteresis control simulation - zero load

(a) Graph of v_{cap} versus $Z_0 i_d$

(b) Graph of i_α versus i_β

(c) Graph of v_{cap} versus time

(d) Graph of i_a versus time

v_{cap} maximum	728.4	i_d maximum	5.5
v_{cap} minimum	682.8	i_d minimum	-7.7

Table E-3 Results

Chatter Control (Zero Load)

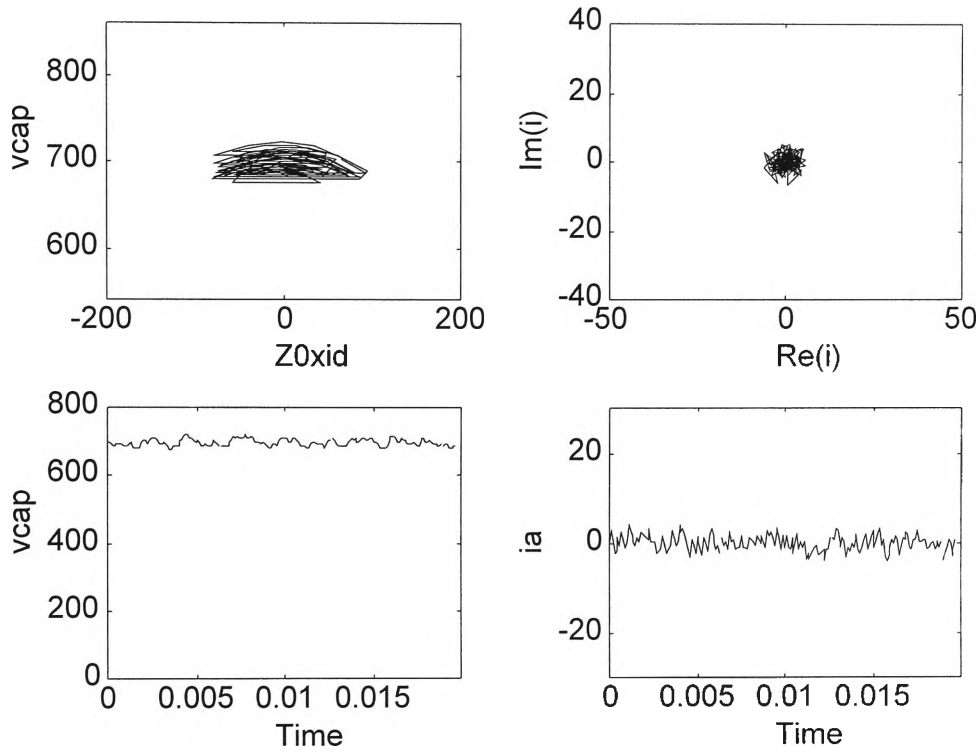

Figure E-3 – Chatter control simulation - zero load

(a) Graph of v_{cap} versus $Z_0 i_d$

(b) Graph of i_α versus i_β

(c) Graph of v_{cap} versus time

(d) Graph of i_a versus time

v_{cap} maximum	722.0	i_d maximum	5.5
v_{cap} minimum	675.8	i_d minimum	-4.7

Table E-4 Results

Simple Control (Zero Load)

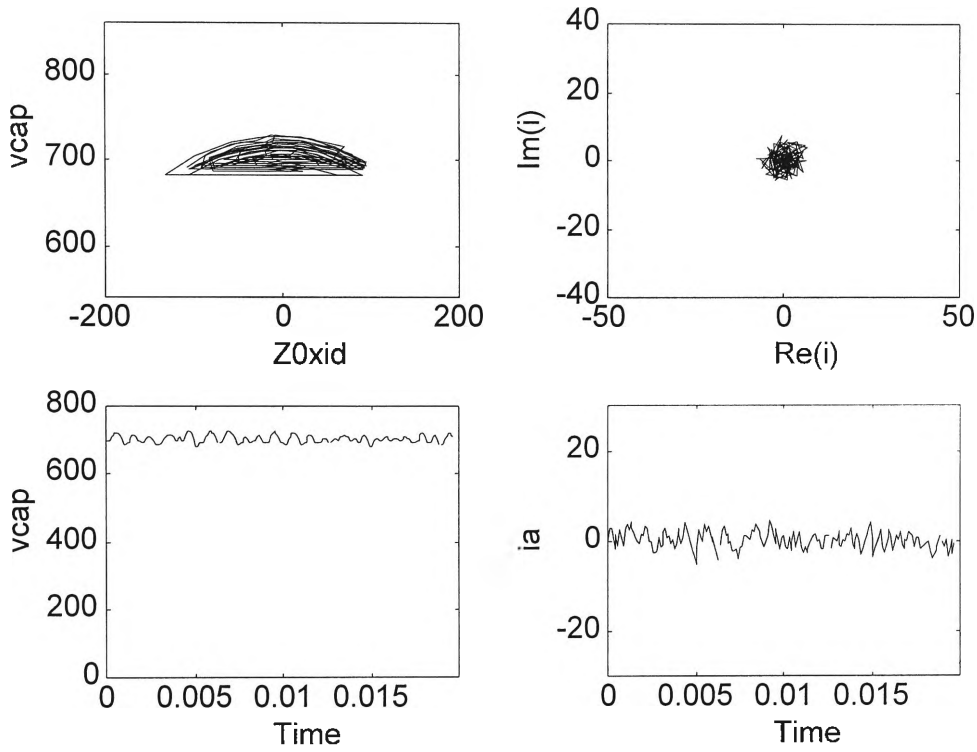

Figure E-4 – Simple control simulation - zero load

(a) Graph of v_{cap} versus $Z_0 i_d$

(b) Graph of i_α versus i_β

(c) Graph of v_{cap} versus time

(d) Graph of i_a versus time

v_{cap} maximum	728.4	i_d maximum	5.5
v_{cap} minimum	682.8	i_d minimum	-7.7

Table E-5 Results

E.4 Steady State Conditions (Full Load)

Optimal Control (Full Load)

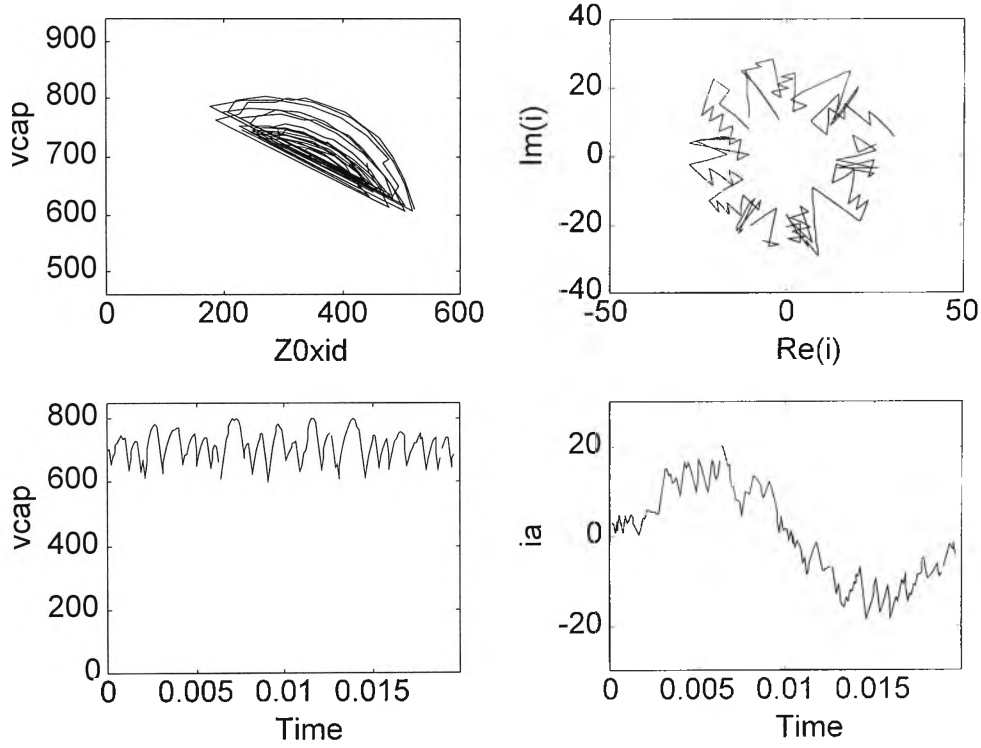

Figure E-5 – Optimal control simulation - full load

(a) Graph of v_{cap} versus $Z_0 i_d$

(b) Graph of i_α versus i_β

(c) Graph of v_{cap} versus time

(d) Graph of i_a versus time

v_{cap} maximum	803.2	i_d maximum	30.2
v_{cap} minimum	604.4	i_d minimum	10.1

Table E-6 Results

Hysteresis Control (Full Load)

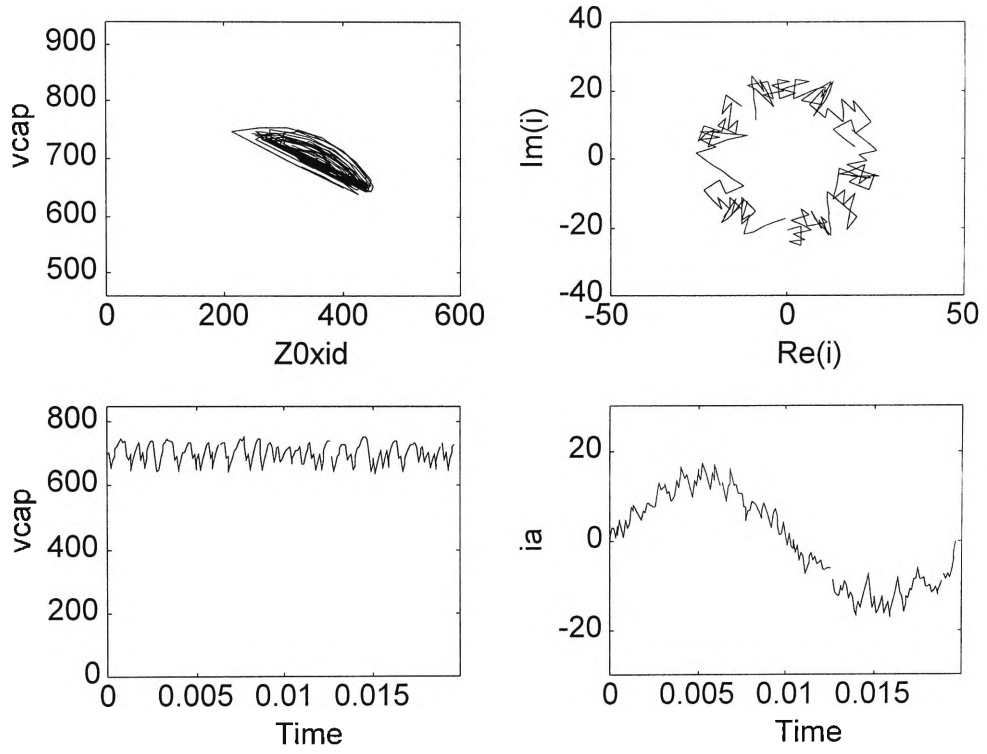

Figure E-6 – Hysteresis control simulation - full load

(a) Graph of v_{cap} versus $Z_0 i_d$

(b) Graph of i_α versus i_β

(c) Graph of v_{cap} versus time

(d) Graph of i_a versus time

v_{cap} maximum	755.2	i_d maximum	26.1
v_{cap} minimum	637.7	i_d minimum	12.2

Table E-7 Results

Chatter Control (Full Load)

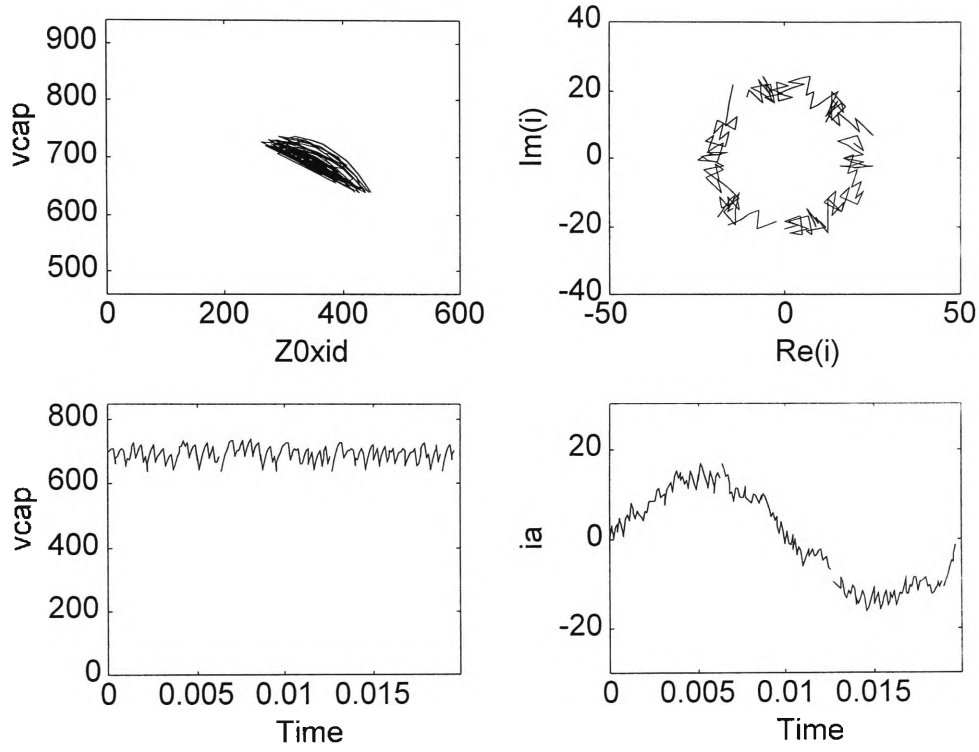

Figure E-7 – Chatter control simulation - full load

(a) Graph of v_{cap} versus $Z_0 i_d$

(b) Graph of i_α versus i_β

(c) Graph of v_{cap} versus time

(d) Graph of i_a versus time

v_{cap} maximum	738.6	i_d maximum	25.8
v_{cap} minimum	638.0	i_d minimum	15.2

Table E-8 Results

Simple Control (Full Load)

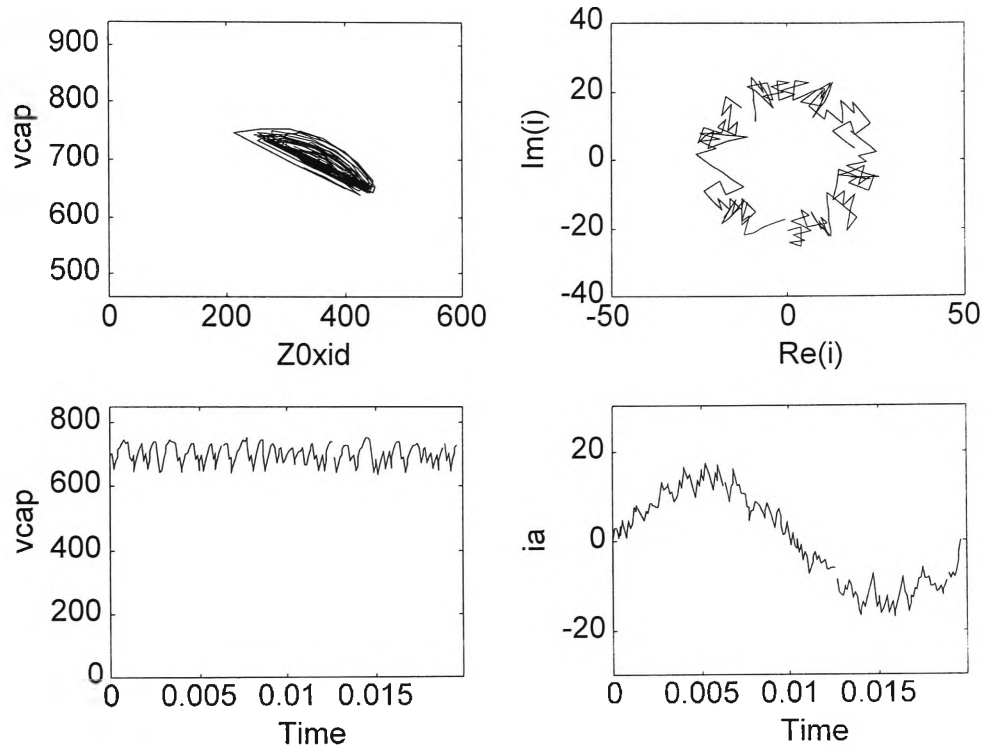

Figure E-8 – Simple control simulation - full load

(a) Graph of v_{cap} versus $Z_0 i_d$

(b) Graph of i_α versus i_β

(c) Graph of v_{cap} versus time

(d) Graph of i_a versus time

v_{cap} maximum	755.2	i_d maximum	26.1
v_{cap} minimum	637.7	i_d minimum	12.2

Table E-9 Results

E.5 Transient Conditions (Output Current Ramping Up)

Optimal Control (Output Current Ramping Up)

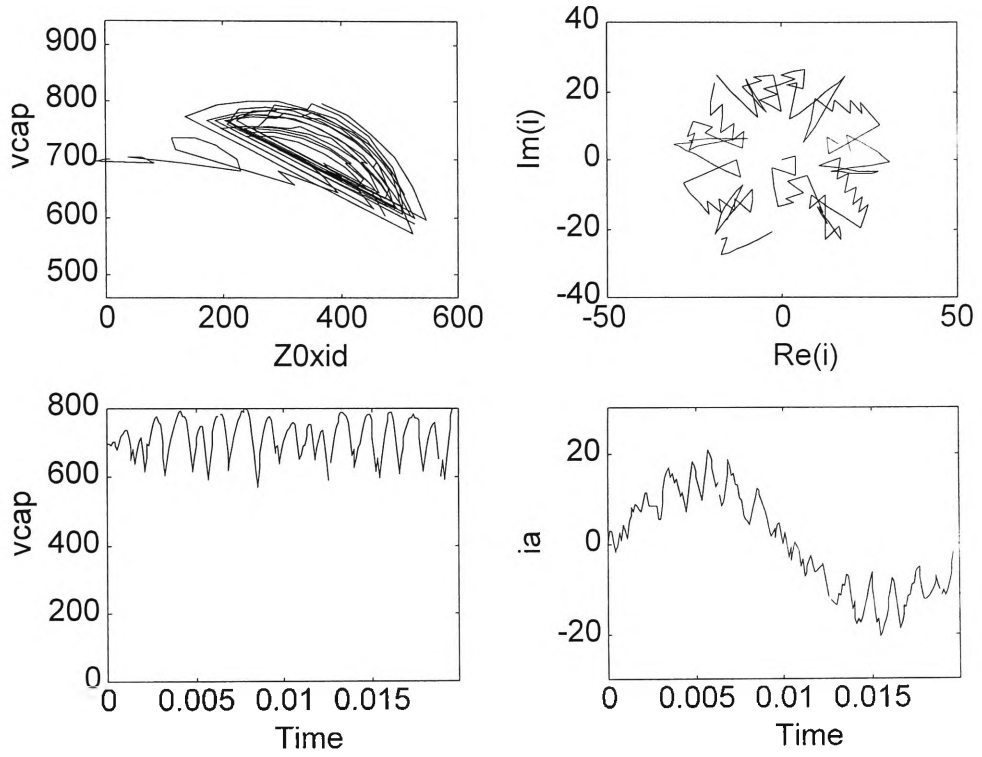

Figure E-9 – Optimal control simulation – output current ramping up

(a) Graph of v_{cap} versus $Z_0 i_d$ (b) Graph of i_α versus i_β
(c) Graph of v_{cap} versus time (d) Graph of i_a versus time

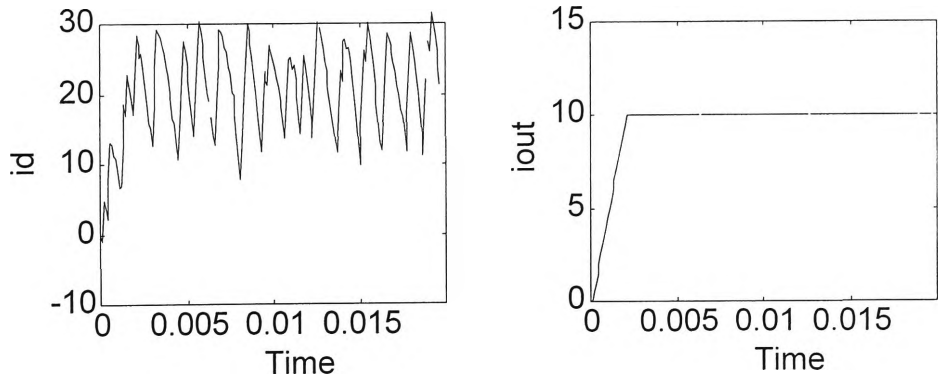

Figure E-10 – Optimal control simulation – output current ramping up

(a) Graph of i_d versus time (b) Graph of i_{out} versus time

v_{cap} maximum	808.3	i_d maximum	31.5
v_{cap} minimum	573.0	i_d minimum	-1.1

Table E-10 Results

Hysteresis Control (Output Current Ramping Up)

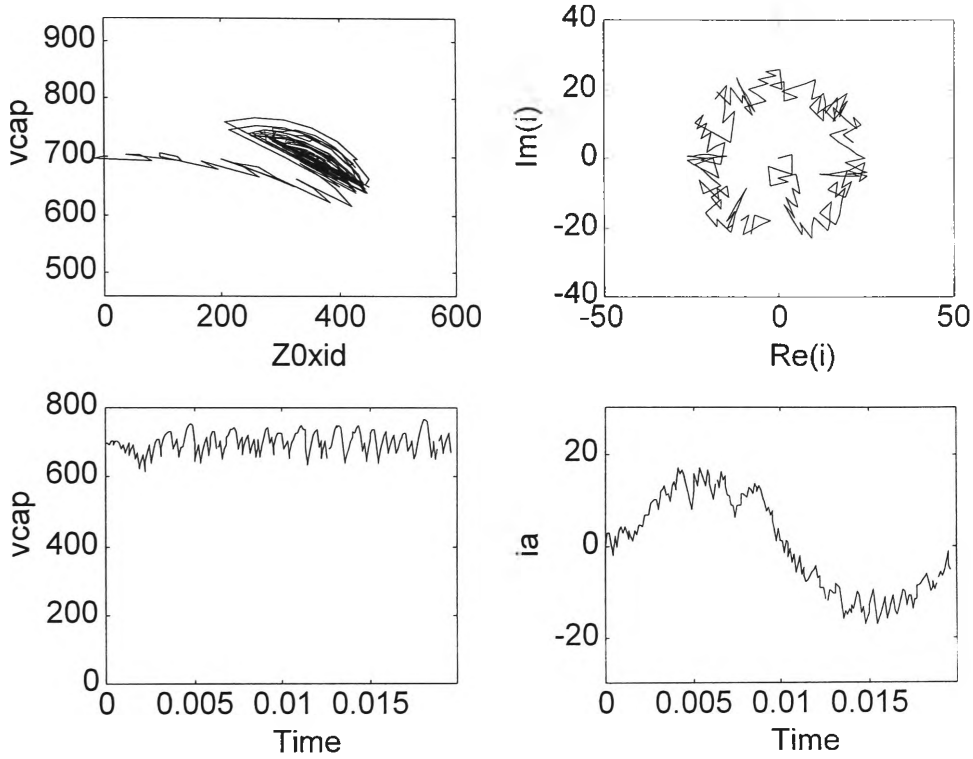

Figure E-11 – Hysteresis control simulation – output current ramping up

(a) Graph of v_{cap} versus $Z_0 i_d$ (b) Graph of i_α versus i_β

(c) Graph of v_{cap} versus time (d) Graph of i_a versus time

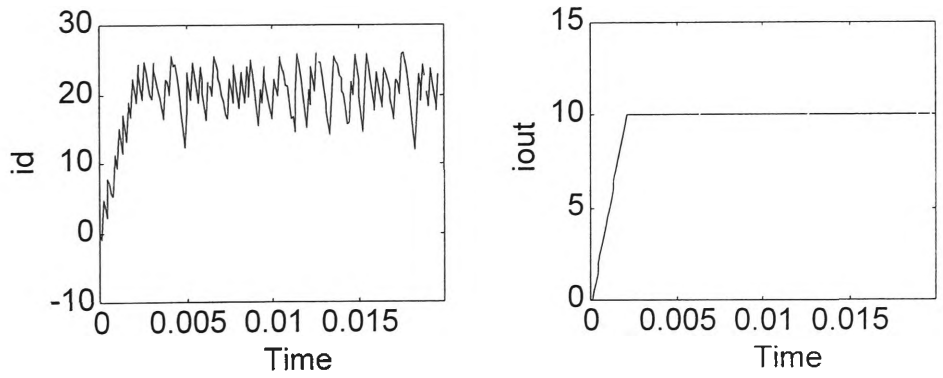

Figure E-12 – Hysteresis control simulation – output current ramping up

(a) Graph of i_d versus time (b) Graph of i_{out} versus time

v_{cap} maximum	766.9	i_d maximum	26.1
v_{cap} minimum	614.5	i_d minimum	-1.1

Table E-11 Results

Chatter Control (Output Current Ramping Up)

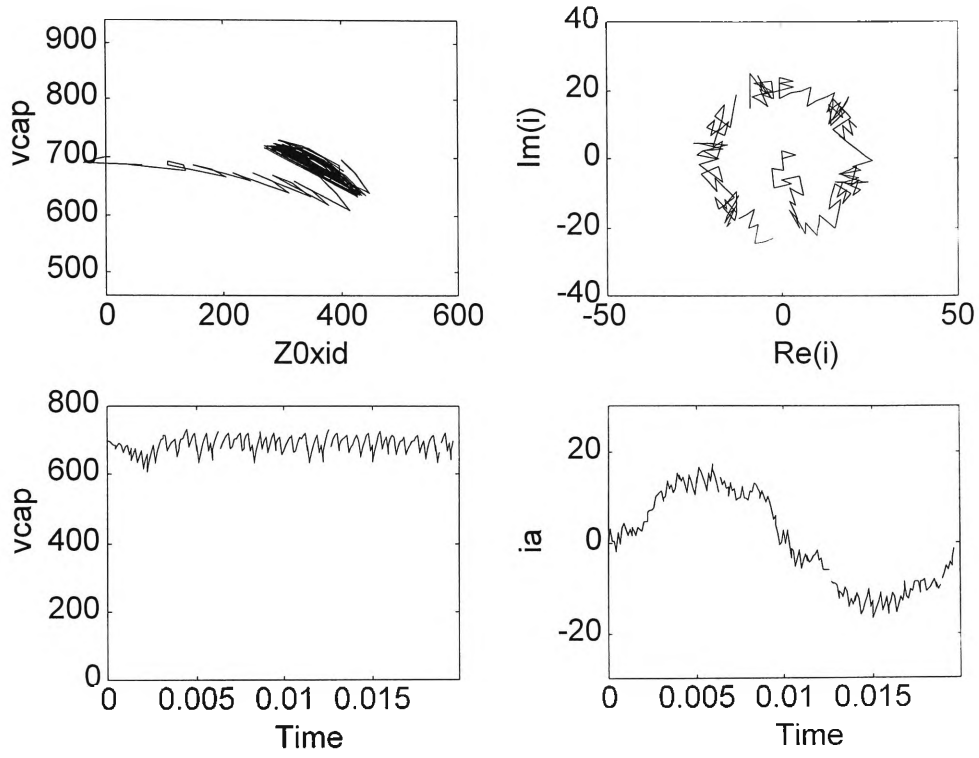

Figure E-13 – Chatter control simulation – output current ramping up

(a) Graph of v_{cap} versus $Z_0 i_d$

(b) Graph of i_α versus i_β

(c) Graph of v_{cap} versus time

(d) Graph of i_a versus time

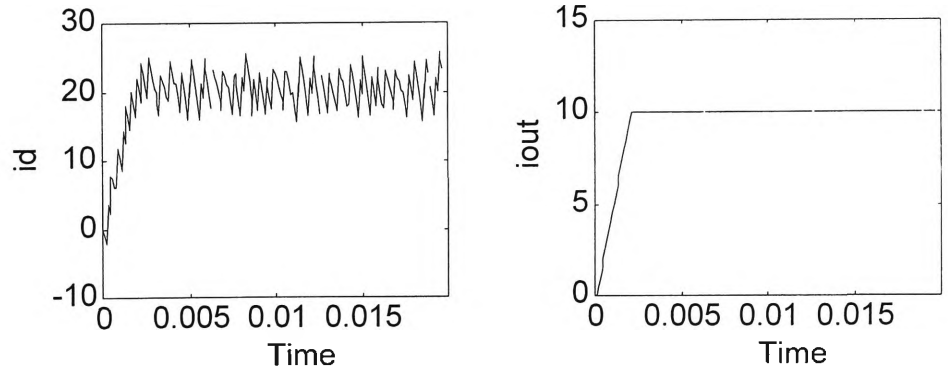

Figure E-14 – Chatter control simulation – output current ramping up

(a) Graph of i_d versus time

(b) Graph of i_{out} versus time

v_{cap} maximum	732.5	i_d maximum	25.8
v_{cap} minimum	609.6	i_d minimum	-2.1

Table E-12 Results

Simple Control (Output Current Ramping Up)

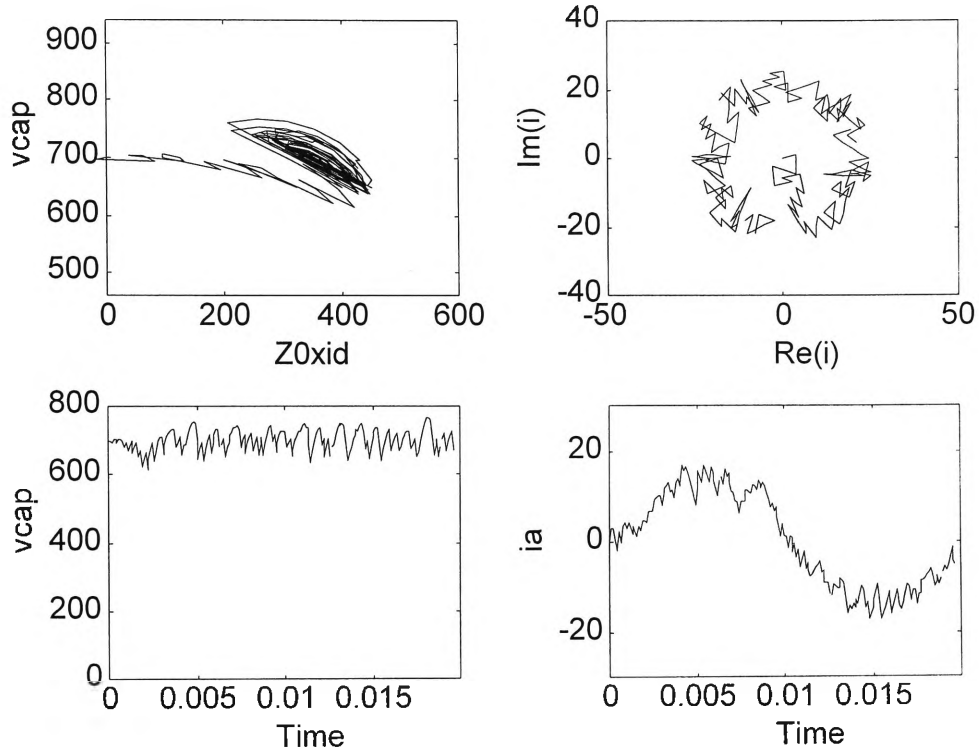

Figure E-15 – Simple control simulation – output current ramping up

(a) Graph of v_{cap} versus $Z_0 i_d$

(b) Graph of i_α versus i_β

(c) Graph of v_{cap} versus time

(d) Graph of i_a versus time

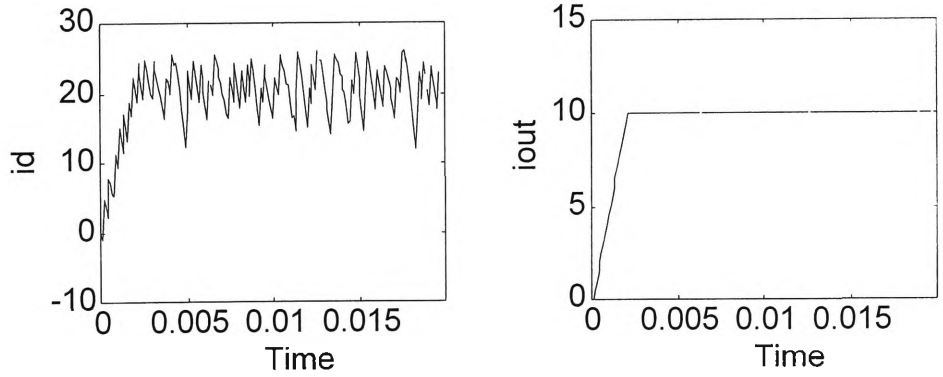

Figure E-16 – Simple control simulation – output current ramping up

(a) Graph of i_d versus time

(b) Graph of i_{out} versus time

v_{cap} maximum	766.9	i_d maximum	26.1
v_{cap} minimum	614.5	i_d minimum	-1.1

Table E-13 Results

E.6 Transient Conditions (Output Current Ramp Down)

Optimal Control (Output Current Ramping Down)

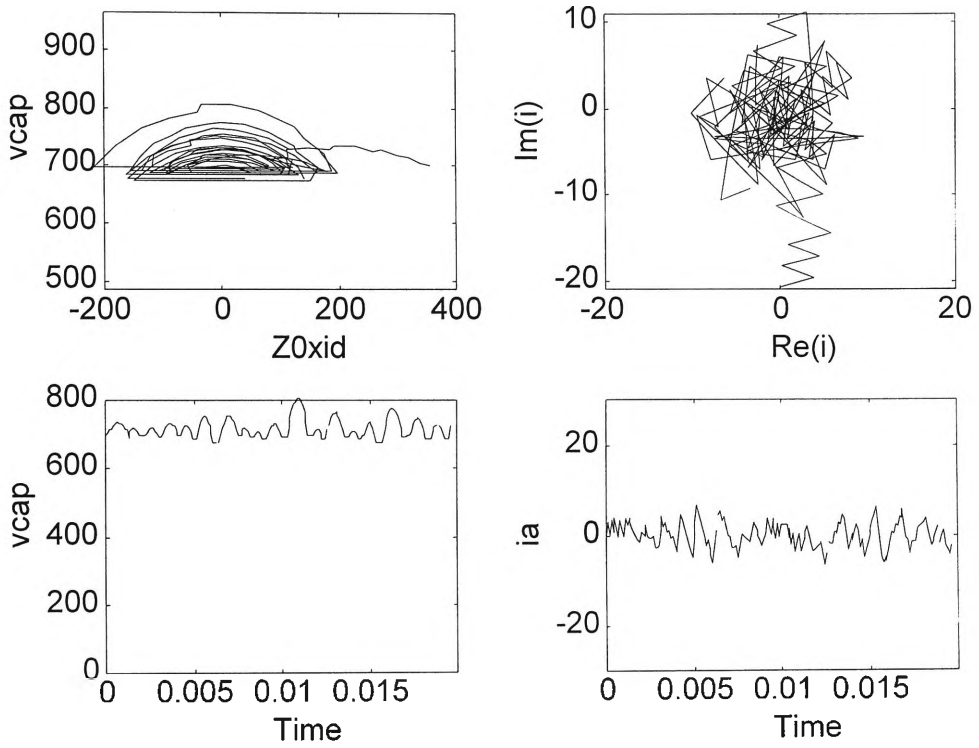

Figure E-17 – Optimal control simulation – output current ramping down

(a) Graph of v_{cap} versus $Z_0 i_d$ (b) Graph of i_α versus i_β
(c) Graph of v_{cap} versus time (d) Graph of i_a versus time

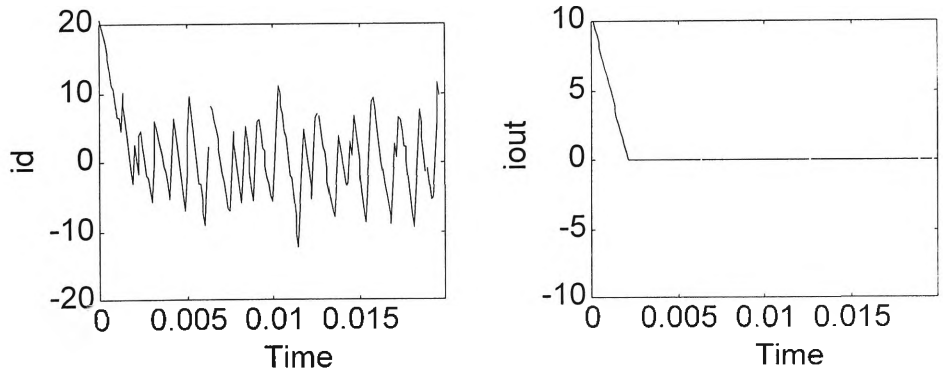

Figure E-18 – Optimal control simulation – output current ramping down

(a) Graph of i_d versus time (b) Graph of i_{out} versus time

v_{cap} maximum	805.9	i_d maximum	20.6
v_{cap} minimum	674.0	i_d minimum	-12.5

Table E-14 Results

Hysteresis Control (Output Current Ramping Down)

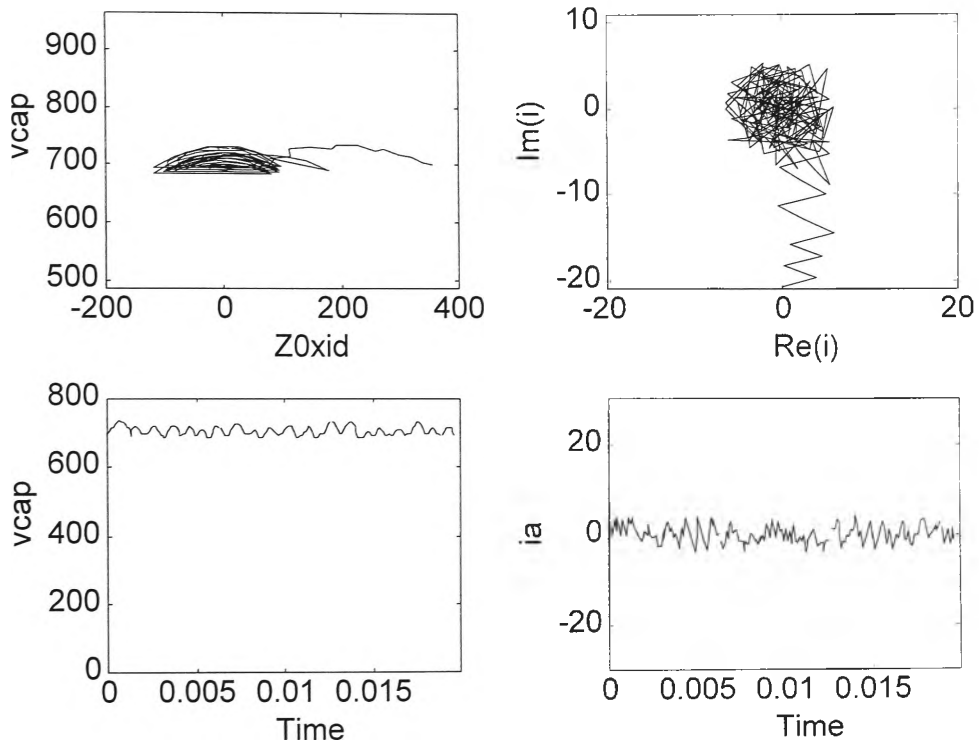

Figure E-19 – Hysteresis control simulation – output current ramping down

(a) Graph of v_{cap} versus $Z_0 i_d$

(b) Graph of i_α versus i_β

(c) Graph of v_{cap} versus time

(d) Graph of i_a versus time

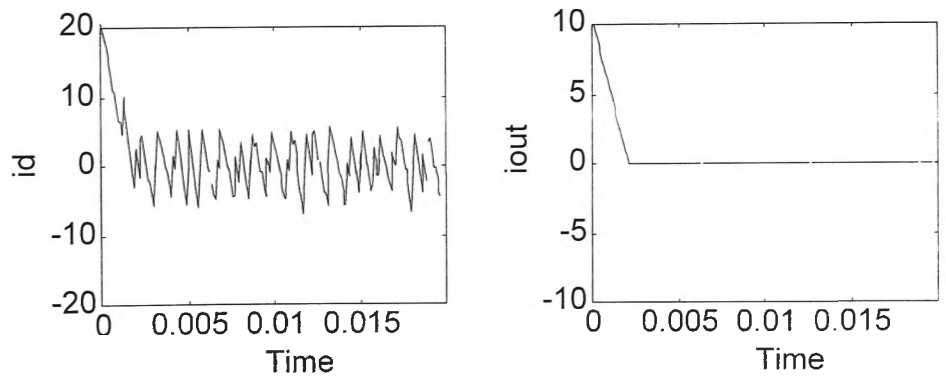

Figure E-20 – Hysteresis control simulation – output current ramping down

(a) Graph of i_d versus time

(b) Graph of i_{out} versus time

v_{cap} maximum	735.5	i_d maximum	20.6
v_{cap} minimum	684.2	i_d minimum	-6.9

Table E-15 Results

Chatter Control (Output Current Ramping Down)

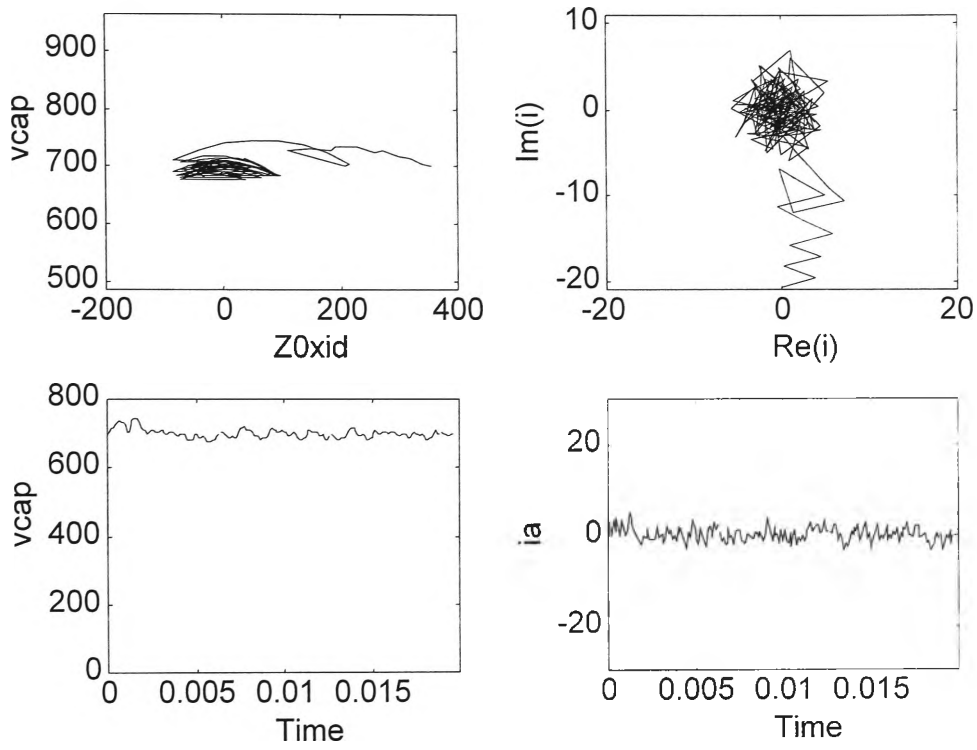

Figure E-21 – Chatter control simulation – output current ramping down

(a) Graph of v_{cap} versus $Z_0 i_d$ (b) Graph of i_α versus i_β

(c) Graph of v_{cap} versus time (d) Graph of i_a versus time

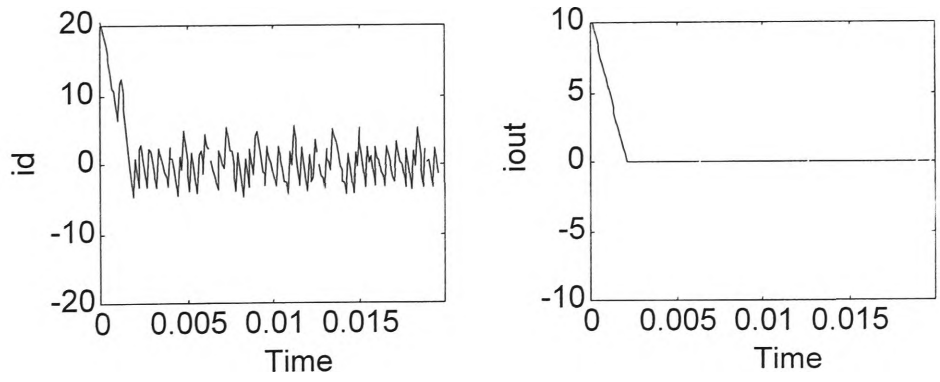

Figure E-22 – Chatter control simulation – output current ramping down

(a) Graph of i_d versus time (b) Graph of i_{out} versus time

v_{cap} maximum	746.1	i_d maximum	20.6
v_{cap} minimum	676.2	i_d minimum	-4.9

Table E-16 Results

Simple Control (Output Current Ramping Down)

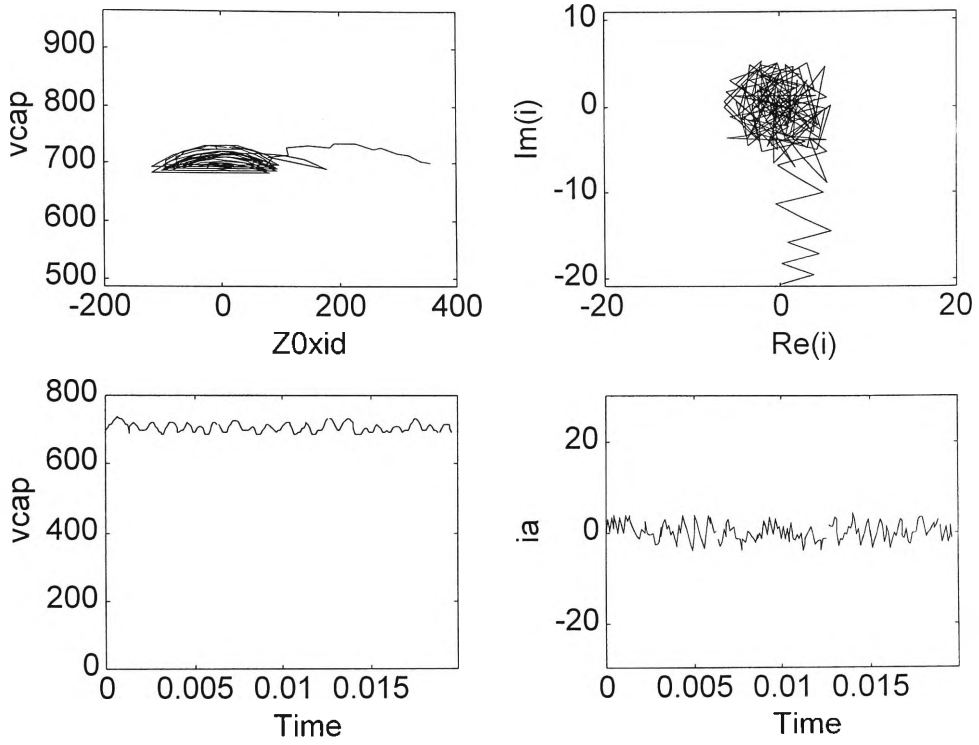

Figure E-23 – Simple control simulation – output current ramping down

(a) Graph of v_{cap} versus $Z_0 i_d$

(b) Graph of i_α versus i_β

(c) Graph of v_{cap} versus time

(d) Graph of i_a versus time

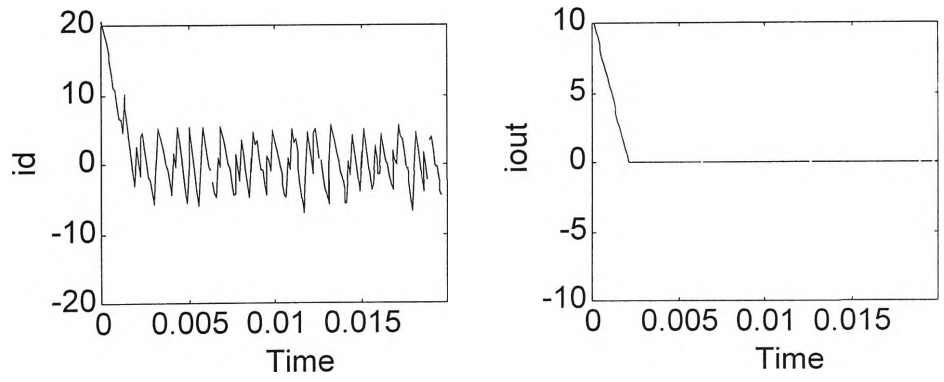

Figure E-24 – Simple control simulation – output current ramping down

(a) Graph of i_d versus time

(b) Graph of i_{out} versus time

v_{cap} maximum	735.5	i_d maximum	20.6
v_{cap} minimum	684.2	i_d minimum	-6.9

Table E-17 Results

E.7 Transient Conditions (Output Current Step Up)

Optimal Control (Output Current Stepping Up)

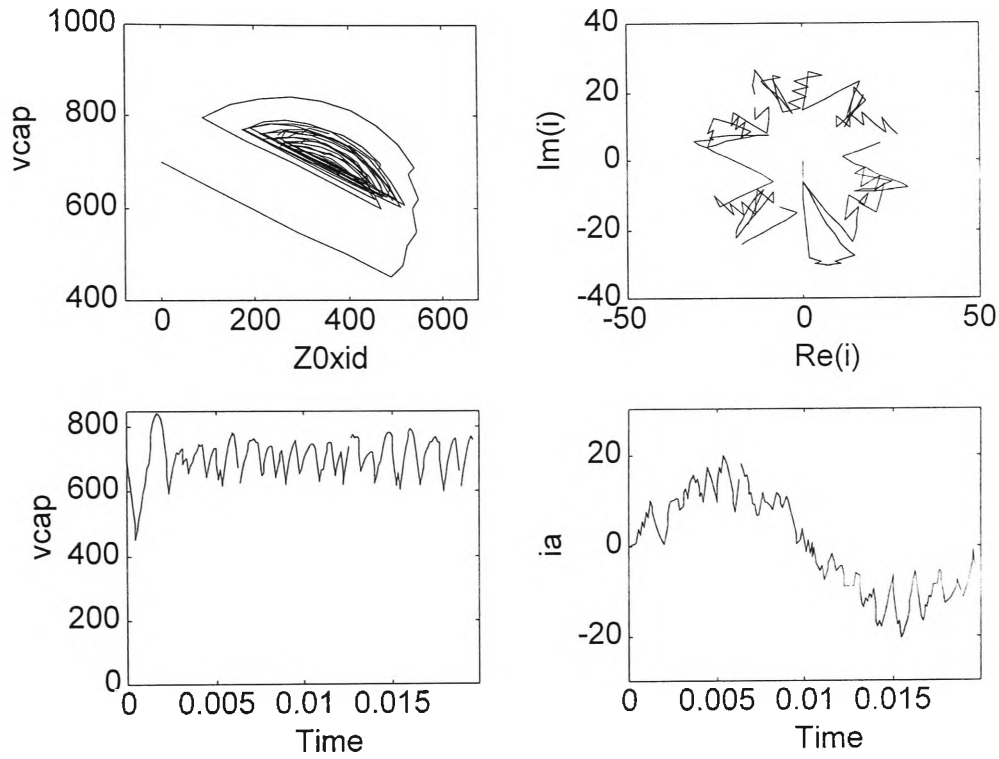

Figure E-25 – Optimal control simulation – output current stepping up

(a) Graph of v_{cap} versus $Z_0 i_d$
(b) Graph of i_α versus i_β
(c) Graph of v_{cap} versus time
(d) Graph of i_a versus time

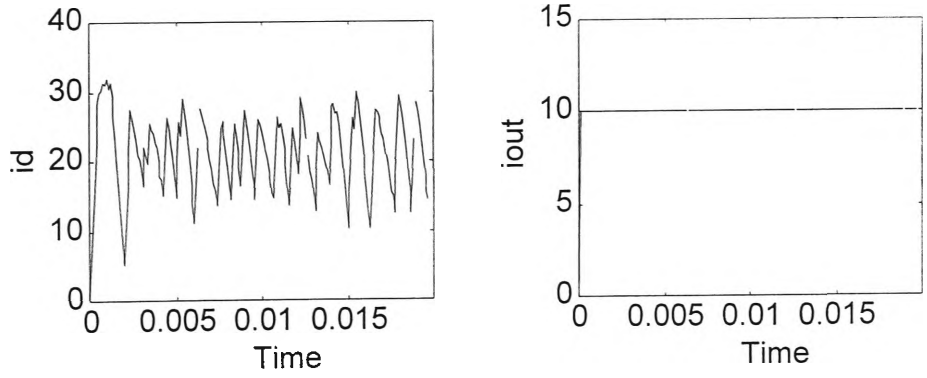

Figure E-26 – Optimal control simulation – output current stepping up

(a) Graph of i_d versus time
(b) Graph of i_{out} versus time

v_{cap} maximum	843.4	i_d maximum	31.8
v_{cap} minimum	450	i_d minimum	0
Cycles to reach target:	22	Time to reach target:	2.2 ms

Table E-18 Results

Hysteresis Control (Output Current Stepping Up)

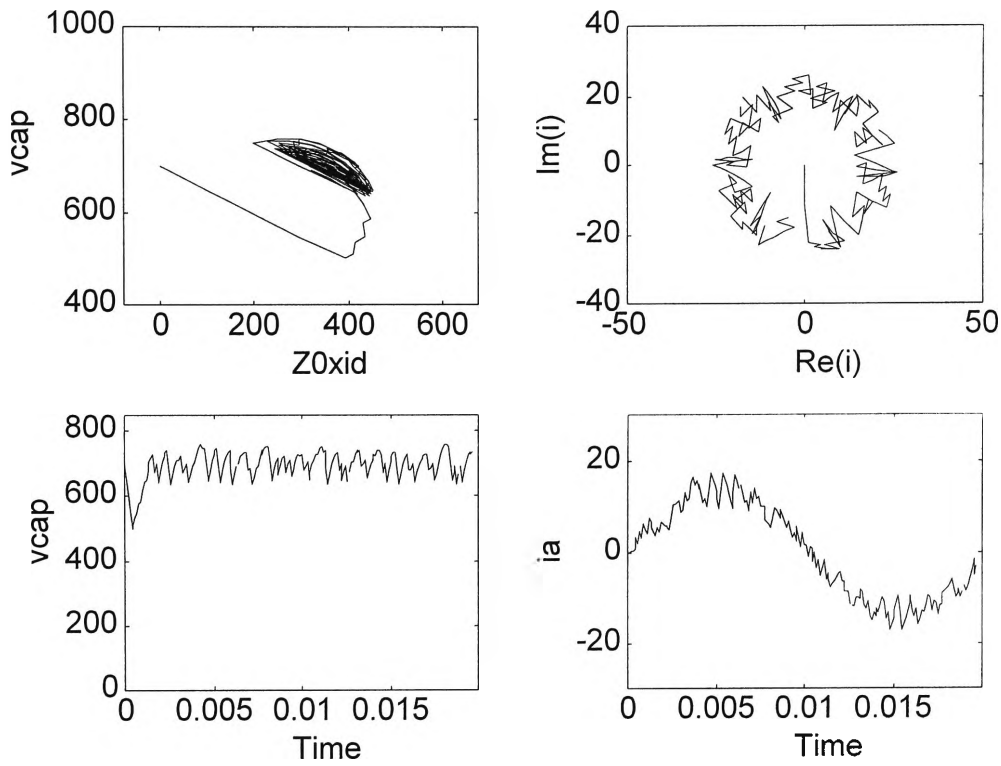

Figure E-27 – Hysteresis control simulation – output current stepping up

(a) Graph of v_{cap} versus $Z_0 i_d$ (b) Graph of i_α versus i_β
(c) Graph of v_{cap} versus time (d) Graph of i_a versus time

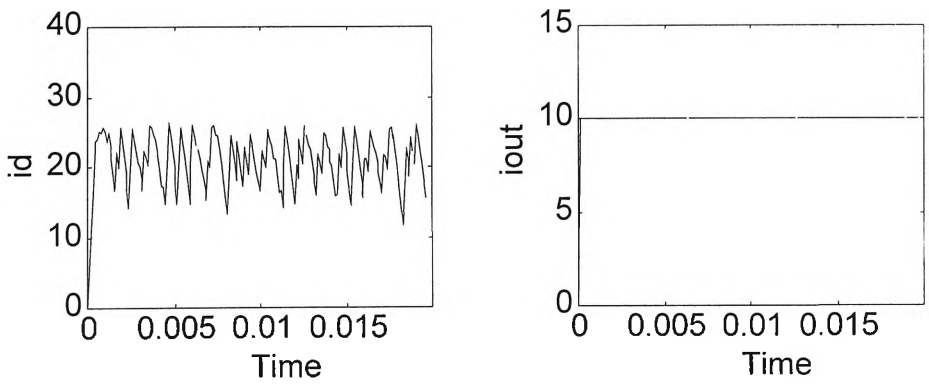

Figure E-28 – Hysteresis control simulation – output current stepping up

(a) Graph of i_d versus time (b) Graph of i_{out} versus time

v_{cap} maximum	759.1	i_d maximum	26.1
v_{cap} minimum	500	i_d minimum	0
Cycles to reach target:	14	Time to reach target:	1.4 ms

Table E-19 Results

Chatter Control (Output Current Stepping Up)

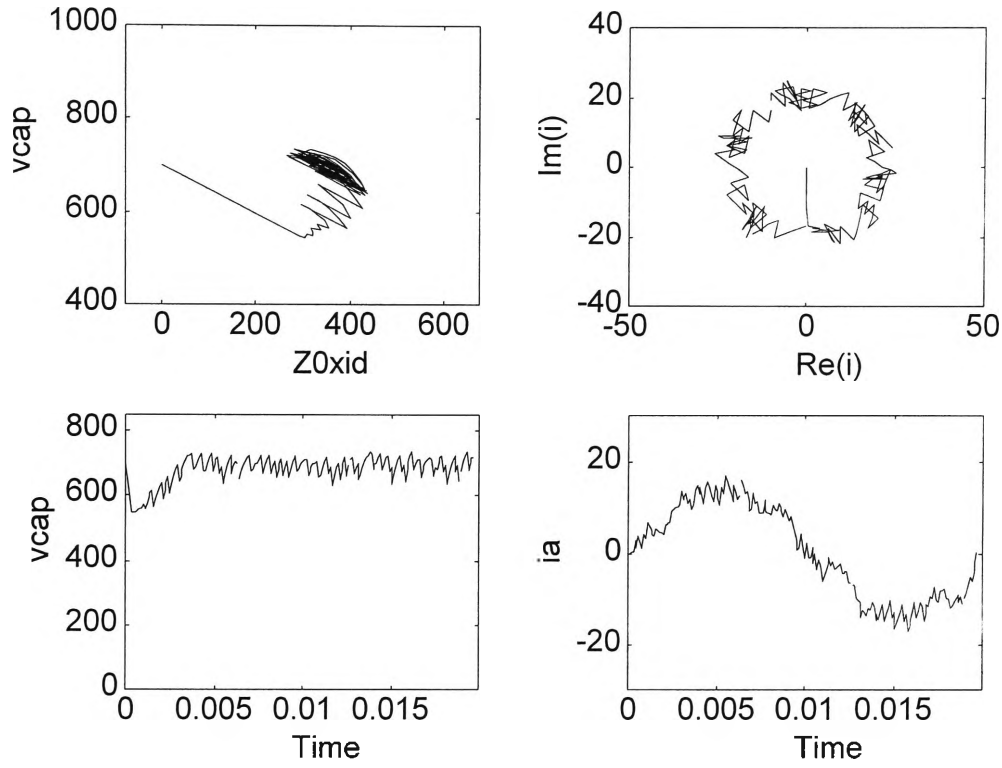

Figure E-29 – Chatter control simulation – output current stepping up

(a) Graph of v_{cap} versus $Z_0 i_d$ (b) Graph of i_α versus i_β
(c) Graph of v_{cap} versus time (d) Graph of i_a versus time

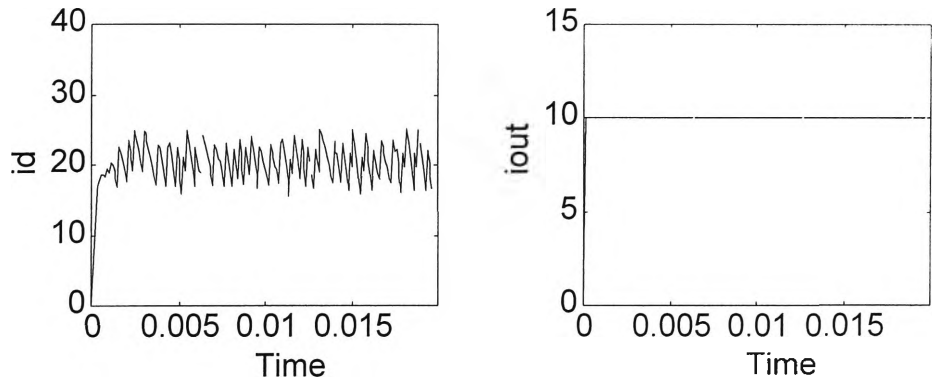

Figure E-30 – Chatter control simulation – output current stepping up

(a) Graph of i_d versus time (b) Graph of i_{out} versus time

v_{cap} maximum	734.1	i_d maximum	25.2
v_{cap} minimum	545.6	i_d minimum	0
Cycles to reach target:	28	Time to reach target:	2.8 ms

Table E-20 Results

Simple Control (Output Current Stepping Up)

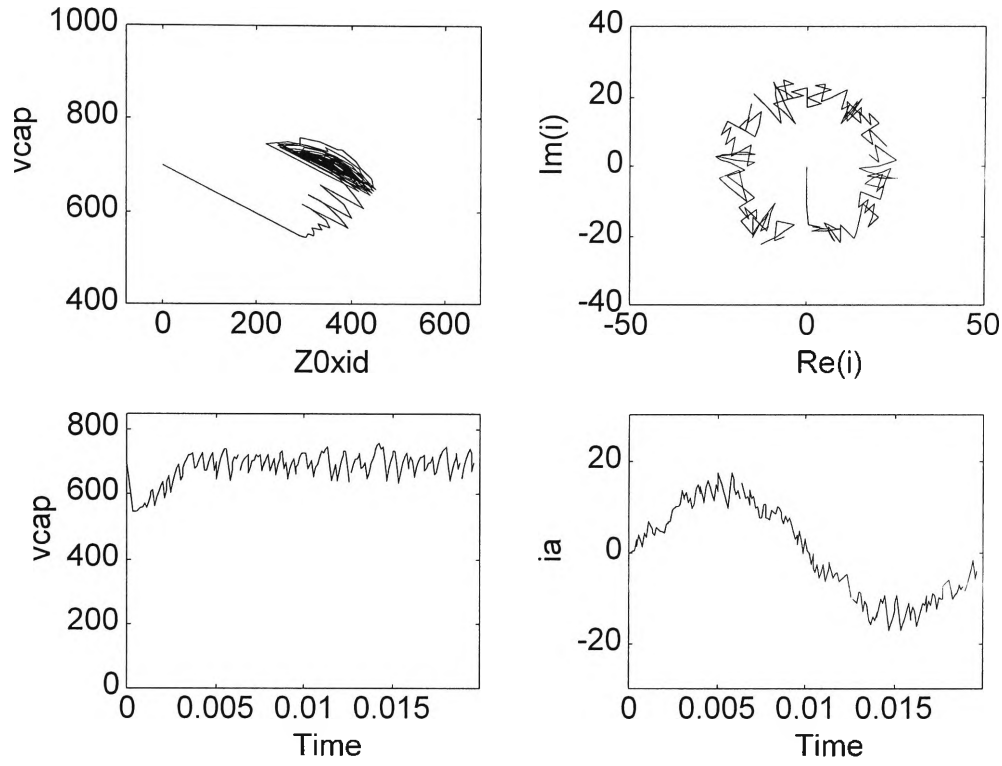

Figure E-31 – Simple control simulation – output current stepping up

(a) Graph of v_{cap} versus $Z_0 i_d$ (b) Graph of i_α versus i_β
(c) Graph of v_{cap} versus time (d) Graph of i_a versus time

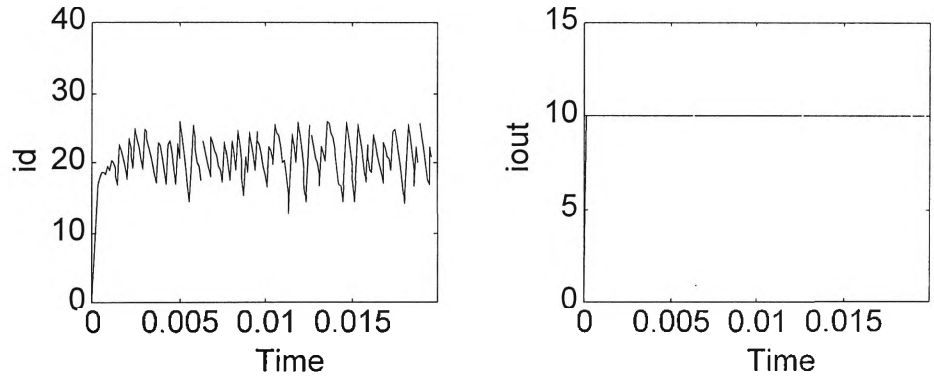

Figure E-32 – Simple control simulation – output current stepping up

(a) Graph of i_d versus time (b) Graph of i_{out} versus time

v_{cap} maximum	758.2	i_d maximum	26.0
v_{cap} minimum	545.6	i_d minimum	0
Cycles to reach target:	28	Time to reach target:	2.8 ms

Table E-21 Results

E.8 Transient Conditions (Output Current Step Down)

Optimal Control (Output Current Stepping Down)

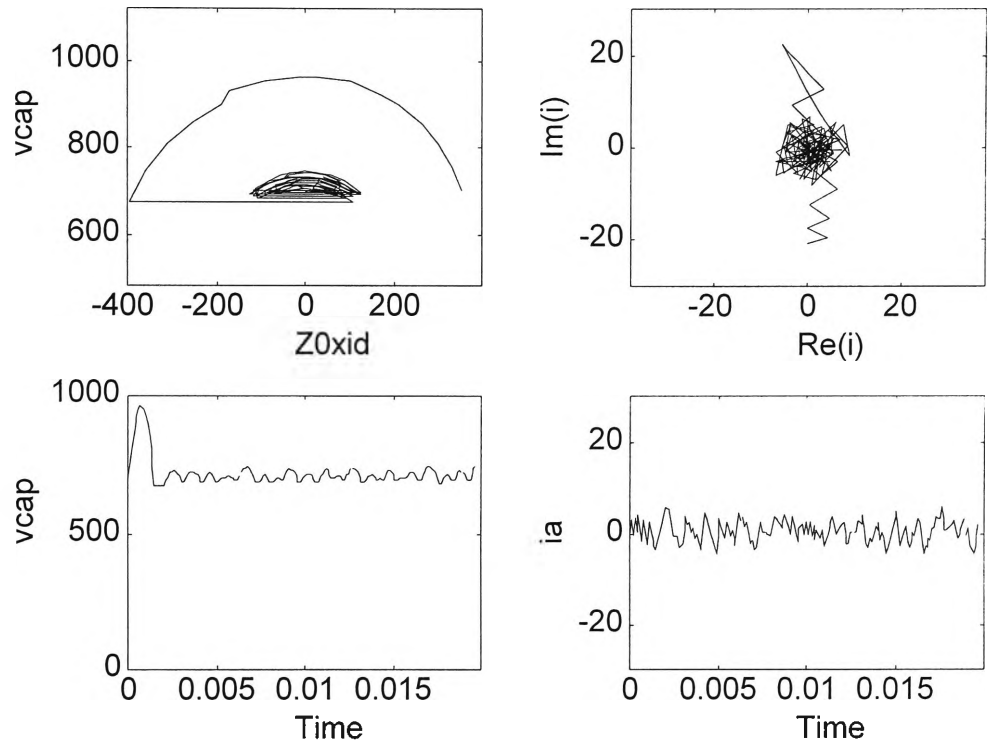

Figure E-33 – Optimal control simulation – output current stepping down

(a) Graph of v_{cap} versus $Z_0 i_d$ (b) Graph of i_α versus i_β
(c) Graph of v_{cap} versus time (d) Graph of i_a versus time

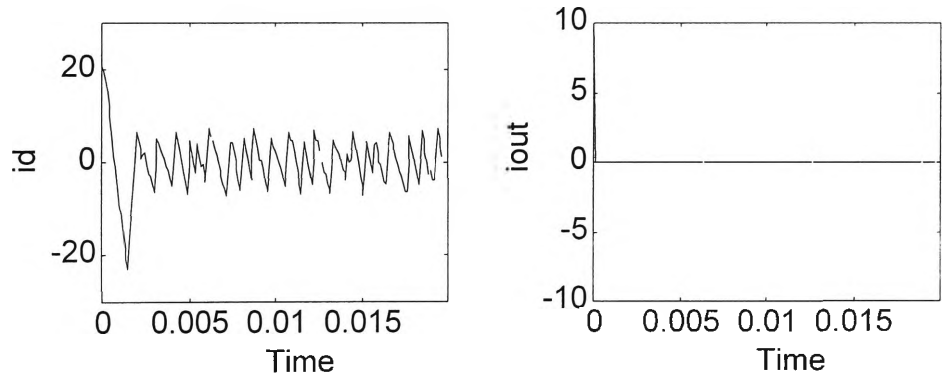

Figure E-34 – Optimal control simulation – output current stepping down

(a) Graph of i_d versus time (b) Graph of i_{out} versus time

v_{cap} maximum	961.5	i_d maximum	20.6
v_{cap} minimum	676.1	i_d minimum	-22.8
Cycles to reach target:	19	Time to reach target:	1.9 ms

Table E-22 Results

Hysteresis Control (Output Current Stepping Down)

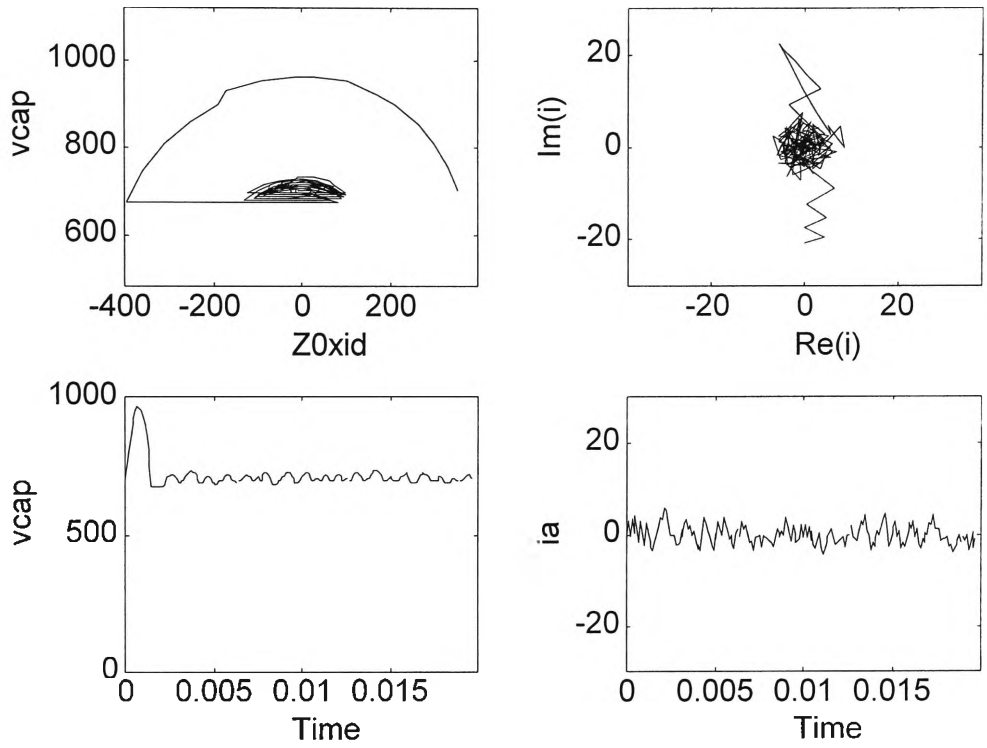

Figure E-35 – Hysteresis control simulation – output current stepping down

(a) Graph of v_{cap} versus $Z_0 i_d$ (b) Graph of i_α versus i_β
(c) Graph of v_{cap} versus time (d) Graph of i_a versus time

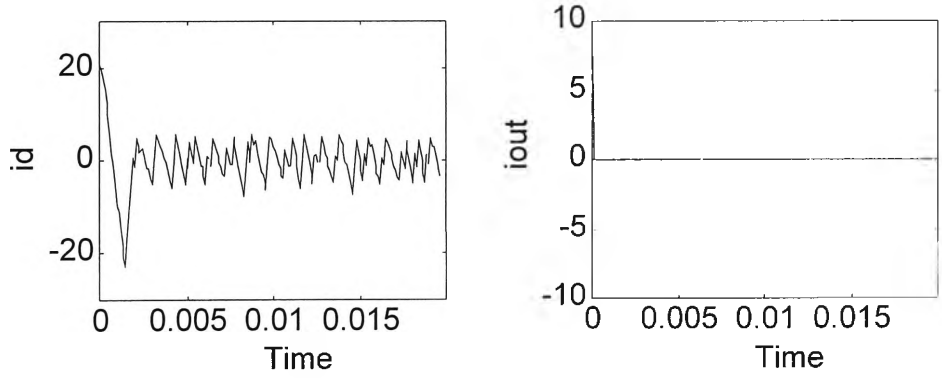

Figure E-36 – Hysteresis control simulation – output current stepping down

(a) Graph of i_d versus time (b) Graph of i_{out} versus time

v_{cap} maximum	961.5	i_d maximum	20.6
v_{cap} minimum	673.8	i_d minimum	-22.8
Cycles to reach target:	20	Time to reach target:	2.0 ms

Table E-23 Results

Chatter Control (Output Current Stepping Down)

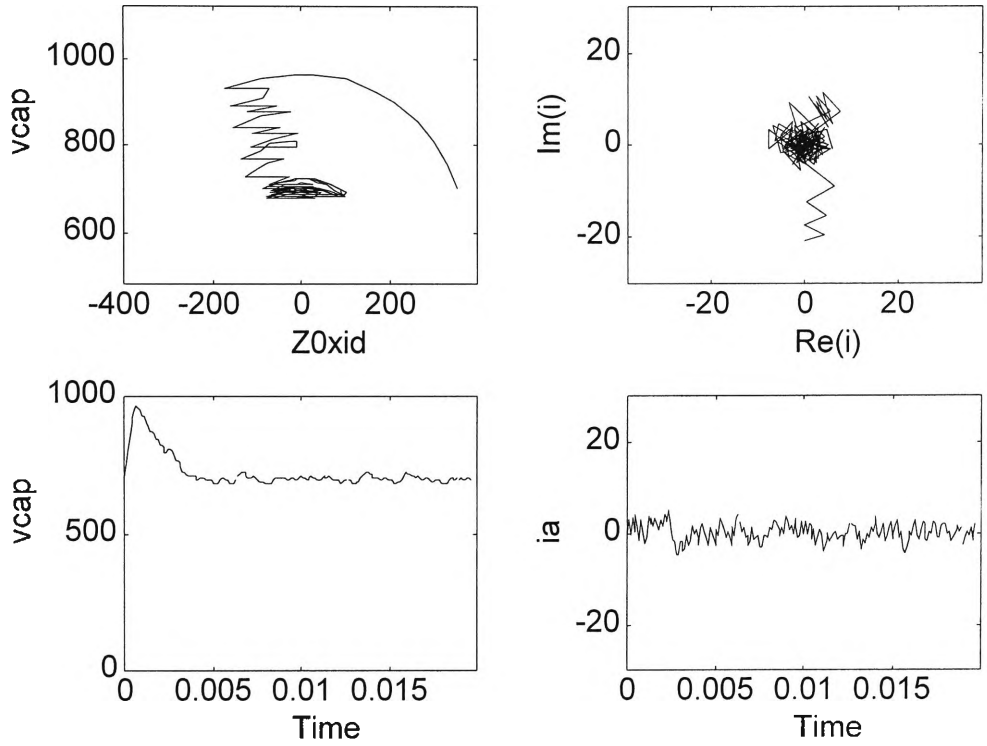

Figure E-37 – Chatter control simulation – output current stepping down

(a) Graph of v_{cap} versus $Z_0 i_d$ (b) Graph of i_α versus i_β
(c) Graph of v_{cap} versus time (d) Graph of i_a versus time

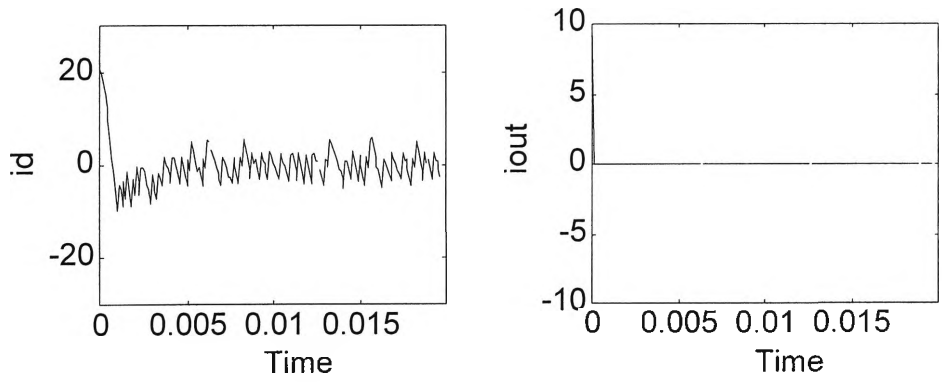

Figure E-38 – Chatter control simulation – output current stepping down

(a) Graph of i_d versus time (b) Graph of i_{out} versus time

v_{cap} maximum	961.5	i_d maximum	20.6
v_{cap} minimum	678.5	i_d minimum	-9.7
Cycles to reach target:	36	Time to reach target:	3.6 ms

Table E-24 Results

Simple Control (Output Current Stepping Down)

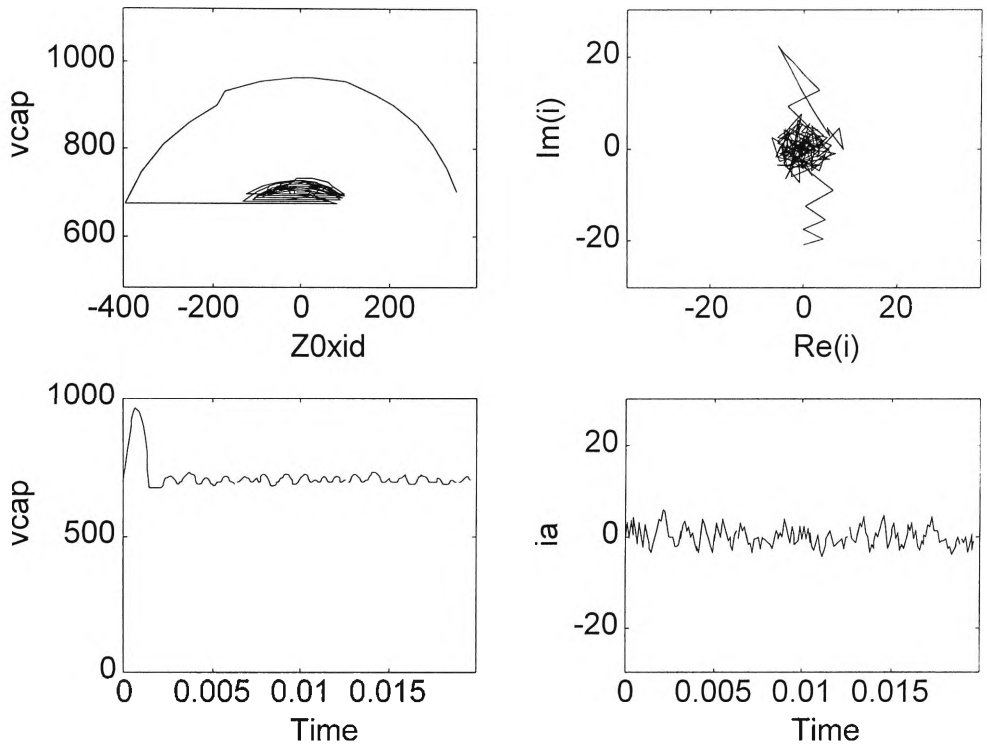

Figure E-39 – Simple control simulation – output current stepping down

(a) Graph of v_{cap} versus $Z_0 i_d$ (b) Graph of i_α versus i_β
(c) Graph of v_{cap} versus time (d) Graph of i_a versus time

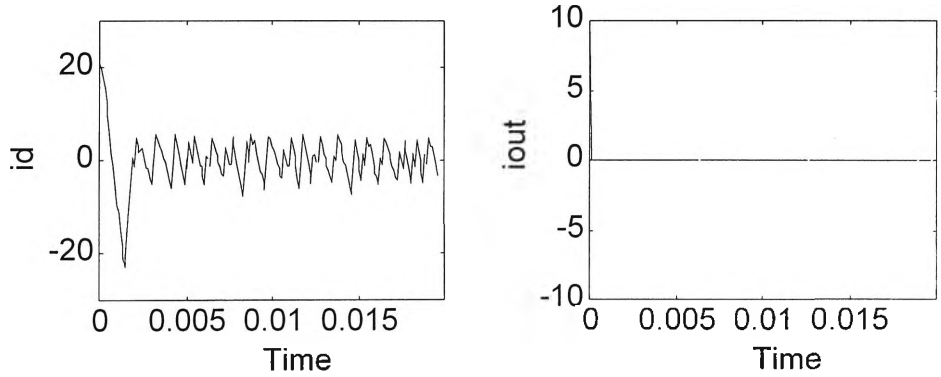

Figure E-40 – Simple control simulation – output current stepping down

(a) Graph of i_d versus time (b) Graph of i_{out} versus time

v_{cap} maximum	961.5	i_d maximum	20.6
v_{cap} minimum	673.8	i_d minimum	-22.8
Cycles to reach target:	20	Time to reach target:	2.0 ms

Table E-25 Results